UNIVERSIDADE ESTADUAL DE CAMPINAS
Faculdade de Engenharia Elétrica e de Computação

CAROLINA FRANCISCANGELIS

TOWARDS VIBRATION SENSING APPLICATIONS BASED ON PHASE-OTDR TECHNIQUES

APLICAÇÕES DE MÉTODOS DE SENSORIAMENTO DE VIBRAÇÃO BASEADOS EM TÉCNICAS DE PHASE-OTDR

CAMPINAS
2017

UNIVERSIDADE ESTADUAL DE CAMPINAS
FEEC – Faculdade de Engenharia Elétrica e de Computação

CAROLINA FRANCISCANGELIS

TOWARDS VIBRATION SENSING APPLICATIONS BASED ON PHASE-OTDR TECHNIQUES

APLICAÇÕES DE MÉTODOS DE SENSORIAMENTO DE VIBRAÇÃO BASEADOS EM TÉCNICAS DE PHASE- OTDR

Thesis presented to the School of Electrical and Computer Engineering and of the University of Campinas in partial fulfillment of the requirements for the degree of Doctor, in the area of Electronics, Microelectronics and Optoelectronics

Tese apresentada à Faculdade de Engenharia Elétrica e de Computação da Universidade Estadual de Campinas como parte dos requisitos exigidos para a obtenção do título de Doutora em Engenharia Elétrica, na Àrea de Eletrônica, Microeletrônica e Optoeletrônica

Supervisor/*Orientador*: FABIANO FRUETT
Co-supervisor/*Co-orientador*: CLAUDIO FLORIDIA

ESTE EXEMPLAR CORRESPONDE À VERSÃO FINAL TESE DEFENDIDA PELA ALUNA CAROLINA FRANCISCANGELIS E ORIENTADA PELO PROF. DR. FABIANO FRUETT

CAMPINAS
2017

Agência(s) de fomento e nº(s) de processo(s): CNPq, 202816/2015-0; CAPES

Ficha catalográfica
Universidade Estadual de Campinas
Biblioteca da Área de Engenharia e Arquitetura
Luciana Pietrosanto Milla - CRB 8/8129

F847t

Franciscangelis, Carolina, 1989-
Towards Vibration Sensing Applications Based On Phase-OTDR Techniques / Carolina Franciscangelis. – Campinas, SP : [s.n.], 2017.

Orientador: Fabiano Fruett.
Coorientador: Claudio Floridia.
Tese (doutorado) – Universidade Estadual de Campinas, Faculdade de Engenharia Elétrica e de Computação.

1. Vibração. 2. Acústica. I. Fruett, Fabiano, 1970-. II. Floridia, Claudio. III. Universidade Estadual de Campinas. Faculdade de Engenharia Elétrica e de Computação. IV. Título.

Informações para Biblioteca Digital

Título em outro idioma: Aplicações De Métodos De Sensoriamento De Vibração Baseados Em Técnicas De Phase-OTDR
Palavras-chave em inglês:
Vibration
Acoustics
Área de concentração: Eletrônica, Microeletrônica e Optoeletrônica
Titulação: Doutora em Engenharia Elétrica
Banca examinadora:
Fabiano Fruett [Orientador]
Livia Ribeiro Alves
Roberto Ricardo Panepucci
Peter Jürger Tatsch
Cristiano Monteiro de Barros Cordeiro
Data de defesa: 04-12-2017
Programa de Pós-Graduação: Engenharia Elétrica

COMISSÃO JULGADORA – TESE DE DOUTORADO

Candidata: Carolina Franciscangelis RA: 072905

Data da Defesa: 4 de dezembro de 2017

Título da Tese (inglês): ”Towards vibration sensing applications based on phase-OTDR techniques”
Título da Tese (português): “Aplicações de métodos de sensoriamento de vibração baseados em técnicas de phase-OTDR”

Prof. Dr. Fabiano Fruett (Presidente, FEEC/UNICAMP)
Dra. Livia Ribeiro Alves (INPE)
Dr. Roberto Ricardo Panepucci (CTI)
Prof. Dr. Peter Jürger Tatsch (FEEC/UNICAMP)
Prof. Dr. Cristiano Monteiro de Barros Cordeiro (IFGW/UNICAMP)

A ata de defesa, com as respectivas assinaturas dos membros da Comissão Julgadora, encontra-se no processo de vida acadêmica do aluno.

ACKNOWLEDGEMENTS

Firstly, I thank God for life and all these amazing opportunities!

I thank my parents, Rosangela and Batista for all the fantastic support along my whole life, for inspiring me so much and for teaching me how to chase my dreams and make them come true.

I thank my stepfather, Fernando, for all the support, inspiration, motivation and for always believing in me and in my goals.

Thanks also to my stepmother, Silvana, for all the love, support and friendship.

I am grateful to my grandparents, Jubeide, Orlando, Josephina and Antônio (*in memoriam*), for all the love and comfort.

Thanks to my dear Frímann, for the love, comfort, support, inspiration, smiles and chocolates.

I am very grateful to my supervisor at Unicamp. Prof. Dr. Fabiano Fruett, for supporting and guiding me through all these years during my bachelor studies, master and PhD. I deeply thank you for all your knowledge, patience, experience and support.

I deeply thank Dr. Walter Margulis, my supervisor during my one-year PhD sandwich period at RISE Acreo facilities in Sweden. Dr. Margulis great experience and knowledge in optical fibers were essential for the development of this work and its relevant results. Thank you very much, Walter, for being an example as scientist as well as for teaching me and supporting me so much.

Thanks to my co-supervisor at CPqD, Dr. Claudio Floridia, for supervising me since my first internship in optical fiber sensors. During both my master's and PhD studies, Dr. Floridia shared his extensive knowledge in optical fiber monitoring, which was of great importance for all the obtained results.

I thank all the amazing team at RISE Acreo: Sebastian, Carola, Magnus, Johan, Sasha, Leif, João, Pär and Pierre-Yves. Special thanks to Erik Zetterlund and Åsa Claesson, group and department managers respectively, who greatly supported me and gave me fantastic opportunities!

I thank Saab AB for all the support that made my PhD sandwich feasible, specially to Lars Sjöström for his interest in this work. Special thanks also to my Saab

supervisor, Dr. Ingemar Söderquist, to Dr. Tonny Nyman, Mikael J. Petersson and to Dr. Per Hallander for all the great technical discussions.

I also thank KTH, especially Prof. Dr. Fredrik Laurell and Prof. Dr. Stefan Hallström for all the technical discussions and advises.

I hugely thank the amazing friends (family, actually!) that I made in Stockholm during my PhD sandwich: Alexandra, Nikoletta, Reihaneh, Argiro, Cristine, Antonios, Efthimios, Carlos, Adriana, Janna, Naiara, Ibrahim, among other amazing people that made my year fantastic!

I thank my beloved friends in Brazil, that supported me with love and comprehension during all these years: Marselle, Camila R., Camila B., Camila D., Camila P., Caike, Monike, Ricardo R., Guilherme M., Guilherme S., Thais, Fernando, Bruna, William, Raudiner, Paulo, Micheli, Michele, Aline, Gabriel, Tatiane, Anapaula, Ulysses, Getúlio, Glauco.

My huge thanks to the great team at LSMO – CPqD, for all the support, lessons and friendship: João Rosolem, Rivael, Ariovaldo, Felipe, Fábio, João Fracarolli, Danilo and Eduardo.

I thank my friends and colleagues at LSM – Unicamp: Giuliano, José, Luciane, Pedro, Ricardo and Diego.

I thank CISB for all the finantial support during my PhD sandwich.

I thank CAPES and CNPq funding agencies for the finantial support.

"A man must shape himself to a new mark directly the old one goes to ground."

(Sir Ernest Henry Shackleton)

ABSTRACT

Distributed optical fiber sensors have been increasingly employed for monitoring several parameters, such as temperature, vibration, strain, magnetic field and current. When compared to other conventional techniques, these sensors are advantageous due to their small dimensions, lightweight, immunity to electromagnetic interference, high adaptability, robustness to hazardous environments, less complex data multiplexing, the feasibility to be embedded into structures with minimum invasion, the capability to extract data with high resolution from long perimeters using a single optical fiber and detect multiple events along the fiber.

In particular, distributed acoustic sensors (DAS) based on optical time domain reflectometry (OTDR), are of high interest, due to their capability to be used in applications such as structural health monitoring (SHM) and perimeter surveillance. Through the frequency analysis of a structure, for instance an aircraft, a bridge, a building or even machines in a workshop, it is possible to evaluate its condition and detect damages and failures at an early stage. Also, OTDR based solutions for vibration monitoring can be easily adapted with minimum setup modifications to detect intrusion in a perimeter, a useful tool for surveillance of military facilities, laboratories, power plants and homeland security.

The same OTDR technique can be used as a non-destructive diagnostic tool to evaluate vibrations and disturbances on both small structures with some dozens of centimeters' resolution and in big structures or perimeters with some meters of spatial resolution and hundreds of kilometers of reach. Another useful feature of this optical fiber-based solution is the possibility to be combined with high-performance digital signal processing techniques, enabling fast disturbance detection and location, real-time intrusion pattern recognition and fast data multiplexing of structure surfaces for SHM applications.
The main goal of this thesis is to make use of these features to employ DAS techniques as key enabling technologies solutions for several applications. In this work, OTDR based techniques were studied and the thesis main contributions were focused on bringing innovative solutions and validations for SHM and surveillance applications.

This PhD had a sandwich period at Acreo AB, Stockholm, Sweden, where experimental tests were performed, and it was part of the 42ª CISB/Saab/CNPq Call.

RESUMO

Sensores à fibra óptica distribuídos têm sido empregados para monitorar vários parâmetros, tais como temperatura, vibração, tensão mecânica, campo magnético e corrente elétrica. Quando comparados a outras técnicas convencionais, tais sensores são vantajosos devido a suas pequenas dimensões, imunidade a interferências eletromagnéticas, alta adaptabilidade, robustez a ambientes nocivos, dentre outros. Sensores acústicos distribuídos em particular são interessantes devido a sua capacidade em serem usados em aplicações tais como monitoração de saúde de estruturas e vigilância de perímetros.

Através da análise em frequência da estrutura, por exemplo uma aeronave, uma ponte, um edifício ou mesmo máquinas em uma fábrica, é possível avaliar sua condição e detectar danos e falhas em um estágio primário. Tais soluções podem cobrir ambas as aplicações de detecção de intrusão e monitoração estrutural com mínimas adaptações no sistema sensor.

Desta forma, vibrações e distúrbios pequenas estruturas com resolução de dezenas de centímetros e em grandes estruturas ou perímetros com alguns metros de resolução espacial e centenas de quilômetros de alcance podem ser detectadas. Outra característica útil desta solução baseada em fibra óptica é a possibilidade de ser combinada com técnicas de processamento digital de sinais, permitindo a detecção e localização de perturbações rápidas, reconhecimento de padrões de intrusão em tempo real e multiplexação de dados de superfícies estruturais para aplicações SHM.

O principal objetivo desta tese é fazer uso desses recursos para empregar técnicas de DAS como soluções de tecnologias- chave para várias aplicações. Neste trabalho, as técnicas de phase-OTDR foram estudadas e as principais contribuições da tese focaram em trazer soluções inovadoras e validações para aplicações de vigilância e vigilância. Como resultado, artigos foram publicados em revistas e congressos internacionais.

Este doutorado teve um período sanduíche nas instalações da RISE Acreo AB, Estocolmo, Suécia, onde experimentos foram realizados e foi parte da 42ª Chamada CISB/Saab/CNPq.

ABBREVIATIONS LIST

ADC	Analog to Digital Converter
ANN	Artificial Neural Network
APC	Angled Physical Contact
APD	Avalanche Photodetector
B-OTDR	Brillouin-Optical Time Domain Reflectometer
BP	Back Propagation
BRAM	Block Random Access Memory
DAS	Distributed Acoustic Sensor
DOFS	Distributed Optical Fiber Sensor(s)
DSP	Digital Signal Processing
EDFA	Erbium Doped Fiber Amplifier
FBA	Fiber Brillouin Amplification
FDM	Frequency Domain Multiplexed
FIFO	First In First Out
FPGA	Field Programmable Gate Array
FUT	Fiber Under Test
IIR	Infinite Impulse Response
NA	Numerical Aperture
NAR	Nuisace Alarm Rates
NLL	Narrow Linewidth Laser
OFDR	Optical Frequency Domain Reflectometer
OTDR	Optical Time Domain Reflectometer
PC	Physical Contact
phase-OTDR	phase-sensitive Optical Time Domain Reflectometer
PMD	Polarization Mode Dispersion
SHM	Structural Health Monitoring
SMF	Single Mode Fiber
SMOS	Sinusoid Modulated Optical Signals
SNR	Signal-to-Noise Ratio
SOA	Semiconductor Optical Amplifier
VHDL	Very High Speed Integrated Circuits Hardware Description Language

SYMBOLS LIST

η	Attenuation coeficiente
P_{BS}	Backscattered signal
K	Constant that depends on the fiber core compositon
G	Derivative
E	Light electrical field
θ	Maximum trace angle of light guided mode
V	Normalized frequency
M	Number of reflecting sections
α_A	Optical fiber absorption coeficiente
z	Optical fiber length
NA	Optical fiber numerical aperture
α_R	Optical fiber Rayleigh scattering coeficient
n	Optical fiber refractive index
I	Optical intensity
P	Optical power attenuation
P_R	Optical power loss due to Rayleigh scattering
v_g	Optical pulse group velocity
T_{Max}	Optical pulse repetition rate
τ	Optical pulse width
Δt_W	Optical pulse width
ΔSR	OTDR spatial resolution
$\Delta\varphi$	Phase difference between two backscattered waves
α	Scattering center amplitude
φ	Scattering wave phase
c	Speed of the light
t	Time
α_T	Total attenuation optical fiber coefficient
L	Total fiber length
λ	Wavelength

SUMMARY

CHAPTER 1

1. INTRODUCTION

Distributed optical fiber sensors (DOFS) have been increasingly employed for monitoring several parameters, such as temperature, vibration, strain, magnetic field and current [1]. When compared to other conventional techniques, these sensors are advantageous due to their small dimensions, lightweight, immunity to electromagnetic interference and high adaptability [2]. Also, these solutions can be also robust to hazardous environments, require less complex data multiplexing and can be embedded into structures with minimum invasion. Differently from point or multi-point solutions where the insertion of single or multiple sensing elements in the fiber is required, in DOFS the whole fiber itself is a continuous sensing element [3]. This feature allows to extract data with spatial resolution of centimeters from perimeters of kilometers lengtht using a single optical fiber and to detect multiple simultaneous events along it. In particular, distributed acoustic sensors (DAS) based on Rayleigh scattering and phase-sensitive optical time domain reflectometry (phase-OTDR), this thesis' subject of study, are of high interest due to their capability to be used in applications such as structural health monitoring (SHM) and perimeter surveillance. When compared to other fiber optics sensing solutions, the phase-OTDR technique features a relevant compromise between spatial resolution, reach and dynamic measurement limits. This method can be adjusted to cover hundreds of kilometers [4], to deliver a 20 cm spatial resolution [5] or measure frequencies from mHz to hundreds of kHz [6], revealing, thus, flexibility and the capability to attend the wide SHM and surveillance applications requirements.

The SHM solutions can detect cracks and material fatigue inside structures. One highly effective non-destructive diagnostic tool for SHM is the damage identification based upon changes in the vibration characteristics of the structure. Usually, frequency information is the most important parameter in vibration sensing [7]. Through the frequency analysis of a structure provided by the phase-OTDR technique, for instance an aircraft, a bridge, a building

or even machines in a workshop, it is possible to evaluate its condition and detect damages and failures at an early stage [8].

It is also known that DAS solutions based on phase-OTDR can be employed for surveillance applications [9]. Perimeter security is an issue of major concern in environments such as: military facilities, electrical plants, oil pipelines, dams, private properties and others. In these facilities, it is important to employ robust, high performance and cost-effective monitoring systems which enables multi-zone disturbance detection and localization capabilities. In this scenario, the phase-OTDR technique rises as a feasible solution, because it can monitor hundreds of kilometers with a meter spatial resolution and needs access to one fiber end only [4]. In these solutions, the sensing fiber can be buried a few meters in the ground, guaranteeing the sensor camouflage from the intruders. Together with parallel hardware architecture approaches, this method allows implementing real-time detecting and locating invasion, enabling a fast response towards the intruder.

It is worth stressing that minimum setup modifications in a phase-OTDR system can make it capable to evaluate vibration frequencies and disturbances locations on both structures that some dozens of centimeters of spatial resolution and also on structures that demand spatial resolutions in the order of meters. Thus, this DAS method can be classified as a key enabling technology solution for several SHM and surveillance applications.

This PhD had a sandwich period at Acreo AB, Stockholm, Sweden, where experimental tests were performed. It was part of the 42ª CISB/Saab/CNPq Call and all the research presented here was performed to present to Saab AB solutions in SHM and surveillance.

1.1. MOTIVATIONS AND CONTRIBUTIONS

The main goal of this thesis is to make use of the phase-OTDR features to employ this DAS technique as key enabling technology solution for applications concerning SHM and surveillance. The motivations rely on the fact that both areas can be covered using the same phase-OTDR method with minor setup changes, which highlights the adaptability feature of this DAS approach. In this work, phase-OTDR based techniques were investigate and the thesis main contributions were focused on bringing innovative solutions and validations for SHM and surveillance applications, described in the subsections below.

A. Structural Health Monitoring

Fiber optic sensors for aircraft SHM allow evaluating both: new aeronautic materials and the behavior of aircraft structures under harsh environmental conditions of pressure, temperature and acoustic disturbance. As previously explained, distributed optical fiber sensors features allow the fiber to be embedded into aircraft structures in a nearly non-intrusive way to sense and measure vibrations along every point along the fiber length. The capability of measuring vibrations on aircraft composite structures is of interest when concerning the study of the material fatigue or the occurrence of undesirable phenomena like flutter.

Therefore, the contribution of this thesis regarding aircraft SHM was the evaluation of the phase-OTDR technique to measure vibration frequencies in carbon composites using embedded optical fibers. Frequencies ranging from 0 to 1000 Hz were correctly measured in two layers of the investigated composite board and this work was published in the SPIE Smart Structures NDE Conference, 2107. Also, a literature review was also performed in order to evaluate the influence of the embedded optical fibers in the composite reinforcing carbon fibers, showing that no significant resistance reduction is observed when the optical fibers are embedded in parallel with respect to the material carbon fibers.

B. Perimeter surveillance

Perimeter surveillance usually requires real-time multi-zone processing of disturbance signals. In this scenario it is important to have: (i) a high performance and reliable computational approach that receives and filters the data at the sampling frequency allowing multiple disturbances to be detected and located; (ii) a scalable and easy configurable processing solution that can be adapted to different scenarios and follows the optical distributed sensors along incremental perimeters and structures.

This thesis contribution to the intrusion detection field based on DAS is the propose of using parallel hardware architectures to implement real-time detecting and locating perturbations through a phase-OTDR distributed vibration sensor. In this multidisciplinary investigation, hardware architectures of the iterative moving average filter and the Sobel filter were mapped on field programmable gate arrays, exploring the intrinsic parallelism in order

to achieve real-time requirements. Experimental results validate the employment of this DAS technique allied with FPGA solutions for surveillance applications. The experimental results were published in the 14th EEE International Conference on Networking, Sensing and Control, 2017.

C. Structural Health Monitoring & Perimeter surveillance: distributed optical fiber microphone

The use of DAS as a distributed microphone allows extracting information from sound which is useful to monitor perimeter security and equipment in industrial plants, since it allows spatially locating the acoustic disturbance and its frequency content. Recently, a distributed fiber microphone was reported based on the phase-OTDR. The amount of data generated by a system used to monitor the acoustic response of the entire fiber all the time is massive, and data acquisition to a memory followed by off-line processing is required. This is a serious limitation, and most DAS systems reported in the literature involve a posteriori analysis of recorded data. In that publication, for example, consecutive phase-OTDR curves were acquired and processed off-line to recover the sound signal.

In some cases, it would be very advantageous to listen to the acoustic signal in real-time, without additional signal processing. In this thesis, a novel proposal is demonstrated to solve this issue, employing a phase-OTDR with direct detection. The method comprises a sample-and-hold circuit capable of both tuning the receiver to an arbitrary section of the fiber considered of interest and to recover in real-time the detected acoustic wave. The system allows listening to the sound of a sinusoidal disturbance with variable frequency, music and human voice with ~60 cm of spatial resolution through a 300 m long optical fiber. The experimental results were published in the Optics Express journal, 2016, as show in Appendix A.

The developed system distributed capability allied with the real-time spatial tuning makes it also suitable for listening to several machines in a workshop, one at a time. Thus, the phase-OTDR real-time microphone technique was also employed to listen to two different machines, a drill and a cooling water system pump, using a single optical fiber. Both machines were attached to two different sections of the optical fiber and they were both working

simultaneously. By triggering the sample-and-hold device, both machines were successfully listened to, along with the recording of their soundwaves. Also, the knocking sounds on the carbon composite border evaluated in the previous SHM section were also listened to, a result that reinforce the use of this microphone for SHM.

These experiments shown the quality limits of an optical fiber as microphone when employing the phase-OTDR technique, which proved to be satisfying when using a proper transducer. It is expected that these results will feed further researches regarding sound coupling and analysis in optical fibers.

1.2. THESIS OUTLINE

This thesis next chapters are organized as follow:

Chapter 2 – Scattering in optical fibers for distributed sensing applications

This chapter shows a literature review in scattering in optical fibers applied to distributed sensing. Firstly, an overview of the Brillouin, Rayleigh and Raman scattering. Then, a detailed section is dedicated to explain the Rayleigh scattering phenomenon, which is the one employed in the phase-OTDR technique, the method explored in this thesis. This section is followed by an explanation about the phase-OTDR vibration sensing method and a literature review of its applications for surveillance and SHM.

Chapter 3 – Multipoint simultaneous intrusion detection for surveillance systems based on phase-OTDR

In this chapter, the application of the phase-OTDR technique for multiple intrusion detection for surveillance systems is presented. Experimental results containing both the traditional method and the joint research between DAS and FPGA methods are shown. The advantages and limitations of this application are discussed.

Chapter 4 – Vibration measurement on composite material with embedded optical fiber based on phase-OTDR

This chapter stresses about one of the phase-OTDR applications covered: the measurement of vibration on composite material. The chapter introduces concepts of carbon composite material and its adherence with embedded optical fibers. Also, the fabrication process of these materials is explained and the results of the validation regarding vibration frequencies measurements in two layers of the material is presented.

Chapter 5 – Real-time distributed optical fiber microphone based on phase-OTDR

In this chapter, a novel distributed microphone based on phase-OTDR technique is be presented along with experimental results and discussions regarding its capacity limits and future challenges.

Chapter 6 – Conclusions

This chapter will summarize this thesis main achievements and contributions along with a discussion regarding future works.

Appendix A – Published papers

Bibliography

CHAPTER 2

2. SCATTERING IN OPTICAL FIBERS FOR DISTRIBUTED ACOUSTIC SENSING

This chapter begins with a review about scattering phenomenon in optical fibers for distributed sensing. The theoretical fundaments behind the main scattering types, Raman, Rayleigh and Brillouin, are stressed with an emphasis on the Rayleigh scattering which is the one explored. Next, the operating principle of the phase-sensitive Optical Time Domain Reflectometer (phase-OTDR) technique, main subject of this thesis, is explained, including a detailed literature review.

2.1. OVERVIEW

Scattering of electromagnetic waves in any medium is related to the heterogeneity of that medium: heterogeneity on the molecular scale or on the scale of aggregations of many molecules [10]. An optical fiber is a non-homogeneous waveguide in which properties such as density, composition and structure vary along its length. When a light beam propagating through an optical fiber encounters these material irregularities, it suffers scattering [11]. If the propagating light doesn't affect the optical properties of the medium, the scattering phenomenon is classified as spontaneous and the irregularities are excited by thermal effect.

However, if the light intensity is enough to produce these properties fluctuations, then the scattering is called stimulated. Part of the scattering light goes back to the input of the fiber and is known as backscattered light [12]. When converted

from frequency/time domain to spatial domain, it represents the phase/amplitude behavior of light along the fiber length. Since these parameters can be sensitive to phenomena as temperature, strain and vibration, this small fraction of the light is the one employed for distributed optical fiber sensors (DOFS) techniques. Since these fluctuations, also known as scattering centers, occurs within micrometers of distance from each other, the DOFS methods are capable to reach a high spatial resolution and extract information continuously along the fiber length [13].

In distributed optical fiber sensing approaches, three spontaneous scattering phenomena are usually employed: Brillouin, Raman and Rayleigh [14], which are all summarized in Figure 2.1.

The Raman scattering is caused by the interaction between the propagating light and the medium molecular vibrations, also known as optical phonons, i. e. photons are scattered by the effect of vibrational and rotational transitions in the bonds between neighboring atoms [12].

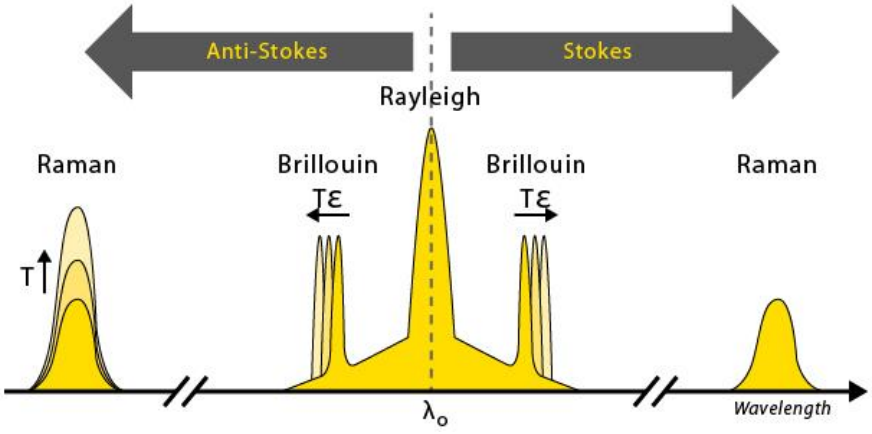

Figure 2.1. Representation of Raman, Brillouin and Rayleigh scattering spectra.

The Raman scattering is classified as an inelastic process, in which an absorbed photon is re-emitted with lower energy and the difference in energy between the incident photons and scattered photons corresponds to the energy required to excite a molecule to a higher vibrational mode [12]. This inelastic interaction causes a frequency shift between the incident and the scattered photons, of around teraherz, generating two spectral peaks known as Stokes and anti-Stokes, where the last one is

sensitive to temperature changes while the other is not. Thus, the Raman backscattering is widely employed for temperature sensing but is insensitive to strain or vibration monitoring. Therefore, this scattering type will not be further addressed in this thesis, which is focused on vibration sensing only.

The Brillouin scattering is also an inelastic process in which part of the power is lost from the optical wave and absorbed by the transmission medium [15]. However, in this case the contribution comes from the acoustic phonons, i. e. the phonons in which the atoms motions are in phase, differing from Raman where the atoms motions are out of phase. Thus, the Brillouin scattering also generates scattered photons with shifted frequencies when compared to the incident photon, but within gigaherz shift only, as depicted in Figure 2. This Brillouin backscattered light is sensitive to temperature and strain [12] and some applications in DOFS involve the simultaneous measurement of strain and temperature. However, the dynamic strain measurements, i. e. the capacity of measuring vibrations of solutions based on this scattering are very limited when compared to Rayleigh based solutions [12].

The Rayleigh scattering, the basis phenomenon for the phase-OTDR technique, is an elastic process. In this situation, the incident and scattered photons have the same energy, thus the same frequency [11]. This scattering type is caused by the optical fiber density fluctuations with a size much smaller than the propagating light wavelength, usually less than 10% [16]. Part of the scattered light backscatters and, when analyzed at the sensor receiver-side, delivers a curve that represents the light intensity along the fiber length.

This elastic scattering has been widely used for temperature, strain, polarization-mode dispersion (PMD), vibration and attenuation sensing, for both telecommunications and sensors applications. It has been explored in techniques such as Optical Frequency Domain Reflectometer (OFDR), Optical Time Domain Reflectometer (OTDR), polarization-OTDR (pOTDR) and phase-OTDR [12]. The last one, explored for dynamic disturbances detection since the 90’s, is the main subject explored and will be further addressed in this chapter.

Since the understanding of the Rayleigh scattering mechanism is demanding for the comprehension of the phase-OTDR technique for vibration sensing, the next section is fully dedicated to exploring its theoretical fundaments and applications.

2.2. THE RAYLEIGH SCATTERING THEORY

In a medium like an optical fiber, its molecules are immersed in a strong internal electromagnetic field. This field is responsible for the constant readjust of the molecules' electron clouds. These readjustments cause a chain reaction that propagates to the neighboring molecules, causing local charge density changes [11]. Thus, fluctuations in the molecule position in the medium are observed in distances in the fiber in the order of some hundreds of nanometers, which is around ten times a molecule size and smaller than the propagating light wavelength. These fluctuations result in an inhomogeneity of the fiber refractive index along its length, in points called scattering centers [17].

When light propagates into an optical fiber, its electromagnetic field rearranges the orientation of these fluctuating molecular electron clouds in the scattering centers, causing a joint response to the electromagnetic field that results in light scattering in all directions [18], as shown in Figure 2.2.

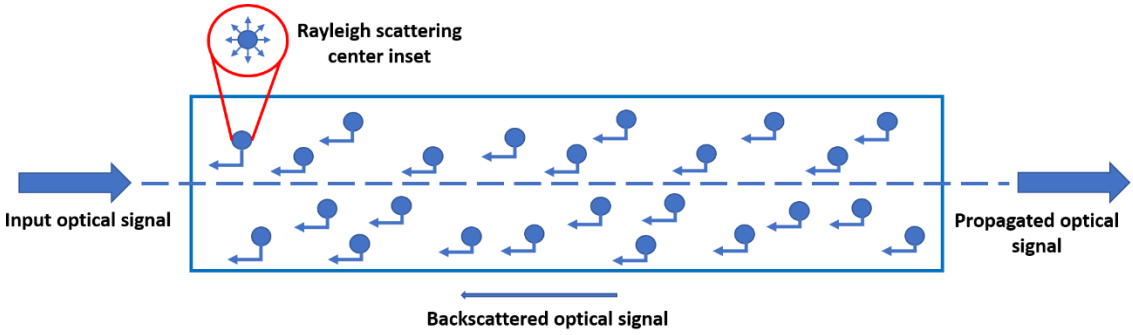

Figure 2.2. Illustration of the backscattering concept in optical fibers, highlighting the presence of the Rayleigh scattering centers.

Some of the scattered light is collected by the optical fiber and guided in the backward direction, a fraction of light called backscattering.

In general, the optical characteristics of scattering depend on the size of scatter in comparison to the optical signal wavelength. In optical fibers, the scatter, i. e. the refractive index fluctuations, are usually smaller than the optical signal wavelength, which explains the presence of the Rayleigh scattering. This scattering causes a continuously decrease in the power of the propagating light beam along the optical fiber. The shorter the wavelength, λ, the stronger the Rayleigh scattering coefficient, which can be expressed for silica optical fibers according to the following equation [11]:

$$\alpha_R = \frac{K}{\lambda^4} \tag{2.1}$$

where K is a constant that depends on the fiber core composition and it ranges around 0.7 ~ 0.9 (dB/km)μm^4.

Regarding the total loss in optical fibers, expressed in dB/km, it can be caused by both the Rayleigh scattering and the material absorption phenomenon coefficient, α_A. Thus, the total attenuation coefficient, α_T, can be represented as following [11]:

$$\alpha_T = \alpha_R + \alpha_A \tag{2.2}$$

Also, the input optical power attenuation along the optical fiber length, which exhibits an exponential pattern, can be expressed according to the equation below:

$$P(z) = P_0 exp\{-\int_0^z [\alpha_T(z)]dx\} \tag{2.3}$$

If the Rayleigh scattering in the fiber is modeled by the scattered caused by every short fiber section of length dz, then the optical power loss due to the scattering inside this section is:

$$dP_R(z) = P(z)\alpha_R(z)dz \tag{2.4}$$

However, only a small fraction of this scattered energy is coupled to the waveguide and propagates back to the optical fiber input side. Therefore, the backscattered light resulting from each *dz* section is calculated as follow [19]:

$$dP_{BS} = P(0)\eta\alpha_R(z)dzexp\{-2\int_0^z \alpha_T(x)dx\} \quad (2.5)$$

where η is a parameter called conversion efficiency. When Rayleigh scattering occurs in an optical fiber, each scattering center scatters the light into all directions, filling the entire 4π solid angle [19]. However, only a small part of the scattered light whose angle lies within the numerical aperture (NA) can be converted into guided mode inside the fiber core and become the backscatter that travels back to the fiber input. The rest of the scattered light will be radiated into the cladding and lost. Thus, the ratio between the captured light and the total scattered optical power is given by the following equation [19]:

$$\eta = \frac{2\pi(1-cos\theta)}{4\pi} = \frac{1-cos\theta}{2} \quad (2.6)$$

where 4π is the total area of the unit sphere that represents the scattering center, θ is the maximum trace angle of the guided mode with respect to the fiber axis and $2\pi(1-cos\theta)$ is the area of the spherical cap in the shadowed blue area shown in Figure 2.3.

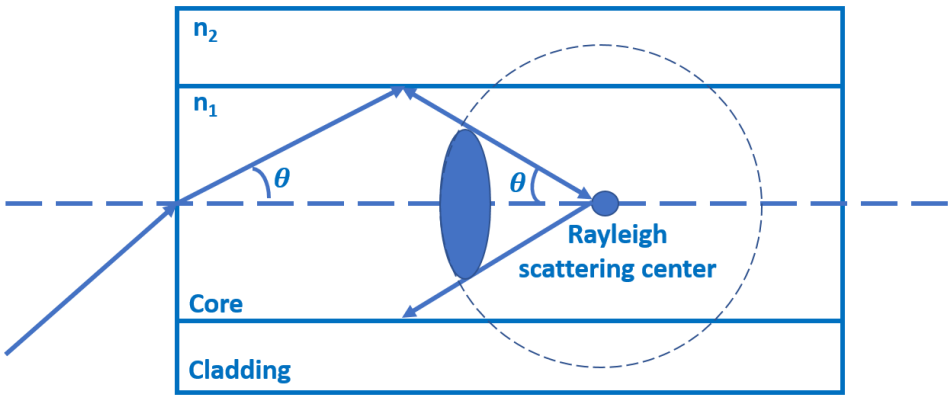

Figure 2.3. Detailed illustration of the Rayleigh scattering mechanism in optical fiber cores.

The optical fiber NA is the maximum acceptance angle at a fiber optics input:

$$NA = \sqrt{n_1^2 - n_2^2} \tag{2.7}$$

Considering a normalized frequency, V < 2.4, the required for single mode fibers, the conversion efficiency can be expressed as following [19]:

$$\eta \approx \frac{1}{4.55}\left(\frac{NA}{n_1}\right) \tag{2.8}$$

Thus, the amount of captured backscattered light is directly dependent on the optical fiber numerical aperture. This knowledge is suitable to maximize the amplitude of the phase-OTDR traces for vibration sensing, as shown in further chapters.

If an optical pulse of certain width, τ, is launched into an optical fiber at the time t_0, neglecting the effect of chromatic dispersion and fiber nonlinearities, the locations of the pulse leading and trailing edges at time t are $z_l = v_g(t-t_0)$ and $z_t = v_g(t-t_0-\tau)$, where v_g is the optical pulse group velocity [19]. In this case, the backscattered signal, P_{BS}, that returns to the fiber originated from a short fiber section of length $\Delta z/2 = (z_l - z_t)/2 = v_g\tau$ has its amplitude defined by the following equation:

$$P_{BS}(z) = \frac{v_g\tau}{2} P(0)\eta\alpha_R(z)\exp\left\{-2\int_0^z \alpha_T(x)dx\right\} \tag{2.9}$$

It is also worthy stressing that the collected backscatter power is usually very low, ranging around -50 dBm or even lower [19]. The operating principles of the phase-OTDR technique are explored in the next section.

2.3. THE PHASE-OTDR TECHNIQUE BASED ON RAYLEIGH SCATTERING

This section stresses about the main principles involved in the phase-OTDR method, including historical context, basic setup and summarized main applications. In order to better understand the phase-OTDR operation mechanisms, an overview of the traditional OTDR method is firstly presented.

2.3.1. THE BASIC OTDR METHOD

The parameters that characterize an optical fiber, such as losses and optical power attenuation can be modified due to environmental conditions: humidity, temperature, mechanical stress, vibrations, among others. These properties were always of interest in installed optical fiber communication cables, since the attenuation profile of an optical fiber determines directly its loss, affecting the transmission system quality.

In this context, the traditional and oldest method to measure insertion loss in optical fibers is also a very destructive one, since it requires the fiber link to be cut in tracks and the loss measured in the end of each track [19]. This method was widely used until 1976, where Barnoski and Jensen, the authors of the first publication regarding backscattering in optical waveguides [20] proved the application of the scattering phenomenon in optical monitoring. They developed, thus, the first OTDR, a distributed method sensitive enough to measure Rayleigh backscatter in optical fibers within hundreds of kilometers of range, a spatial resolution that nowadays can achieve centimeters and requires access to one fiber ending only.

The OTDR analysis techniques also evolved along the decades in such way that now this distributed monitoring method is widely used for optical network monitoring, measuring the attenuation of the transmitted signal along the fiber length and detecting undesirable events such as insertion loss, splice loss, bending and bad connections [19].

A basic OTDR setup is depicted in Figure 2.4.

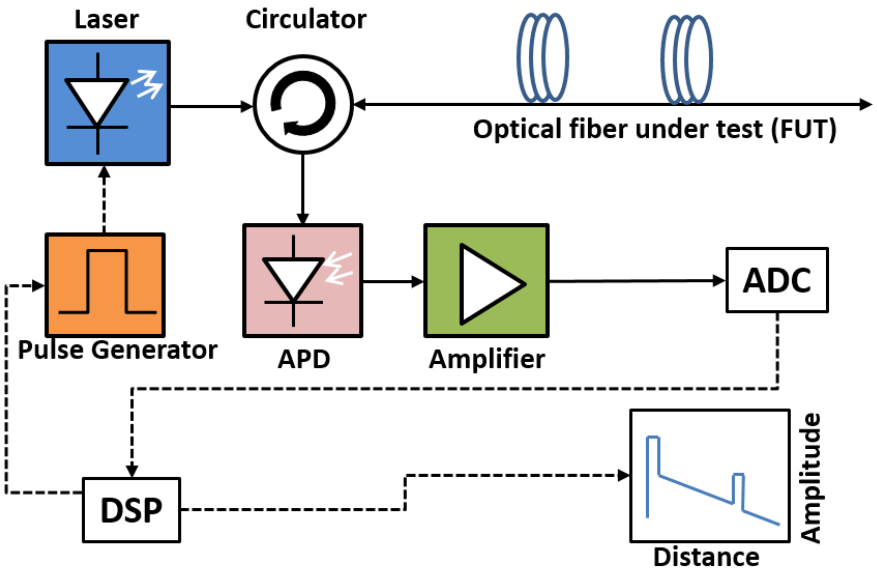

Figure 2.4. Block diagram of a basic OTDR setup.

A pulse generator is triggered by a digital signal processing unit and used to modulate the intensity of a broadband laser. In conventional OTDRs, this triggering signal is usually a rectangular pulse with certain duration, which depends on the required spatial resolution and sensitivity. The optical pulse is directed to the optical fiber under test (FUT) by a circulator and the Rayleigh backscattering signal that returns from the FUT is directed to a photodetector. In order to avoid the superposition of backscattered signals, only one pulse can travel in the fiber at a time, as shown in Figure 2.5 a. Thus, the repetition rate at which the pulses are sent in the FUT is limited by the roundtrip flight time of the pulse in the fiber, limited by the fiber length, L, as follows [13]:

$$T_{Max} = \frac{2Ln}{c} \tag{2.10}$$

where c is the speed of light and n is the optical fiber refractive index. Assuming that the Rayleigh scattering centers previously explained are homogeneously distributed along the FUT, each infinitesimal part of the traveling optical pulse will generate a counter-propagating Rayleigh backscattered signal while the pulse travels in the fiber [13]. At each instant, t, a backscattered signal with the same width of the propagating pulse, Δt_W, will be generated from the pulse position in the fiber, as depicted in Figure

2.5 b. Thus, the backscattered signal is continuously generated and signals generated from different parts and times can overlap at the photodetector at the OTDR receiver-side (z_0), as shown in Figure 2.5 c.

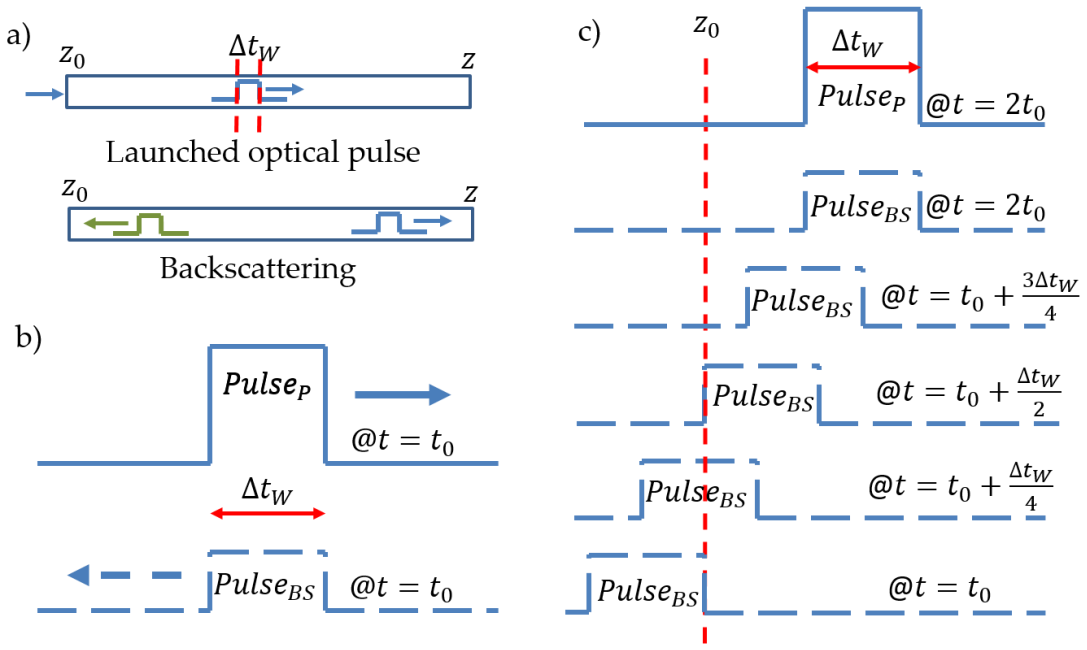

Figure 2.5. a) Depiction of the backscattering generated by an optical pulse in an optical fiber; (b) details of the generated backscattered pulse: less amplitude and same width as the original pulse; (c) illustration of the overlap of different backscattered signal at the OTDR receiver.

The OTDR photodetector is usually an avalanche photodetector (APD) or a p-i-n photodiode. The reason is the need for a high sensitive detector capable to detect low power signals such as the Rayleigh backscattered light around -60 dBm or less. The light detected by the photodetector is converted into an electric signal and conditioned by a linear amplifier and then acquired by an analog-to-digital converter (ADC) and digitally processed. The ADC sampling rate defines the spatial separation between consecutive data samples. This type of detection shown in Figure 2.4 is known as direct detection and is the simplest configuration of OTDR based sensors. In this topology, two main noises are limiting in the system: the shot and the thermal noise of the detection system [19].

The main goal of an OTDR measurement is to read the impulse response of an optical fiber. Since the OTDR pulses approach an ideal Dyrac delta function, the result

is a convolution between the fiber response and a pulse of finite temporal duration, resulting in a smoothed version of the impulse response.

Figure 2.6 [21] shows the typical trace exhibited by an OTDR after a measurement. The vertical axis represents the backscattered signal in arbitrary unit, usually in decibels (dB). The horizontal axis corresponds to the distance between the instrument and a location in the FUT. Since an OTDR can only measure time, t, this axis is converted to distance along the fiber, L, according to the following equation:

$$L = \frac{ct}{2n} \tag{2.11}$$

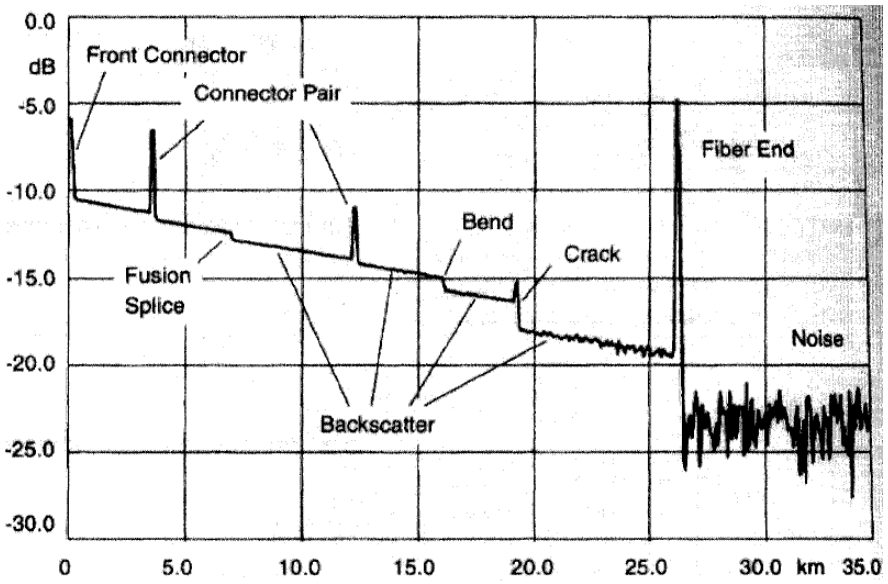

Figure 2.6 Typical OTDR trace [21].

The typical OTDR trace, as shown in Figure 2.6, exhibits three main characteristics: straight descending lines caused by distributed Rayleigh backscattering, positive peaks caused by reflections in some fiber tracks and steps. These last ones can be either positive or negative, depending on the fiber physical properties [19].

The first noticeable event in the trace is the reflection from the front connector that links the instrument to the FUT. This undesirable event might be reduced by using a good quality connector with low reflectance, in order to avoid masking information

from the beginning of the fiber. An unsuitable connector reduces the launched optical power in the fiber due to insertion loss and might cause a new reflection in the backscattered light, generating the so called “ghost patterns” [19]. These patterns are characterized as peaks that doesn’t represent a feature of the fiber itself and might be minimized by using angled physical contact (APC) connectors instead of physical contact (PC).

Since the OTDR traces represent optical power *versus* distance, the trace slopes provide the fiber attenuation in dB/km. Splices between two optical links cause a reduce of the backscattered optical power level and if both links are the same fiber type, then the insertion loss value is determined by this drop. Another event shown in the OTDR trace are the fiber twists and bends, which result in the reflection of part of the propagating light to outside of the fiber core and cladding, causing a power loss.

Another remarkable event is a crack between two fiber links, resulting in a small air gap between then and, consequently, in a high reflection and an abrupt slop in the optical power level. Lastly, there is the remote fiber end, an open ending responsible for causing an intense reflection. It there is a transition between fiber and air after this ending, more than 4% of the propagating signal optical power can be reflected to the OTDR input. No optical signal is detected beyond the fiber end, thus the OTDR curve experiences an attenuation to the receiver noise level, limiting the lowest power level capable to be detected by the instrument.

The characterization of an optical fiber using an OTDR is based in three parameters: dynamic range, dead zone and spatial resolution. The dynamic range is the difference between the backscattered signal level in the input of the fiber and the noise level where the signal-to-noise ratio (SNR) is equal to 1 dB. This parameter is dependent on the OTDR launched pulse width and determines the maximum fiber length possible to be measured by the OTDR, considering the attenuation in the fiber itself and in the splices and connections. There is a trade-off between dynamic range, pulse width and spatial resolution: the shorter the pulse width, the higher the spatial resolution, the smaller the pulse energy and thus the shorter the dynamic range.

The spatial resolution, ΔSR, indicates the precision that the OTDR provides the location of the events long the optical fiber length. This parameter is defined by the pulse width, Δt_W, and is expressed as follows [13]:

$$\Delta SR = \frac{c\Delta t_W}{2n} \tag{2.12}$$

It is worth stressing that a high spatial resolution requires narrow optical pulses, which demands a broader bandwidth in the photodetector at receiver-side of the instrument, increasing its total cost [19]. The last parameter is the dead zone, which is caused by the reflections in the beginning of the FUT that saturate the OTDR receiver system. When these reflections occur, the returned signal is then superimposed at the receiver-side due to saturation caused by the high-power reflections, resulting in an information loss concerning the beginning of the fiber. The dead zone depends on the pulse width, wavelength, receiver bandwidth and optical fiber reflectance.

All the parameters and features shown in this section about an OTDR also suits a phase-OTDR as well. The only difference is the use of a narrow linewidth laser in a phase-OTDR instead of a broadband one usually employed in the OTDR setup. This characteristic as well as the phase-OTDR principle of operation will be explained in next section.

2.3.2. FUNDAMENTALS OF THE PHASE-OTDR TECHNIQUE

The phase-OTDR was first proposed and demonstrated by W. Lee and H. F. Taylor, in 1993 [22]. It was initially developed and employed as a distributed intrusion sensor capable to detect and localize disturbances along a perimeter. The reported system is practically identical to a common OTDR already shown in Figure 2.4, the only difference is the employment of a narrow linewidth laser that presents minimum frequency shift and thus is very coherent, instead of a broadband light source.

If the coherence length of the phase-OTDR light source is equal or longer than the spatial width of the probe optical pulse, the backscattered light fields from the Rayleigh scattering centers will coherently interfere within the pulse, since these fields maintain a fixed and predictable phase relationship between each other. These

coherent interferences will result in a speckle-like pattern along the phase-OTDR trace instead of a smooth OTDR trace, as depicted in Figure 2.7 [11, 13]. It is relevant to stress that this pattern is undesirable for OTDR applications, it is considered coherent noise and may mask relevant OTDR trace information like a bend or a bad connection [23]. However, it is essential for the phase-OTDR operation to detect dynamic disturbances, since this jagged trace remains constant over time unless it experiences an external disturbance, i. e. the Rayleigh backscattered light at the disturbed region experiences an extra phase shift compared to the stable state [24].

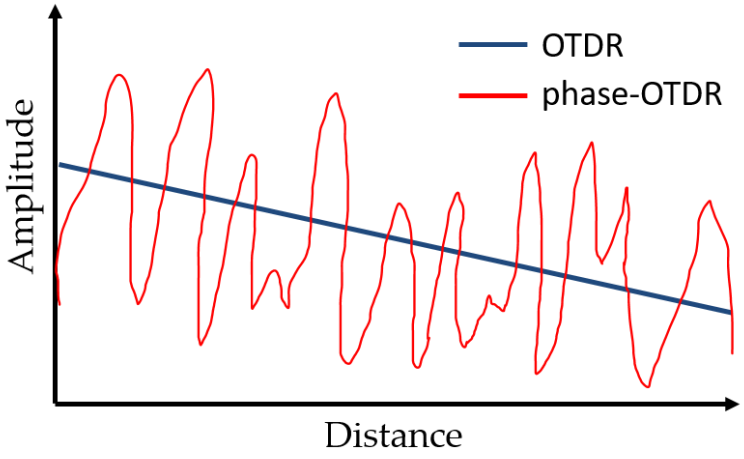

Figure 2.7. Illustration of an OTDR and a phase-OTDR trace.

This phenomenon can be understood and modeled from the calculation of the optical intensity, I, resulting from the addition of two backscattered waves from two Rayleigh scattering centers inside the pulse width, $\boldsymbol{E}_1$ and $\boldsymbol{E}_2$ [19]:

$$I(t) = E(t)_1^2 + E(t)_2^2 + 2E_1E_2\cos\left(\theta(t)_p\right)\cos(\Delta\varphi(t)) \tag{2.13}$$

where $\theta(t)_p$ is the relative polarization angle and $\Delta\varphi(t)$ the phase difference between the two backscattered waves. If the light source was broadband, both fields would interfere incoherently due to the fact that $\Delta\varphi(t)$ varies randomly over time and, thus, the interference term is averaged away. This explains why an OTDR shows a smooth trace that is sensitive to intensity variations only.

On the other hand, if a coherent source was employed, e. g. in a phase-OTDR, the fields would interfere coherently and the interference terms would have a value dependent on $\Delta\varphi(t)$. Thus, the optical intensity of the resulting interference signal would be sensitive to variations of the relative phase among the backscattered fields, caused by external disturbances such as phase shifts caused by vibrations, strain or temperature, as previously explained.

This analysis can also be extrapolated to multiple scattering centers, employing a model [25] in which the optical fiber of length z is divided into M reflecting sections of equal length $\Delta z = z/M$, each one containing N scattering centers, as shown in Figure 2.8.

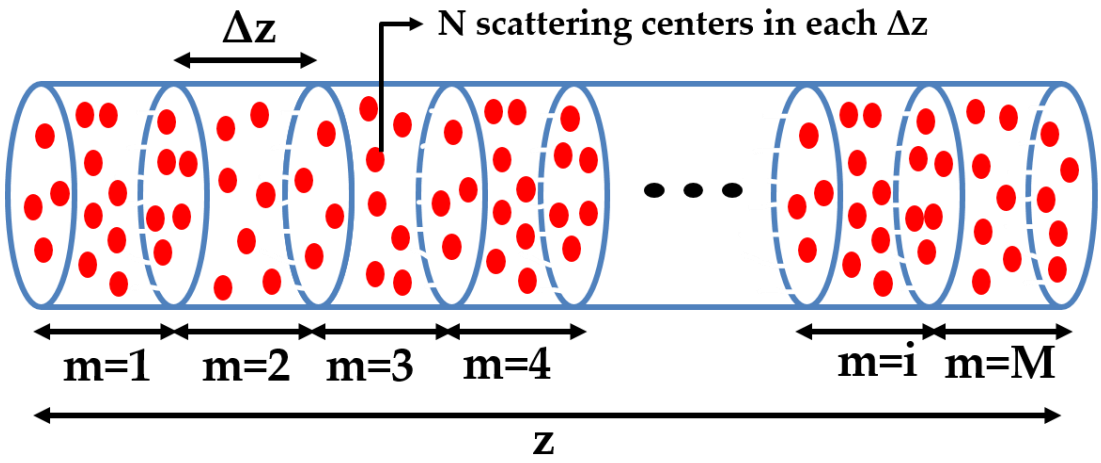

Figure 2.8. Illustration of a model of the Rayleigh backscattering in an optical fiber.

Thus, in this model the Rayleigh backscattering in the fiber section is represented by the M reflecting sections. The interference field of the Rayleigh backscattering signal at the position m = i is defined by the following expression:

$$\vec{E}_{BS}(z_i) = E_0 e^{-\alpha_T (i-1)\Delta z} \sum_{k=1}^{N} a_k^i e^{j\varphi_k^i} \tag{2.14}$$

where E_0 is the propagating pulse electrical field intensity, α_T is the optical fiber attenuation coefficient previously explained, α_k^i is the amplitude of the k-th scattering center at m = i and φ_k^i is its phase. According to this equation, the interference among

the Rayleigh backscattering light is represented by the complex sum of the scattering centers amplitude and phase in each section, which can be interpreted as the spatial width of the propagating optical pulse. Simulations already presented in literature using this model show as result typical phase-OTDR traces with a jagged appearance, as expected, which is due to the random position of the Rayleigh scattering centers along the optical fiber [25].

It is worthy stressing that the phase-OTDR method presents a non-cumulative effect in the result traces, i. e. the signal detected from one section in the fiber is totally independent from another section if the distance between both is not within the sensor spatial resolution defined by the spatial width of the optical pulse. This concept is shown in Figure 2.9a, where two consecutive phase-OTDR from before and after a disturbance in the section between 360 m and 380 m of a 1 km optical fiber are displayed. It is visible from the figure and from the inset zoom that the trace only changes where the disturbance is applied. In Figure 2.9b this is even more evident, since a peak is observed only in the disturbed region of the differential curve between both traces. This feature is advantageous when compared to cumulative methods such as the pOTDR, which can detect only where the disturbance begun but not where it ends.

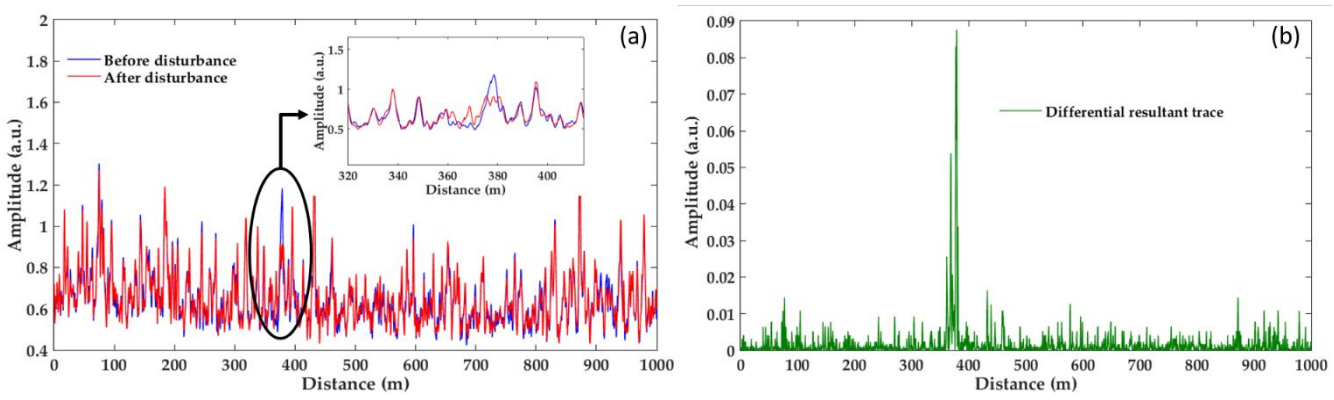

Figure 2.9. a) Two consecutive phase-OTDR traces: before (blue) and after (red) a disturbance in ~20 m section (inset) of a 1 km optical fiber; b) Trace resultant from the subtraction of the two-consecutive phase-OTDR traces.

In the case of detecting dynamic disturbances, i. e. mechanical vibrations, the phase-OTDR trace will show local amplitude variations that are synchronized with the applied vibration frequency, which makes possible to measure the frequency profile of the disturbance [27]. In order to do so, several consecutive phase-OTDR traces are acquired and processed. The time-domain signal is rebuilt from the amplitude variation of the disturbed point along the traces, as shown in Figure 2.10a, which shows the time-domain waveform of a 1000 Hz vibration disturbance acquired with the phase-OTDR technique. Also, Figure 2.10b shows the frequency profile of the acquired signal, where it is possible to see a high predominant peak at 1000 Hz, as expected.

The maximum frequency that can be acquired using this technique and correctly rebuilt is limited by the Nyquist theorem, which stresses that, in theory, a signal can be rebuilt if it is sampled with a frequency that is at least twice as higher as the signal's frequency. Thus, in order to be capable to acquired and rebuilt signals of 20 kHz, for instance, the phase-OTDR pulse frequency must be at least 40 kHz. However, there is a trade-off between the maximum frequency that can be measured and the maximum distance achieved by the system: the highest the frequency to be measured, the highest the required pulse frequency and, thus, the shorter the maximum fiber length that can be probed.

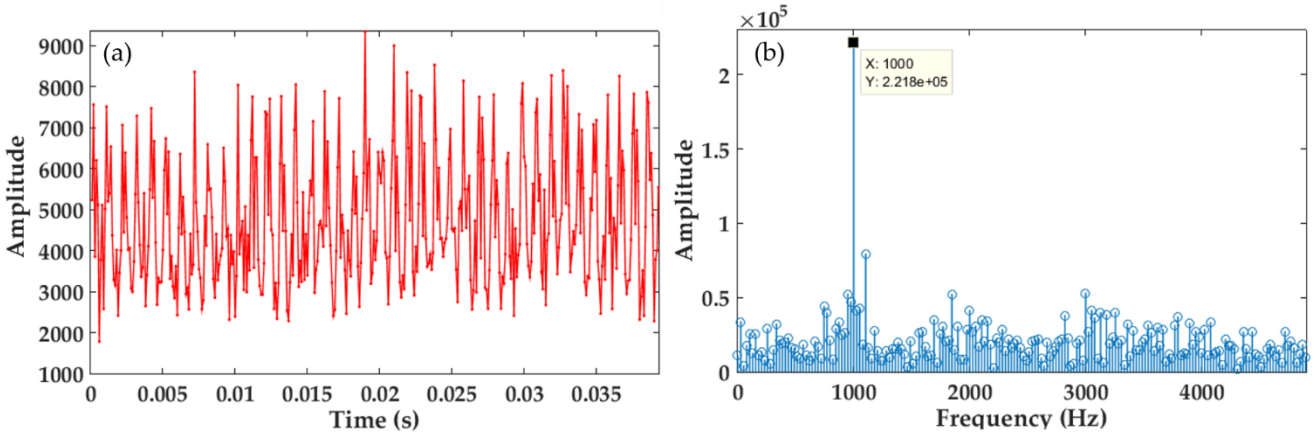

Figure 2.10. a) Time domain waveform of the 1000 Hz vibration signal measured with the phase-OTDR technique; b) Frequency profile of this acquired signal.

Table I summarizes the parameters involved in the project of a phase-OTDR system.

Table I. Parameters of a phase-OTDR system.

Parameter	Observations
Optical pulse frequency	Limits the maximum vibration frequency that can be detected, as previously stressed in the Nyquist theorem.
Optical pulse width	Defines the spatial resolution of the phase-OTDR system. The shorter the pulse the higher the spatial resolution.
Optical pulse period	Limits the maximum length of the optical fiber sensor. The longer the period the longer the fiber that can be evaluated through the phase-OTDR system.
Photodetector bandwidth	Limits the width of the probing optical pulse. The wider the bandwidth the shorter the probing pulse.
Laser linewidth	Defines the coherence of the probing optical pulse. The narrower the laser linewidth, the higher the coherence length and thus the phase-OTDR probing pulse width can be longer as well.

This section presented the main concepts about the operating principle of the phase-OTDR technique. From the parameters provided in this section, it is visible that this method is flexible and adaptable regarding spatial resolution, distance reach and maximum frequency that can be measured. All these parameters can be changed by varying the system probe pulse width and its frequency, i. e. no hardware

modifications are required. Thus, the phase-OTDR technique flexibility allows it to be employed for several different applications, from environments when high spatial resolution and short range are required, e. g. aircraft structural health monitoring, to situations where long range and short spatial resolution are demanded, for instance, long perimeters surveillance. Also, this method can be used as a distributed microphone as well, since it has enough bandwidth to listen to sound from different sections of the fiber.

The applications mentioned were explored in this thesis and the obtained results will be show and discussed in further chapters. The next section presents a literature review of the phase-OTDR method, its applications and how the technique evolved along the decades, since its first demonstration in the 90's until the most recent publications.

2.3.3. LITERATURE REVIEW OF THE PHASE-OTDR METHOD

In 1984, years before the phase-OTDR technique was proposed and demonstrated, the fading phenomenon was already observed and explained in OTDR methods that employ coherent detection [23]. In these situations, the use of a narrow linewidth laser was necessary, which caused the undesirable jagged appearance in the OTDR curve that could be removed by averaging many independent traces.

Later in the 90's, as previously mentioned, the phase-OTDR method was proposed, first in a patent [22] and then in a paper [24], using the fading phenomenon as a tool to detect local disturbances in an optical fiber, a feature not achieved by a common OTDR. The employed setup was simple, basically a normal OTDR with a long coherence length light source, and the obtained results were still course: qualitative detection and location of intrusion in a 9 km length optical fiber with 400 m of spatial resolution.

After the first publication, several proposals were presented in order to improve and sophisticated this distributed acoustic sensor system. In 2005, a phase-OTDR based DAS for intrusion detection was demonstrated [27]. In this work, a fiber laser

with very narrow linewidth (~3 kHz) was built in the laboratory. The setup was tested both in laboratory and on field, by burying a 44 m section of 14 km of optical fiber at 20 cm depth. Intrusions caused by an 80 kg person stepping in the ground above the cable were detected within 2 km of spatial resolution. It was concluded that this technique could represent a low-cost perimeter security for nuclear power plants, electrical power distribution centers, storage facilities, military bases, national borders, among others.

Later in 2007, the same authors published a field test [28] with the same developed system in desert terrain, where 19 km of optical fiber were monitored in real time by detecting intruders on foot and on vehicles traveling down a road near the cable line. It was observed a sensitivity change by the factor of 4 between different sections of the fiber under test, which was credited to the differences in the cable installation: burial depth, tension or tautness of the cable.

Also in 2007, a brief publication [29] showed that the digital signal processing (DSP) of the detected phase-OTDR traces can be used to identify specific signature characteristics for different types of intruders. Thus, this publication suggested a joint work between this optical sensor method and computational pattern identification techniques, an approach that would be largely employed in the next decades.

In 2008, a distributed intrusion sensor based on the combination of the phase-OTDR and the pOTDR techniques was demonstrated. In this proposal, both methods shared the same optical device and were used together to enhance the veracity of the intrusion detection. Also, the wavelet transform method [30] and the peak-enhancing signal processing technique to improve the system performance, testifying once again the flexibility of the phase-OTDR method to be integrated to DSP approaches.

Ran et al [31] presented in 2009 a scheme to provide security service in passive optical access networks (PON) using a phase-OTDR system. The method was employed to detect intrusion close to the optical network cables and the system was integrated to the PON itself. The only requirement was to choose a wavelength for the phase-OTDR pulse that is sufficiently far from the upstream and downstream traffic

wavelengths. Intrusions along 15 km of optical fiber network were successfully located with 100 m of spatial resolution. This work proved that this distributed sensing technique can be also useful when applied to solve peripheric issues in telecommunications systems.

In 2010, a novel DAS scheme based on coherent detection of phase-OTDR was demonstrated [26], employing also two DSP techniques called moving averaging and moving differential to the acquired traces. In this work, pencil break measurements were used to emulate the acoustic emission of cracks in concrete or steel bridges for early crack identification, thus a useful tool for SHM. The best spatial resolution achieved is 5 m. The use of heterpodyne detection improved the SNR of the detected vibration when compared to direct detection, thus increasing the sensor sensitivity, while the DSP methods reduced the noise power and increased the frequency response range of the sensor. So far, the phase-OTDR was used only to detect intrusions, without exploiting the frequency information of the disturbance. Thus, this work innovates by showing frequency measurements of up to 1000 Hz and also by employing coherent detection in a phase-OTDR system for the first time.

Another coherent detection based DAS was proposed in 2011 [32]. In this work, it was possible to recover the phase of the disturbing signal by using heterodyne detection. The paper also stresses that, when using this type of detection, the phase noise of the laser source becomes an overwhelming noise factor to the measured phase as the fiber length increases. In order to reduce the influence of this noise, the coherent performance of the laser must be enhanced. The authors did so by developing an ultra-low frequency noise narrow linewidth laser source. Also, it is stated that both the interference within pulse duration and the polarization state rotation lead to fading in the beat signal, causing a low SNR where the phase could be hardly demodulated. In order to overcome this issue, the phase modulated paired pulse technique was employed in this work. By injecting paired pulses in the fiber, the detected beat signal is the result of the combination of the two pulses and the local oscillator. For single pulse injection, signal fading is inevitable because the inner-pulse interference result

is random, while for paired pulse case, the fading problem could be overcome by transforming the random inner pulse interference to controllable pulse-pulse interference.

In 2012, Z. Qin et al achieved a 20 cm spatial resolution in a phase-OTDR system [33]. The authors also employed coherent detection and a DSP method, the continuous wavelet transform, to process the DAS signal, where they could evaluate the evolution of the vibration frequency value along time at a specific point in the optical fiber. This technique was capable to provide simultaneously the frequency and time information of the vibration event. Also, a novel DSP method called global wavelet power spectrum was used to find the location of the disturbance. These tools are proven to be useful to evaluate vibration events in SHM applications, e. g. for damage detection in civil or mechanical structures, through the analysis of its frequency profile evolution.

Another approach that explored the use of DSP methods in phase-OTDR systems for disturbance detection was reported in 2013 [34]. In this reference, the SNR and spatial resolution of the sensor is enhanced by employing the Sobel filtering technique and the two-dimensional edge detection method. As result, when the pulse width was 50 ns, 3 m spatial resolution and 8.4 dB SNR was achieved, testifying the approach capability to enhance de performance of phase-OTDR based sensors.

Also in 2013, H. Martins et al [35] presented a direct detection phase-OTDR scheme to measured ultrasonic vibrations. The main novelty of the system is the use of a semiconductor optical amplifier (SOA) to modulate the probing optical pulse. This feature allows to achieve high extinction rate (ER) between pump pulses, decreasing the setup intra-band coherent noise. This paper also presents the concept of visibility in the phase-OTDR traces, which is defined as the ratio between the subtraction of the minimum trace value from the maximum and the addition of both. The highest the visibility of the trace, the better the vibration measurement quality and its reliability. For the first time, vibrations up to 39.5 kHz were measured with the phase-OTDR method in a range that could achieve 1.25 km of distance.

In the same year, T. Zhu et al proposed for the first time a DAS that merged a phase-OTDR setup and a Mach-Zehnder interferometer [36]. Vibration measurement with high-frequency response and high spatial resolution was demonstrated, where modulated pulses were proposed to be used as sensing source. Frequency response and location information were obtained by Mach-Zehnder interferometer and phase-OTDR technology, respectively. In order to simulate high-frequency vibration of crack of cable and civil structure, experiments on detection of piezoelectric transducer and pencil-break were carried out. Spatial resolution of 5 m and the maximum frequency response of ~3 MHz were achieved in 1064 m fiber link when the narrow pulse width is 50 ns. So far, this was the highest frequency capable to be measured by a phase-OTDR based sensor.

A work published in 2014 [37] investigated the influences of the laser source in phase-OTDR distributed intrusion sensors. A numerical simulation was performed to illustrate the relationships between trace-to-trace fluctuations and frequency drift rate as well as pulse width, and fluctuations ratio coefficient (FRC) was proposed to evaluate the level of trace-to-trace fluctuations. The simulation results show that the FRC grows with increasing frequency drift rate and pulse width, reaches, and maintains the peak value when the frequency drift rate and/or the pulse width are high enough. Furthermore, experiments were implemented using a phase-OTDR prototype with a low frequency drift laser (<5 MHz⁄min), of which the high frequency drift rate is simulated by frequency sweeping. The good agreement of experimental with simulated results in the region of high frequency drift rate validates the theoretical analysis, and the huge differences between them in the region of low frequency drift rate indicate the place of laser frequency drift among system noises. The conclusion is useful for choosing laser sources and improving the performance of phase-OTDR.

Still in 2014, an extension of the sensing range of the phase-OTDR technique to up to 100 km was experimentally demonstrated by employing counter pumping fiber Brillouin amplification (FBA) [38]. Also, the effect of pump frequency variation was studied, and the system shows reasonable robustness. It should be noted that further

extension of the sensing range can be envisioned by combining counter pumping Brillouin amplification with co-pumping Raman amplification (the first-order or higher-order Raman amplification). In summary, this work shows great potential for FBA to be adopted in many other distributed fiber-optic sensing systems.

Another type of amplification, Raman amplification, was also used in 2014 for increasing the range of a phase-OTDR based DAS to 125 km, the highest achieved so far [39]. In this study, the authors presented an experimental and theoretical description of the use of first-order Raman amplification to improve the performance of a phase-OTDR when used for vibration measurements. The evolution of the φOTDR signal along the fiber is shown to have a good agreement with the theoretical model for different Raman pump powers. The Raman amplification combined with the noise reduction provided by using balanced detection, an SOA and an optical switch allows to greatly increase the SNR and sensing range of the phase-OTDR. The sensor was able to detect vibrations of up to 250/300 Hz in a distance of 125/110 km with a resolution of 10 m and no post-processing. This sensor could be used in the monitoring of intrusions in large structures such as national borders or pipelines, thus being useful for both SHM and surveillance applications. However, use of bi-directional Raman pumping is a clear drawback in this setup, as access to both fiber ends is required.

This distance record was overcome also in 2014 by Peng et al [40], that presented an ultra-long phase-OTDR capable to achieve high-sensitivity intrusion detection over 131.5km fiber with high spatial resolution of 8m, which is the longest phase-OTDR reported to date, to the best of our knowledge. It is found that the combination of distributed Raman amplification with heterodyne detection can extend the sensing distance and enhances the sensitivity substantially, leading to the realization of ultra-long phase-OTDR with high sensitivity and spatial resolution. Furthermore, the feasibility of applying such an ultra-long phase-OTDR to pipeline security monitoring is demonstrated and the features of intrusion signal can be extracted with improved SNR by using the wavelet detrending/denoising method proposed.

In another reported work [41], the phase-OTDR method was also merged to a Michelson interferometer for acoustic measurement. Phase, amplitude, frequency response and location information could be directly obtained at the same time by using the passive 3×3 coupler demodulation. Experiments on detection of two piezoelectric transducers within 200 m detection fibers were carried out. The result shows that the system could well describe each piezoelectric transducer with different intensity, respectively. The system offered a versatile new tool for acoustic sensing and imaging, such as through the formation of a massive acoustic camera/telescope. This proposed technology can be used for surface, seabed and downhole measurements, being useful for both SHM and surveillance applications.

In 2015, a technique to separate and determine the disturbing signals in phase-OTDR was proposed [42]. It is known that a phase-OTDR system is easy to be interfered by ambient noises, and the nonlinear coherent addition of different interferences always makes it difficult to detect real human intrusions and causes high nuisance alarm rates (NARs) in practical applications. In this paper, a temporal signal separation and determination method is proposed to improve its detection performance in noisy environments. Unlike the conventional analysis of transverse spatial signals, the time-evolving sensing signal of phase-OTDR system was at first obtained for each spatial point by accumulating the changing OTDR traces at different moments. Then, its longitudinal temporal signal was decomposed and analyzed by a multi-scale wavelet decomposition method. By selectively recombining the corresponding scale components, it could extract human intrusion signals, and separate the influences of slow change of the system and other environmental interferences. Compared with the conventional differentiation way and fast Fourier transformation denoising method, the SNRs of the detecting signals for the proposed method was raised by up to ~35 dB for the best case. Moreover, from the decomposed components, different event signals could be effectively determined by their energy distribution features, and the NAR can be controlled to be less than 2% in the test.

In the same year, a phase-OTDR system based on phase-generated carrier algorithm was demonstrated [43]. In this work, an unbalanced Michelson interferometer was introduced at the receiving end of the system. The Rayleigh backscattering light from a certain position along the sensing fiber interfered to generate interference light signal over time, whose phase carries the sensing information. Phase-generated carrier demodulation algorithm was proposed and carried out to recover the phase information. A single frequency vibration event was applied to a certain position along the sensing fiber and demodulated correctly. The noise level of the phase-OTDR system was about 3×10^{-3} rad/√Hz and a signal to noise ratio about 30.45 dB was achieved. The maximum sensing length and the spatial resolution of the phase-OTDR system was 10 km and 6 m with pulse repetition rate at 10 kHz and 6 m fiber delay in MI with interrogating pulse width of 30 ns. Thus, this work is one more successful joint application of the phase-OTDR technique with DSP methods.

Also in 2015, a distributed fiber microphone based on phase-OTDR and employing coherent detection was demonstrated [44]. The authors employed coherent detection and performed a comparison study of two different sensing topologies: the sensing fiber as a suspended loop and as a flat package, glued to a metal sheet. It was verified that the last option was the most sensitive and thus the better choice. The multiplexing capability of the microphone was proven with 1.2 km sensing range and 5 m spatial resolution. Human voice was detected and reproduced, indicating a promising solution for acoustic waves detection.

In 2016, C. Baker et al presented a novel approach for the generation of high extinction-ratio square pulses based on self-phase modulation of sinusoid modulated optical signals (SMOS) [45]. A SMOS in a nonlinear medium experiences self-phase modulation induced by the nonlinear Kerr effect leading to the generation of distinct sidebands. A small variation in the peak power of the SMOS leads to a large variation in the power of the sidebands. Impressing a square pulse on the SMOS and filtering a sideband component results in a higher extinction-ratio square pulse. The advantage

of high extinction-ratio pulses was demonstrated by a reduced background noise level in the Rayleigh backscattering traces of a phase-OTDR vibration measurement system.

In the same year, M. Zhang et al demonstrated a method to enhance the performance of DAS systems based on phase-OTDR by using a narrow linewidth light source and signal processing [46]. They employed a combination of segmented unwrapping algorithm, averaging estimation of phase difference, and infinite impulse response (IIR) filtering method. The enhancement of the signal quality was numerically demonstrated, and they also studied the influence resulted from the light source noise on the phase-OTDR performance. The result has shown that when the linewidth of light source used in the phase-OTDR system is narrower, the performance of the system is better. Such a phase-OTDR system could obtain higher quality demodulated signals when the narrower linewidth light source is chosen and the method of averaging estimation phase difference is used. Also, the averaging estimation of phase difference algorithm proved to be more efficient than the traditional method of the direct phase difference for different linewidths.

Also in 2016, a disruptive modulated-pulse based high spatial resolution distributed fiber system for multi-parameter sensing was proposed [47]. The authors demonstrated a hybrid distributed fiber sensing system which is the integration of phase-OTDR and Brillouin optical time domain reflectometry (B-OTDR). This system enabled the measurement of vibration, temperature and strain. Exploiting the fast changing property of vibration and the static property of temperature and strain, the laser pulse width and intensity were modulated and then injected into the single-mode sensing fiber proportionally, so that the three concerned parameters could be extracted simultaneously by only one photo-detector and data acquisition channel. Combining with advanced data processing methods, the modulation of laser pulse brought additional advantages because of trade and balance between the backscattering light power and nonlinear effect noise, which enhanced the signal-to-noise ratio, and enabled sub-meter level spatial resolution together with long sensing distance. The proposed method realized up to 4.8 kHz vibration sensing with 3 m spatial resolution

at 10 km standard single-mode fiber. And measurements of the distributed temperature and stress profile along the same fiber with 80 cm spatial resolution were also achieved concurrently.

Another disruptive phase-OTDR setup modification was also demonstrated in 2016 by A. Garcia-Ruiz [48]. So far, the optical pulses used in phase-OTDR were typically engineered to have a constant phase along the pulse. In this work, it was demonstrated that by acting on the phase profile of the optical pulses, it is possible to introduce important conceptual and practical changes to the traditional phase-OTDR operation, thus opening a door for new possibilities which are yet to be explored. Using a phase-OTDR with linearly chirped pulses and direct detection, the distributed measurement of temperature/strain changes from trace to trace, with 1mK/4nε resolution, was theoretically and experimentally demonstrated. The measurement resolution and sensitivity could be tuned by acting on the pulse chirp profile. The technique does not require a frequency sweep, thus greatly decreasing the measurement time and complexity of the system, while maintaining the potential for metric spatial resolutions over tens of kilometers as in conventional phase-OTDR. The technique allows for dynamic measurements at kHz rates, while maintaining reliability over several hours.

In 2017, a distributed measurement of acoustic vibration location with frequency multiplexed phase-OTDR was demonstrated [49]. So far, phase-OTDR systems couldn't measure high-frequency vibration whose cycle is shorter than the repetition time of the OTDR. That is, the maximum detectable frequency depends on fiber length. In this paper, describe a vibration sensing technique with frequency division multiplexed (FMD) phase-OTDR that detected the entire distribution of a high-frequency vibration thus allowing to locate a high-speed vibration point was presented. The method measured the position, frequency and dynamic change of a high frequency vibration whose cycle is shorter than the repetition time. Both frequency and position were visualized simultaneously for a 5-km fiber with an 80-kHz frequency response and a 20-m spatial resolution.

Also in the same year, an evolution of the chirped pulse technique was demonstrated [50]. In this improved method, the input pulses were temporally stretched by a suitable dispersive device, and the backscattered traces were re-compressed in the optical domain prior to detection. This allows to substantially increase the probe pulse energy, while avoiding nonlinear interaction within the fiber under test, resulting in an increased SNR without compromising the spatial resolution of the sensor. This configuration allows for high resolution measurements without the need for coherent detection or signal post-processing (as required for instance in OPCR). By compressing in the optical domain with a polarization-insensitive element, there is no need for phase detection (which is typically polarization dependent). Thus, this method should exhibit very low polarization dependence. The reported experiment demonstrated an SNR increase of 20 dB over the traditional phase-OTDR architecture in a system with 1.8 cm spatial resolution.

The papers briefly reviewed in this section show the growth of the phase-OTDR method along the years, highlighting the main achievements and enhancements, Figure 2.11 summarizes the publications in a timeline. It was proven how flexible and adaptive this method can be, since it is possible to integrate it with other distributed sensing technologies, such as pOTDR and B-OTDR, and also apply DSP methods to improve its performance. It was demonstrated that this method can cover a large area of applications, from SHM, surveillance and also as a distributed microphone, which can be useful for the other two. The last reports also show the capability of the method to be used for quantitative measurements of dynamic strain, not anymore limited by only frequency measurements, while keeping direct detection. Thus, this review indicates that this method can be seen as a key solution for distributed sensing technologies.

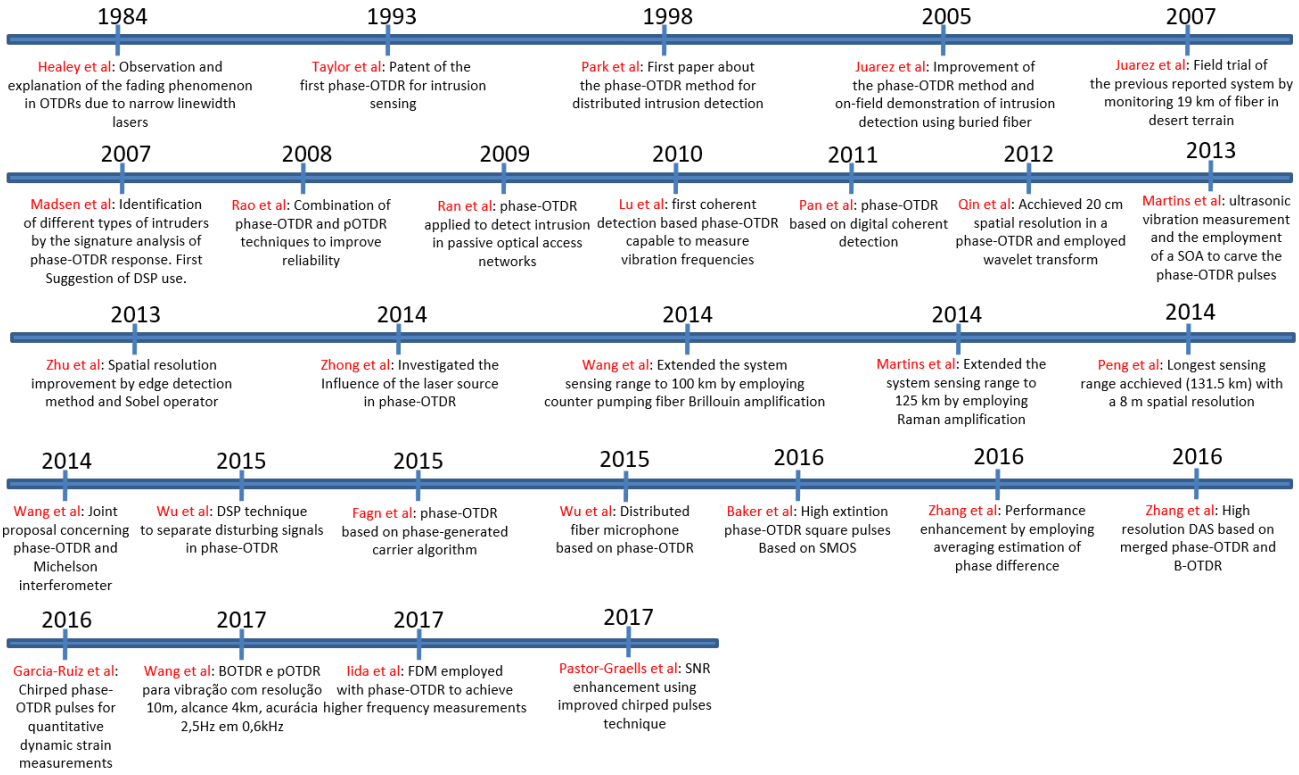

Figure 2.11. Timeline summarizing the main literature publications regarding the phase-OTDR evolution over time.

2.4. CHAPTER CONCLUSION

This chapter provided an overview about scattering phenomenon in optical fibers for distributed sensing, presenting the main theoretical fundaments behind the scattering types: Raman, Rayleigh and Brillouin. The Rayleigh scattering, the phenomenon explored in this thesis, was emphasized and explained through mathematical and physical models. After, the operating principle of the phase-OTDR technique was stressed and a model was also provided for better understand. Lastly, a literature review was presented, showing the evolution of this Rayleigh scattering based DAS along the years, in order to stress its multiple capabilities of integration with other technologies and several applications possibilities in SHM and surveillance.

CHAPTER 3

3. MULTIPOINT SIMULTANEOUS INTRUSION DETECTION FOR SURVEILLANCE SYSTEMS BASED ON PHASE-OTDR

In this chapter, the phase-OTDR method for intrusion detection is explored, both in its most basic setup and in an original contribution where it is merged with Field Programmable Gate Array (FPGA) architectures. The original results obtained in this chapter of the thesis were presented and published at the Proceedings of the 14th IEEE International Conference on Networking, Sensing and Control 2017, Calabria (Italy).

3.1. BACKGROUND ON SURVEILLANCE APPLICATIONS BASED ON PHASE-OTDR

Perimeter security is an issue of major concern in environments such as: military facilities, electrical plants, oil pipelines, dams, private properties and others. In these places, it is necessary a real-time monitoring system to detect invasions in real time, capable to cover the whole perimeter and to feature spatial resolution that allows distinguishing between multiple simultaneous intrusion events [51].

Traditional security systems, including seismic sensors, cameras, motion detectors, and fences, have limited range and several drawbacks. They are deployed above ground, allowing for them to be seen and giving the intruder a chance of dodging detection. Power support is also required, which could be challenging in

remote locations. Long perimeters increase the number of components necessary, adding to the overall complexity of the system [52].

In this scenarium, distributed optical fiber sensor solutions suit the above requirements, since they can cover perimeters of hundreds of kilometers and operate in hazardous environments such electrical plants. Also, these sensors can be buried a few feet under the ground and be almost undetectable, unlike the common above ground solutions [53]. The phase-OTDR method features hundreds of kilometers of reach, dynamic response to intrusions and the capability to be merged with DSP techniques in order to improve performance [42]. As shown in Chapter 2, this method has been widely explored through the decades for surveillance applications.
Figure 3.1 [27] illustrates the concept of the phase-OTDR method applied to intrusion detection.

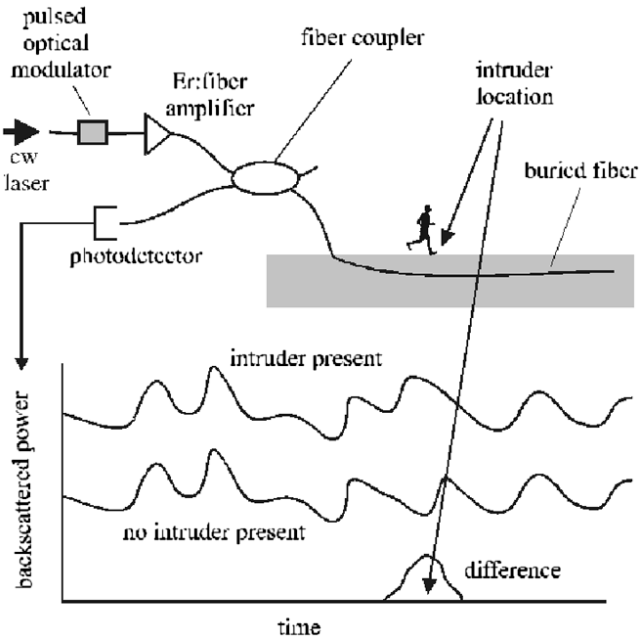

Figure 3.1. Depiction of a phase-OTDR technique used for intrusion detecion in surveillance applications [27].

In this concept, the optical fiber is buried underneath the perimeter to be monitored, providing remote sensing since the active optoelectronic part of the setup, i.e. the transmitter and the receiver side, is away from the sensing element itself, e.g. the fiber optics. As shown in the picture, when an intrusion occurs, the sensor response

will provide the location of this event along the fiber lenght. The reported depth of the buried fiber is so far round 30 ~45 cm [27].

This topology was already tested on field, where 8.5 km of SSMF was buried 30 cm deep into the ground [28]. In this configuration, the phase-OTDR traces were acquired and processed in real time. High sensitivity and consistent detection of intruders on foot and of vehicles traveling down a road near the cable line was achieved.

Also, another reported contribution to this area was the use of digital signal processing of the phase-OTDR curves to identify specific signature characteristics of diferente intruders [29]. In this reference, data was taken with an 80 kg intruder walking towards the buried fiber section, and also the signature of a car traveling at 10-20 mph along a nearby road was recorded, both results shown in Figure 3.2. The footsteps of the intruder are clearly revealed in the extracted signature, and a vehicle can easily be differentiated from a walker based on the difference in signatures. Thus, this approached allowed surveillance based on phase-OTDR to reach another level of integration with DSP techniques and intruder pattern identification.

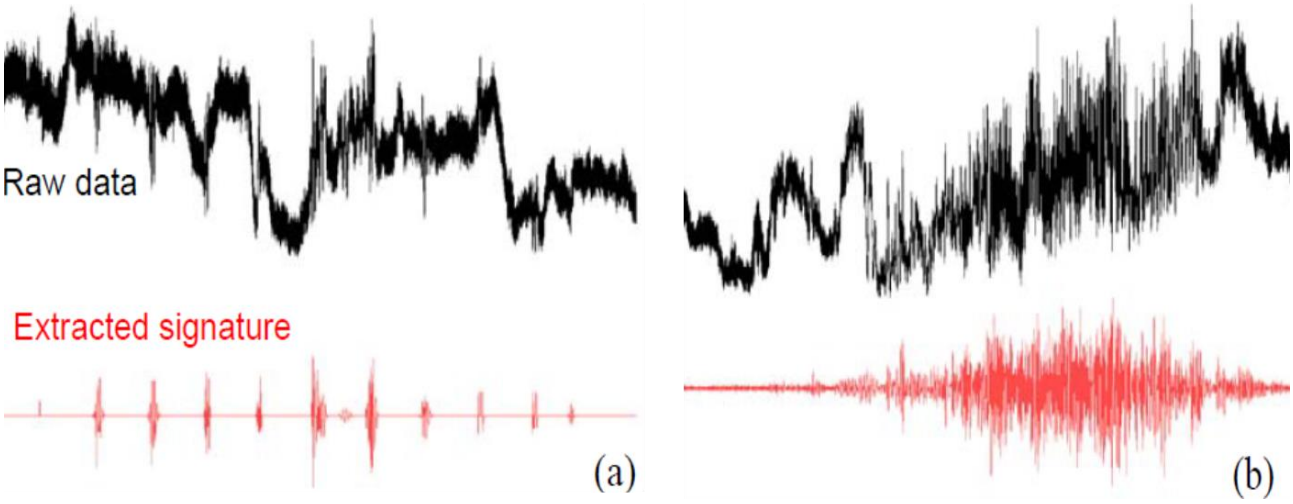

Figure 3.2. Data signature of (a) intruder on foot and (b) car traveling down a nearby road [29].

A recent and relevant contribution was addressed to extract human intrusion events from noisy background in phase-OTDR traces [42]. Instead of using the conventional differential OTDR curve, time-evolving signals for each spatial point are accumulated and analyzed; multi-scale wavelet decomposition and reconstruction

was employed to separate real intrusions from the nonlinearly mixed signals. Different types of signals can be exposed with different distribution features along with the decomposed scales and thus they can be further determined. In this paper, by physically separating real intrusions and other systematic and environmental influences by thewavelet tool, the authors also constructed a 3-layer back propagation (BP) artificial neural network (ANN) network to identify the different distributions of three typical events, no intrusion, human intrusion, and hand clapping for simulating the ambient time-varying sounds and air movements in the environments. Thus, this is one more example of a succesful combination between DSP methods and the phase-OTDR technique.

After stressing in this section the feasibility to use phase-OTDR methods for surveillance applications and its advantages, as well as the performance improvement that can be obtained by merging it with DSP techniques, experiments were performed and an original contribution was achieved.

3.2. EXPERIMENTAL SETUP

In order to perform intrusion experiments for surveillance proposals, a phase-OTDR system was built in the Acreo AB laboratory, in Kista, Stockholm, Sweden. The experimental setup scheme is shown in Figure 3.3.

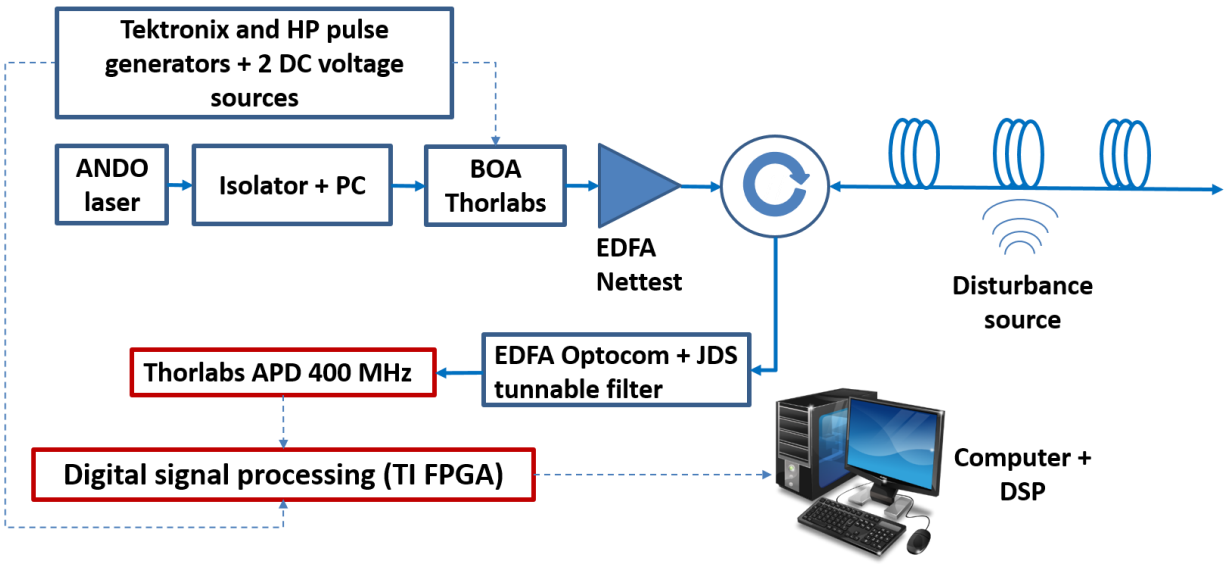

Figure 3.3. Experimental setup of a phase-OTDR for intrusion detection.

The experimental setup comprises an ANDO AQ4321A narrow linewidth laser (NLL) with bandwidth ~200 kHz, a Thorlabs BOA1004PXS gated semiconductor optical amplifier (SOA) to both amplify and trigger the laser light into optical pulses, a GNNettest BT-17 erbium-doped fiber amplifier (EDFA), an optical circulator and optical spools of 0.24 NA single mode optical fiber. The duration of the optical probing pulses is a ~8 ns, thus limiting the spatial resolution to ~80 cm. One or more sections of the fiber spools are disturbed in order to test the intrusion detection capability of the sensor. The circulator directs the Rayleigh backscattered signal into the receiver-side of the setup, which incorporates a second EDFA, a 1-nm wide optical bandpass filter (BPF) tuned to the wavelength of the laser, a 400 MHz avalanche photodetector (APD) and a TSW14J56 analog-to-digital converter (ADC) to acquired and store the phase-OTDR traces. The ADC trigger is locked with the BOA control pulses, thus synchronizing the data capture every phase-OTDR pulse is launched in the fiber.

Although the setup also works with standard telecommunications fiber, the motivation for using high NA fiber is the increase in Rayleigh scattering collection with increased numerical aperture, as previously stressed. This is confirmed with the study of four fibers with different NA values, measuring the average amplitude of the Rayleigh scattering signal detected in each case. An increasing linear relation is found,

as shown in Figure 3.4. Consequently, the use of a high NA fiber is advantageous for measurements with higher amplitude than with a lower NA.

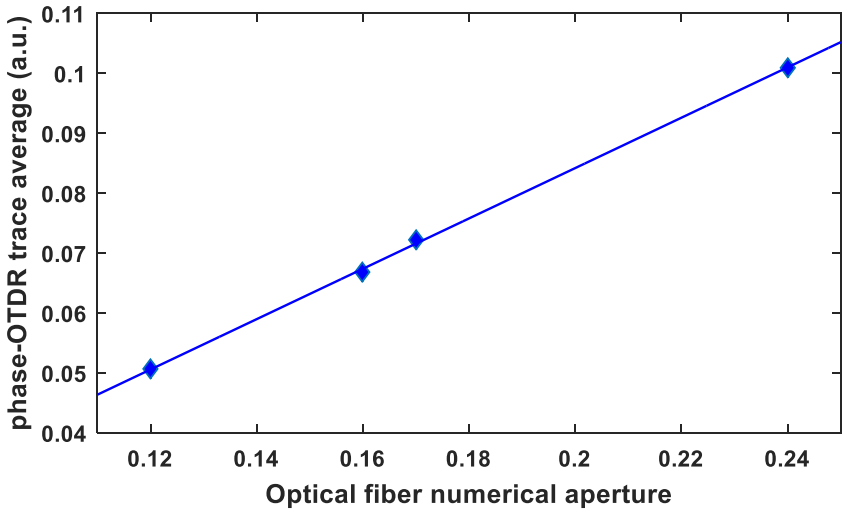

Figure 3.4. Relationship between the optical fiber numerical aperture and the phase-OTDR average amplitude.

After building the setup, experiments were performed regarding single and multipoint detection, 2D surface mapping and a novel proposal merging phase-OTDR and FPGA architectures, as will be shown in the follwing subsections.

3.3. SINGLE AND MULTIPOINT INTRUSION DETECTION

In order to evaluate the system capability to detect intrusion, a single point detection was performed first. The experiment consisted of disturbing a fiber section of a 1 km length optical fiber. The disturbed section was from 360 m to 380 m, as shown in the acquired phase-OTDR traces exhibited in Figure 3.5a. Figure 3.5b shows the differential resultant trace obtained from the phase-OTDR traces, which indicates the disturbed section location. This differential signal is calculated by simple subtracting two consecutive phase-OTDR traces.

The disturbance locations are detected by locating the highest peaks in the differential traces when compared to the noise floor. The value of the noise floor can vary according to the application. It is worth mentioning that this measurement is only qualitative and relative, thus this method is uncappable to measure absolute amplitude values of the disturbances.

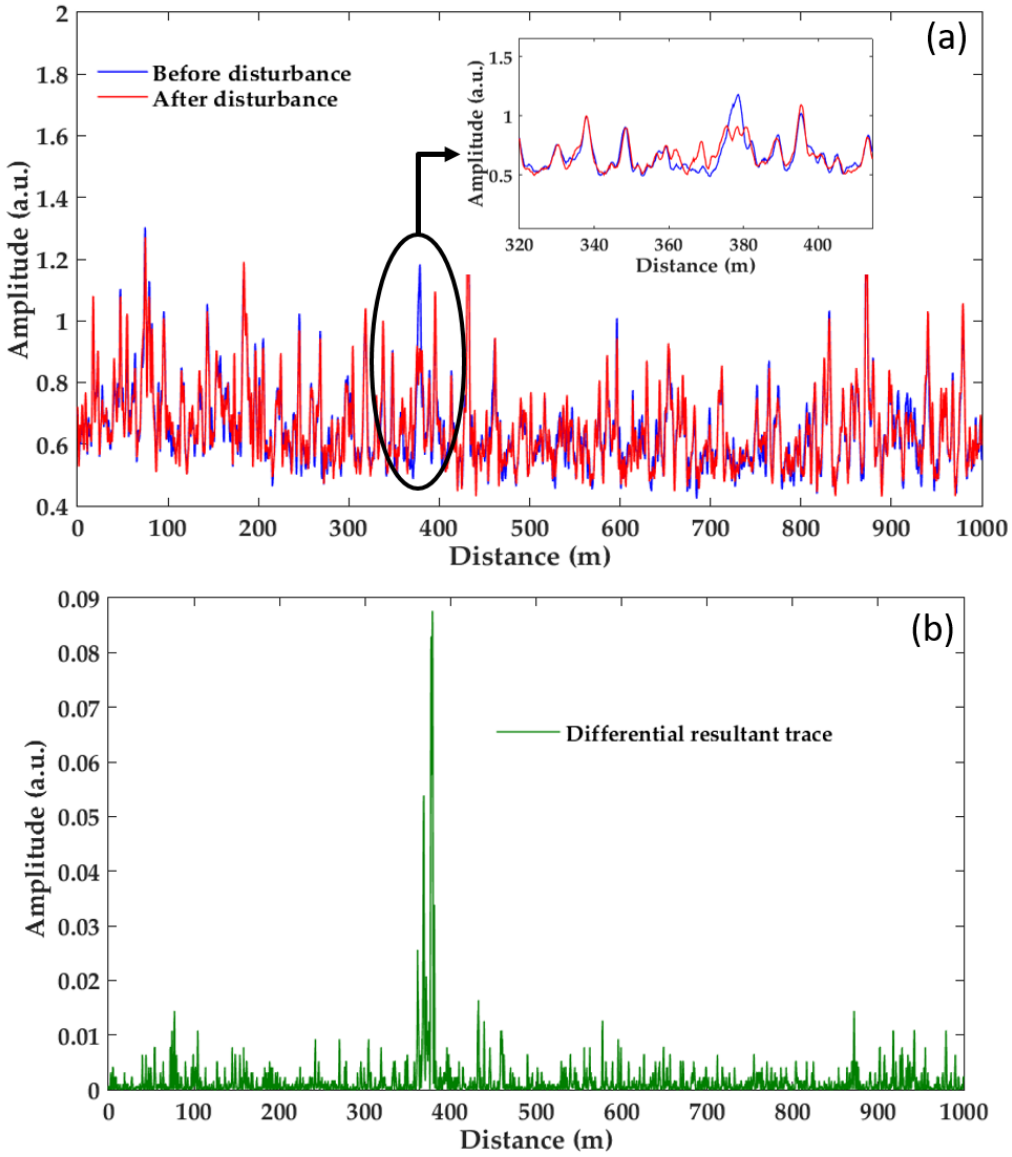

Figure 3.5. Experimental results of a single point intrusion detection: a) Two consecutive phase-OTDR traces: before (blue) and after (red) the disturbance in ~20 m section (inset) of optical fiber; b) Differential resultant trace indicating the location of the disturbed section.

The optical fiber track was glued to an aluminum plate of 40 cm x 40 cm and disturbed by vibrations generated by an electrically controlled shaker placed beneath the plate, as shown in Figure 3.6.

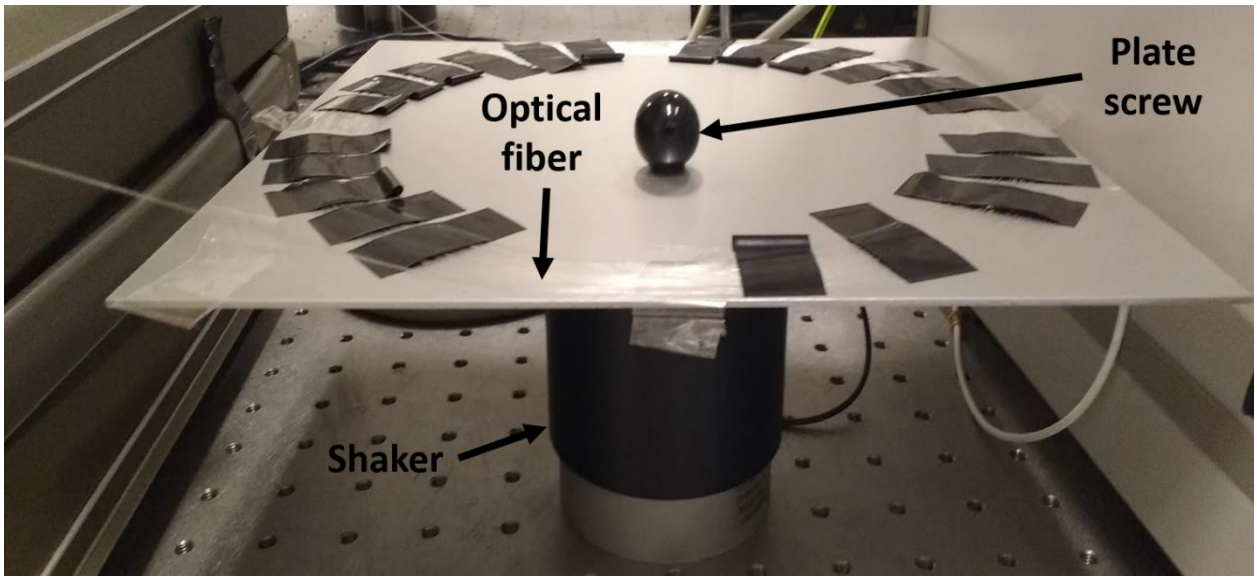

Figure 3.6. Disturbed optical fiber track configuration.

Later, a multiple simultaneous intrusion detection test was performed by pressing two other fiber sections while the shaker was actuating on the one showed in the last experiment. Figure 3.7 shows the experimental result after acquiring and processing data.

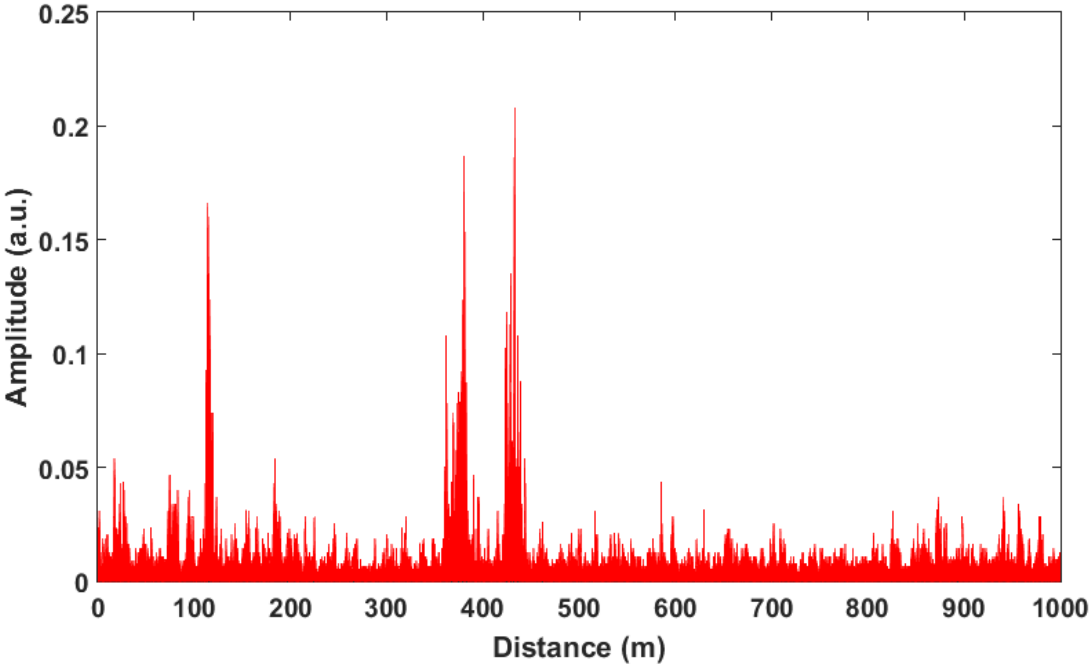

Figure 3.7. Experimental result of three simultaneous disturbance points.

In this approach, the amplitude of the disturbances is not relevant, only their locations are important.

3.4. OPTICAL COILS MESH FOR 2D SURFACE MAPPING

The method uses the basic well known phase-OTDR technique at both transmitter and receiver side. The difference relies on how the sensing fiber is disposed on the monitored surface. Instead of a straight line, the optical fiber is coiled in circles, disposed like a carpet, as shown in Figure 3.8. The technique employs only one fiber. The length of fiber in each coil is longer than the probing pulse length, but now it is the diameter of the coil that limits the spatial resolution of the sensor.

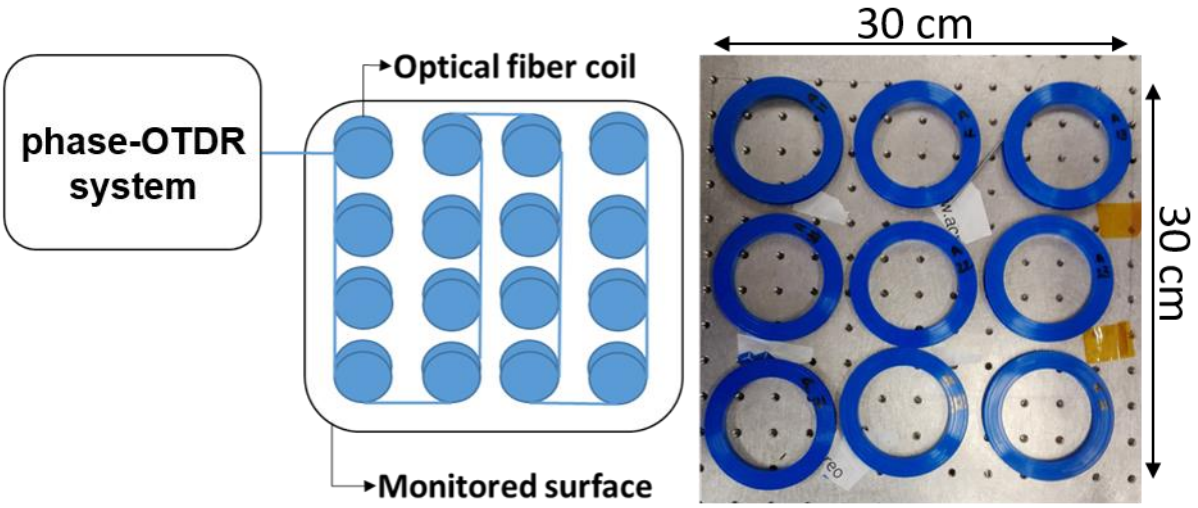

Figure 3.8. phase-OTDR based optical fiber coil mesh concept (left figure) and laboratory implementation example (right figure).

According to Figure 3.8, each coil represents the element of a matrix and can be used to evaluate each part of the surface area. In the experiment, a 30 cm x 30 cm surface was monitored using a fiber coiled in 9 coils of 10 cm diameter each. In order to be capable to resolve all coils, the length of the coiled fiber in every coil must be at least longer than the spatial width of the optical pulse. Thus, 3 m of fiber was wrapped around each one. Every coil represents a region in the phase-OTDR trace that can be mapped to a 2D representation of the monitored surface without employing specialty fibers. This technique can also monitor all the coils at the same time, detecting simultaneous events and providing a complete analysis of the monitored surface.

In order to proof the method concept, each coil was disturbed separately and the average change in amplitude due to the disturbance was mapped into a 2D representation of the analyzed surface, as shown in Figure 3.9. From these graphs, it was able to distinguish each disturbed section of the surface with a 10 cm spatial resolution, which is the diameter of each optical fiber coil. The pulse width used for probing was 8 ns, which in a conventional phase-OTDR would result in an 80 cm spatial resolution. If a higher resolution is required, then smaller coils should be made, respecting the requirement that the fiber length coiled in each coil should be at least

twice the spatial width of the optical pulse launched. Also, the fiber was coiled around rubber disks for simplicity, but for real implementation the coils could be just glued together. The type of glue to be used can be subject of further investigation.

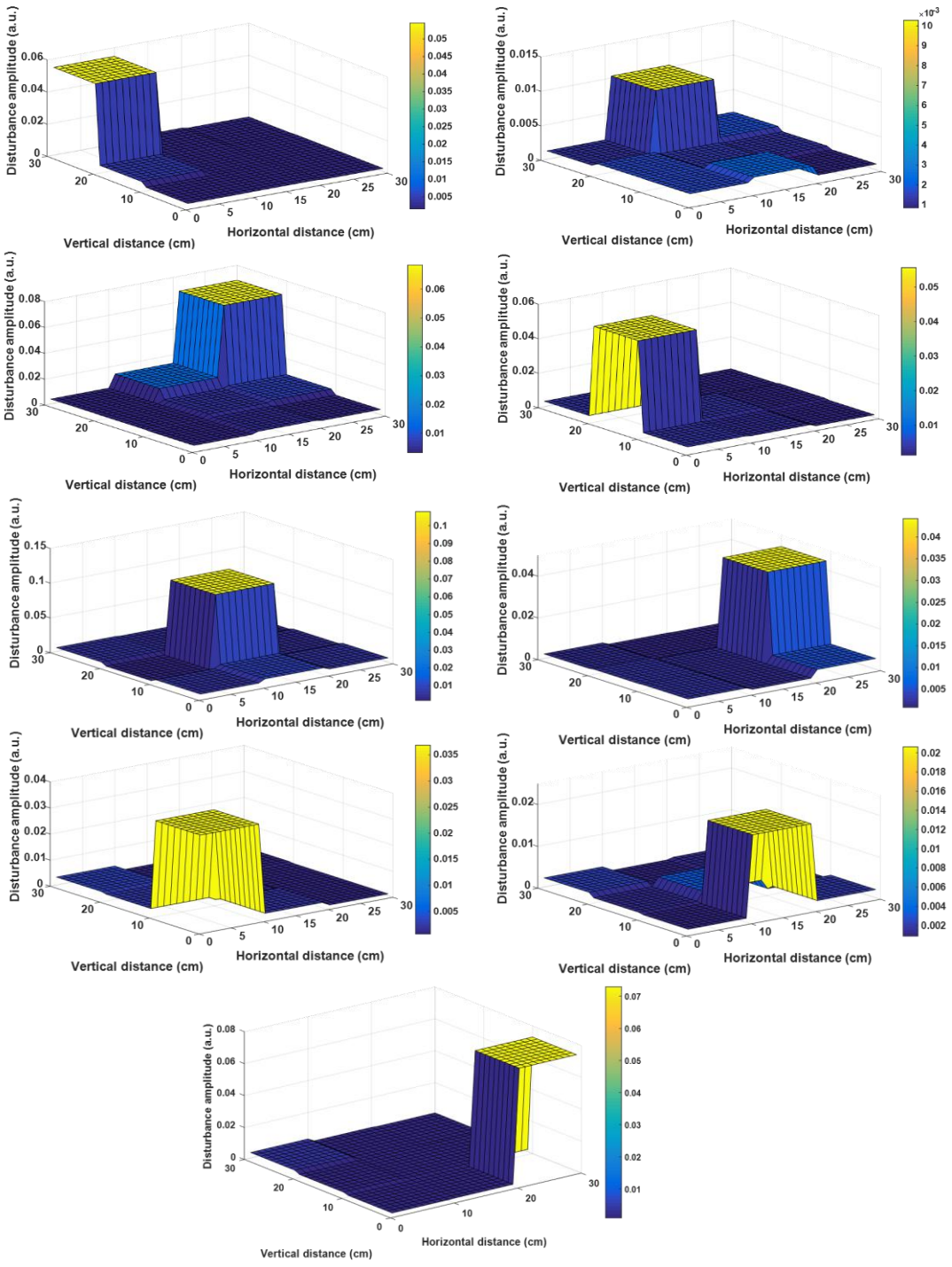

Figure 3.9. Disturbance sensing along the 30 cm x 30 cm surface using the phase-OTDR based optical fiber coil mesh method.

The color map represents the relative amplitude of the disturbance. Also, three coils were disturbed at the same time, in order to prove the simultaneous disturbance detection capability of the method. The result is shown in Figure 3.10, where the three disturbed coils can be distinguished: green, yellow and ochre.

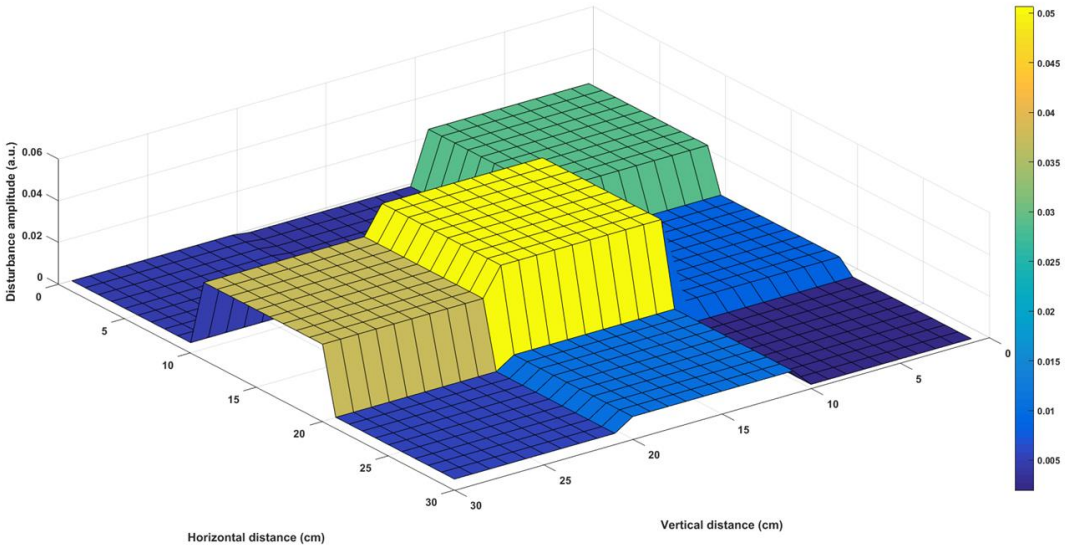

Figure 3.10. Simultaneous disturbance of three coils in the optical fiber coil mesh.

This solution can be useful for mapping disturbances on surfaces of different sizes and shapes.

3.5. INTRUSION DETECTION BASED ON PHASE-OTDR AND FPGA ARCHITECTURES

When it comes to fast location of potential intrusions along oil pipelines, dams, high-voltage cables or military facilities, the capability to deal with real-time multi-zone disturbance signal processing is a key feature. In this scenario, it is important to have: (i) a high performance and reliable computational approach that receives and filters the data at the sampling frequency allowing multiple disturbances to be detected and located; (ii) a scalable and easy configurable processing solution that can be adapted

to different scenarios and follows the optical distributed sensors along incremental perimeters and structures.

In this section, it is shown a joint work that proposed and demonstrated the use of of parallel hardware architectures to implement digital filters for detecting and locating perturbations in a phase-OTDR distributed optical fiber intrusion sensor. It addresses the above described requirements by implementing hardware architectures of the moving average and Sobel filters, exploring their intrinsic parallelism to achieve low latency solutions and to detect and locate multi-zone disturbances along the optical fiber.

This work proposal is focused on these three main contributions: (i) the development of hardware pipelined architectures for real-time processing of --OTDR signals. The architectures were designed to facilitate the adaptability to different optical fiber lengths and resolutions of the analog-to-digital converter (ADC); (ii) the analysis of numerical simulations using experimental data in order to validate the capabilities of the system to detect multiple disturbances; (iii) a scalability analysis of the proposed hardware architectures.

Two different scenarios were tested: one single disturbance and two simultaneous disturbances in the fiber under test. For the single disturbance scenario, we used 57 m length optical fiber and a coiled section of ~3 m upon a plate was disturbed with the shaker. In the two simultaneous disturbances scenario we employed 295 m of optical fiber and disturbed two fiber sections of ~5 m each, 90 m of fiber away from each other. Commonly, the --OTDR signals are acquired, stored in a memory and then digitally processed offline. In general, the digital processing is divided in four main task: filtering, detection, localization and information extraction. This experiments evaluate the real-time processing capabilities of this phase–OTDR setup for the filtering and detection tasks, mapping in hardware the recursive moving average filter and the Sobel filter in order to achieve a low latency solution.

3.5.1. MOVING AVERAGE FILTER

The moving average is a linear filter used for reducing random noise of a signal. It operates by averaging N points of the input signal to create a point of the output signal. Here N represents the window size. The main advantages of the moving average filter are the simplicity and easy implementation capabilities, being optimal for time domain processing, but not suitable for frequency domain signal processing [53]. The main

Algorithm 1 Pseudocode for the recursive moving average filter. The input is the current sample I and the output is the averaged value I_{avg}.

```
Set window size N
Set buffer of N + 1 samples to zero: I_buf[1 : N + 1] = 0
Set prevAvg = I
loop
    for i = 1 to N do
        I_buf[i] = I_buf[i + 1]
    end for
    I_buf[N + 1] = I
    Iavg = prevAvg + (I − I_buf[1])/N
    prevAvg = Iavg
end loop
```

Figure 3.11. Recursive version of the moving average filter.

drawback of the filter is that large window affects the execution time. Thus, for real-time requirements a recursive version of the moving average filter is used, as shown in Figure 3.11.

3.5.2. SOBEL FILTER

There are two main categories for processing and filtering images: frequency domain and space domain processing. The former involves operations over the image frequencies, generally, using the Fourier Transform. The latter consist on the direct manipulation of the image pixels [53]. Most of the space domain filters are based on windowing operations in which a window or a set of input pixels are processed in order to produce one output pixel. These windowing operations are similar to the bi-

dimensional discrete convolution operation in signal processing, as shown in Equation 3.1.

$$K(x,y) \otimes I(x,y) = \sum_{i=-m/2}^{m/2} \sum_{j=-n/2}^{n/2} K(i,j) I(x-i, y-j) \qquad (3.1)$$

where *I* is the input signal and the masks or kernels, *K(x,y)*, assume different sizes and arbitrary values depending on the function to be performed.

In image processing different kernels can be used in order to extract several characteristics. The Sobel filter is an edge detection method based on the assumption that the edge occurs where there is a discontinuity in the intensity of the image. Thus, edges can be detected by applying the gradient across the image, as shown in Equation 3.2, and finding the points where values are significant larger than surroundings. G_x and G_y estimate the derivate along the x and y directions as exhibited in Equation 3.3.

$$\nabla(x,y) = \left[\frac{\partial I}{\partial x} \quad \frac{\partial I}{\partial y}\right]^T = [G_x \quad G_y]^T \qquad (3.2)$$

$$G_x = \begin{bmatrix} -1 & 0 & 1 \\ -2 & 0 & 2 \\ -1 & 0 & 1 \end{bmatrix} \otimes I; \quad G_y = \begin{bmatrix} -1 & -2 & -1 \\ 0 & 0 & 0 \\ 1 & 2 & 1 \end{bmatrix} \otimes I \qquad (3.3)$$

In the context of phase-OTDR, Rayleigh backscattered traces can be treated as an image and disturbances can be located by detecting significant variations in gray level.

3.5.3. FPGA IMPLEMENTATIONS

The moving average and Sobel digital filters were implemented in VHDL hardware description language. For the sake of simplicity all the architectures are based on integer arithmetic and logic operations easily implemented on FPGAs. Since different optical fiber lengths and ADC's resolutions can be used we parametrized the architectures in order to facilitate the scalability and reconfiguration of the circuits to different experimental setups. In order to accomplish real-time requirements the

proposed circuits were developed using pipeline architectures allowing one output per clock cycle to be processed after an initial latency.

3.5.4. phase-OTDR DISTURBANCE DETECTION USING MOVING AVERAGE

Figure 3.12 shows the general architecture for peak detection of phase-OTDR samples using the moving average filter. According to Algorithm 1 a buffer for storing N input samples is required. Here, N was selected to be a power of two simplifying the division operation by a shift right logic operation. Initially the I_{adc} input signals are sequentially displaced and stored into a FIFO (First In, First Out) buffer. When this input buffer is full the oldest sample in the buffer is subtracted from the input signal and a shift right operation performs the division by N.

The result is accumulated in order to obtain the filtered value I_{avg}. Afterward, the square of the differences between sequential phase-OTDR filtered traces are computed. For that, the I_{avg} values are shifted every clock cycle through a new FIFO register composed of the same number of samples along the optical fiber, F.

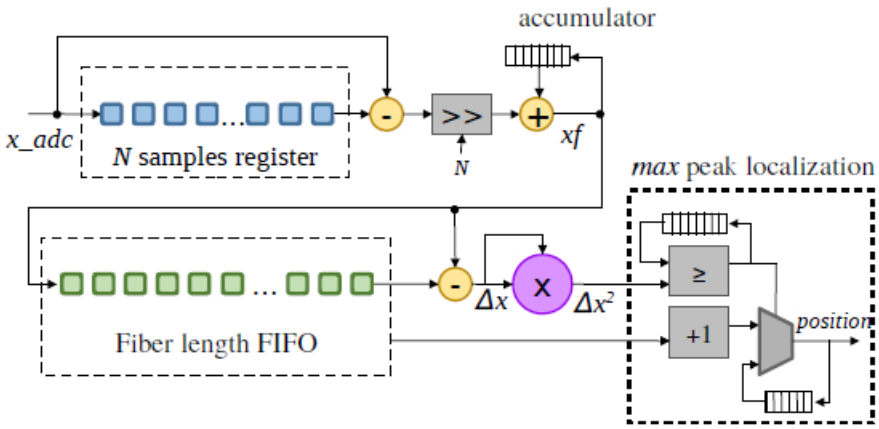

Figure 3.12. General architecture of the recursive moving average filter for peak detection and localization of phase-OTDR signals. The blue blocks denote the FIFO buffer of the moving average and the green blocks represent the FIFO buffer along the optical fiber. The peak localization block was repeated in order to detect two simultaneous perturbation points.

The arithmetic and logic operations are computed in one clock cycle whereas the FIFO has a latency of two clock cycles. Therefore, the initial latency of this architecture is $L = 2F + N + 7$ clock cycles. For a phase-OTDR trace composed of F =9500 samples (295 meters of optical fiber) and a filter with N =32 samples, the latency is L = 19000+32+7 = 19039 clock cycles. After this period, the architecture is able to provide one output per clock cycle.

3.5.5. phase-OTDR DISTURBANCE DETECTION USING SOBEL FILTER

Figure 3.13 shows the proposed hardware architecture for windowing operation, which represents a systolic array. In this approach a two-dimensional image composed of phase-OTDR traces is locally averaging using the edge detection Sobel operator. The architecture is composed of two main components: (i) the neighborhood loading; and (ii) the spatial convolution and threshold detection.

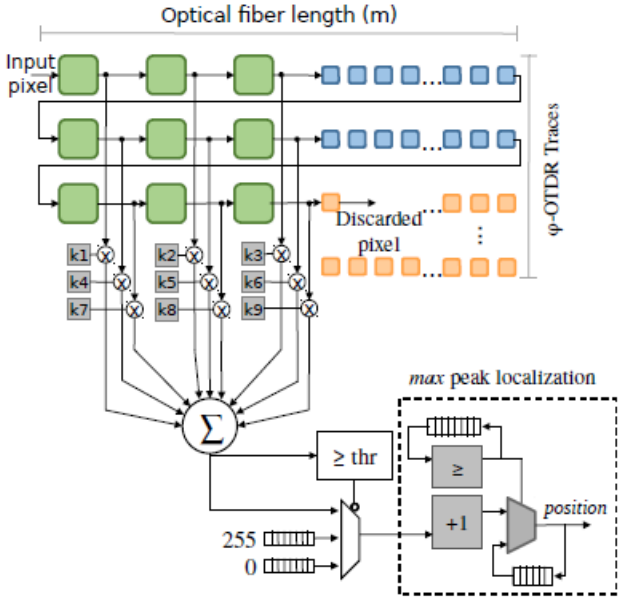

Figure 3.13. Hardware architecture for peak detection and localization of phase-OTDR signals using the Sobel filter. The green, blue and orange blocks denote the pixels in the neighborhood window, the stored pixels and the discarded pixels, respectively. The gray blocks denote the kernel of the convolution

operator. The peak localization block was repeated in order to detect two simultaneous perturbation points.

The neighborhood loading architecture makes use of a buffer for storing the pixels. The structure composed by the green and blue blocks is a FIFO register, where for each cycle of a pixel acquisition all pixels are displaced in the same direction, discarding the oldest and loading the newest. Notice that each line of the shift register is exactly equivalent to the number of samples along the optical fiber. Once the neighborhood is loaded into the FIFO, the image pixels are multiplied by the kernel values in a parallel way. Finally, the multiplications are added and a comparison with a threshold value addresses the output pixel by a multiplexer.

For an image of size G x F and a neighborhood of P x P pixels and taking into account that the FIFO has a latency of two clock cycles, the initial latency of this architecture is equal to $L = (P - 1)2F + P + L_m + L_a + L_t + L_p$, where L_m, L_a, L_c and L_p are, respectively, the latency of the multipliers, the adder, the threshold and the peak localization block. For a phase-OTDR trace composed of F = 9500 samples (295 meters of optical fiber) and a mask of 3x3 pixels, the latency of the proposed architecture is equal to L = (3 - 1) x 2 x 9500 + 3+1+1+1+2 = 38008 clock cycles. After this period, the architecture enables one output pixel per clock cycle.

3.5.6. DETECTION AND LOCALIZATION OF ONE DISTURBANCE POINT

In this experiment 50 traces with 3890 samples each were collected along a distance of 57 m and an acoustic perturbation was applied into a region of 3 m approximately at 39 m. Figure 3.14 presents the results of the recursive moving average for processing phase-OTDR samples with one perturbation point. The hardware solution achieved the same results than Matlab, demonstrating the correctness of the VHDL implementation.

The main differences are related with numerical precision, especially for the division operation since in VHDL integer operations are used whereas Matlab uses floating-point operations. A comparison between VHDL and Matlab implementations of the Sobel filter for processing phase-OTDR samples with one disturbance point is shown in Figure 3.15. In this experiment the samples were rescaled in the range between 0 and 255, allowing them to be used as pixels. It is possible to observe that this gradient-based filter detects the largest intensity variation in the vertical direction, which coincides with the point where the disturbance was applied.

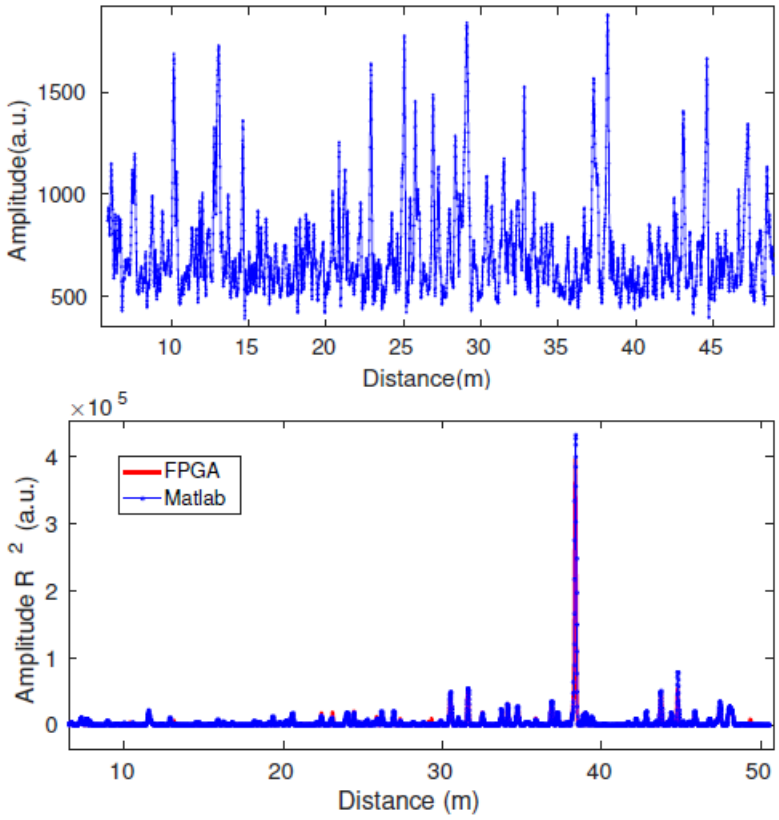

Figure 3.14. Results of the recursive moving average filter for processing phase-OTDR samples with one vibration point. Top: original samples. Bottom: FPGA vs Matlab implementations.

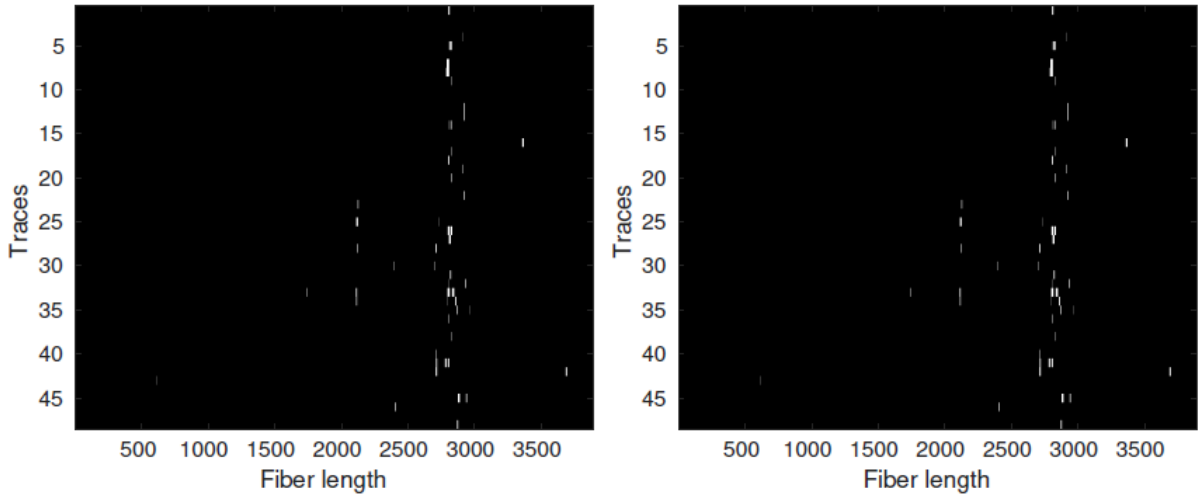

Figure 3.15. Rescale of the Sobel filter results for processing phase-OTDR samples with one disturbance point. Left: Matlab implementation. Right: FPGA implementation.

3.5.7. DETECTION AND LOCALIZATION OF TWO DISTURBANCES POINT

In this experiment, 201 traces with 9500 samples each were collected along a distance of 295 m and two acoustic perturbations were applied 90 m of fiber away from each other at positions 132 m and 32 m. Figure 3.16 shows the achieved results by the Sobel filter for detection of two simultaneous perturbations. The achieved result is presented in the bottom image. It is possible to observe the presence of two groups of pixels at the positions where the disturbances were applied. Sobel filters with large kernels will efficiently remove the noise; however, information containing small vibrations in the fiber can be lost.

Figure 3.17 illustrates the achieved results by the recursive moving average filter where two simultaneous disturbance points were applied to the optical fiber. It was observed the presence of two peaks along the traces whereas the noise was attenuated. The peak detection block was able to localize the perturbations by looking for the two-maximum peak value across the traces. The second highest peak was found looking for the maximum peak out the perturbation region of 5 m of the highest peak.

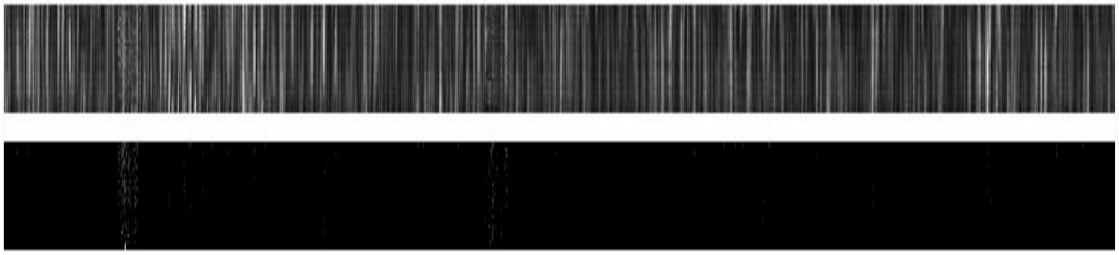

Figure 3.16. Results of the Sobel filter for processing phase-OTDR samples with two simultaneous disturbance. Top: original image. Bottom: FPGA implementation.

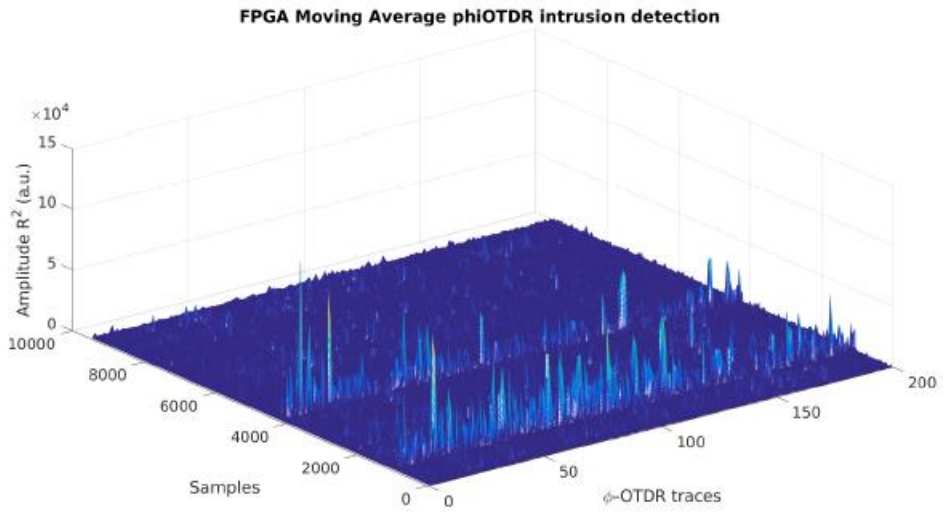

Figure 3.17. Results of the FPGA implementation of the recursive moving average filter for processing phase-OTDR samples with two simultaneous perturbation points.

3.5.8. RESULTS ANALYSIS

In terms of hardware cost, the most remarkable aspect is the BRAM consumption which directly affects the scalability of the architectures for large optical fibers systems. The moving average architecture was configured to analyze 57 m and 295 m of optical fiber. In the former 2 BRAMs to implement FIFO buffers of size 16 bits x 4096 were required. In the later 7.5 BRAMs (7 BRAM36 and 1 BRAM18) implementing a FIFO buffer of size 16 x 16384. Thus, the moving average architecture is able to analyze up to 47.05 m and 483.32 m for the first and second configurations, respectively; however,

using the total available BRAMs resources in the FPGA it can inspect systems up to 3.8 km length.

The Sobel filter architecture achieves better results in term of filtering capabilities; however, it requires more BRAM resources (two phase-OTDR traces instead of one in the moving average) and, as a consequence, it is able to inspect systems up to 1.9 km length. The recursive moving average and Sobel filters were implemented using pipelined architectures, achieving a latency of 0.127 ms and 0.304 ms, respectively. After that initial period, the implemented circuits of the moving average and Sobel filter are able to process one output every 13.2 ns and 16 ns, respectively. This fact points-out the feasibility of the proposed hardware architectures and experimental setup for real-time vibration sensing at frequencies in the order of MHz. It is important to highlight that the FPGA device has enough resources (more than 90%) for implementing parallel classification algorithms allowing to extract information along the optical fiber in a simultaneous way.

As future work will be to explore real-time processing solutions and the FPGA parallelism capabilities to listen to sound disturbances in multiple zones along the optical fiber.

3.6. CHAPTER CONCLUSION

In this chapter, the phase-OTDR method for multi-point intrusion detection was explored, both in its most basic setup and in an original contribution where it is merged with Field Programmable Gate Array architectures. An optical fiber coil mesh was also proposed, showing the versatility of the method and the capability to increase its spatial resolution without employing higher bandwidth expensive ADC solutions. The original results obtained in this chapter of the thesis were presented and published at the Proceedings of the 14th IEEE International Conference on Networking, Sensing and Control 2017, Calabria (Italy).

CHAPTER 4

4. VIBRATION MEASUREMENT ON COMPOSITE MATERIAL WITH EMBEDDED OPTICAL FIBER BASED ON PHASE-OTDR

As previously reported in the early chapters, distributed sensors based on phase-OTDR are also suitable for structure health monitoring. These sensors features allow the fiber embedment into aircraft structures in a nearly non-intrusive way to measure vibrations along its length. The capability of measuring vibrations on airplane composite structures is of interest for what concerns the study of material fatigue [55] or the occurrence of undesirable phenomena like flutter [56]. This chapter is addressed to the vibration measurement on composite material with embedded optical fiber using the phase-OTDR method. Firstly, a brief introduction of the importance of measuring vibrations in aeronautic structures is presented, followed by a previously reported study of fiber embedment into composites, addressing the main challenges. Then, the fabrication process of composite samples with embedded fibers performed for this work is explained. Lastly, vibrations measurements based on phase-OTDR ranging from some dozens of Hz to kHz in two layers of a built composite material board with embedded polyimide coating 0.24 NA SMF are shown and discussed. The results presented here were presented and published at the Proceedings of SPIE Smart Structures and Nondestructive Evaluations 2017, Portland (USA).

4.1. BACKGROUND ON AIRCRAFT COMPOSITE STRUCTURE MONITORING

Nowadays, a great part of aircrafts structural components are made of advanced composite materials integrated into their primary structure [57]. A composite material is made from two or more constituent materials with significantly different physical or chemical properties that, when combined, produce a material with characteristics different from the individual components. The individual components remain separate and distinct within the finished structure. In particular, the carbon fiber composites explored in this work consists of superimposed ply layers containing reinforcing fibers with specific orientations, as shown in Figure 4.1.

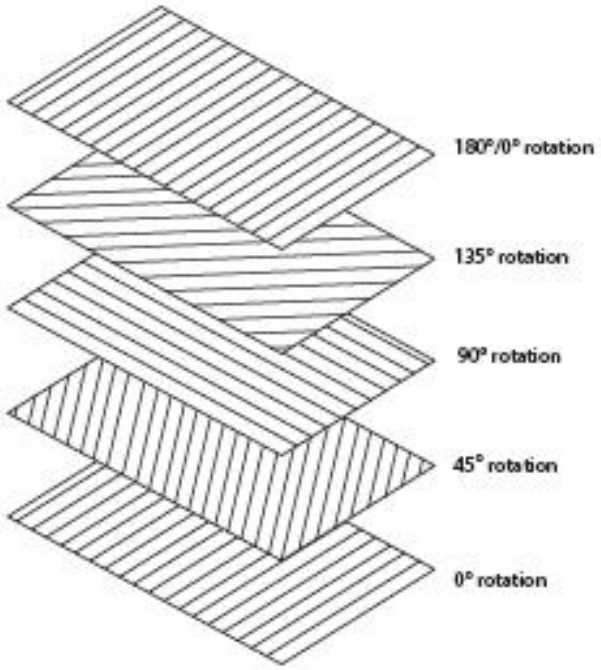

Figure 4.1. Depiction of superimposed reinforced fiber plies to build a carbon composite structure.

The choice of this type of fiber-reinforced material is due to their light weight, resistance to fatigue/corrosion, design flexibility and superior strength properties over conventional aluminum alloys. These features have proven to be a key to improving fuel efficiency, reducing emissions and lowering the manufacturing and operating

costs in both civil and military aircrafts [57]. Figure 4.2 shows the composition of a *Boeing 787* structure, which 50% of its structure is made of composite materials [57].

The expectation is that, over the next years, the percentage of composites in aircrafts grow even more, making them more affordable, safer, cleaner and quieter than the current ones [57]. However, these fiber-reinforced materials are more complex than metallic ones, since their structural anisotropy and their multiphase materials might result in many types of damage with different propagation characteristics, causing the remaining strength and residual life of the structure difficult to predict after a damage.

In these structures, the most common type of damage is caused by impact, such as bird strikes, tool drop during manufacturing and maintenance or even detached ground stones during take-off. These impacts may cause failures in the structure, such as indentation, delamination or reinforcing fibers cracking, compromising the strength and integrity of the structure. Visible damage is more straightforward to detect and solve, while hidden damage is a major concern because failures to detect it may result in an accident.

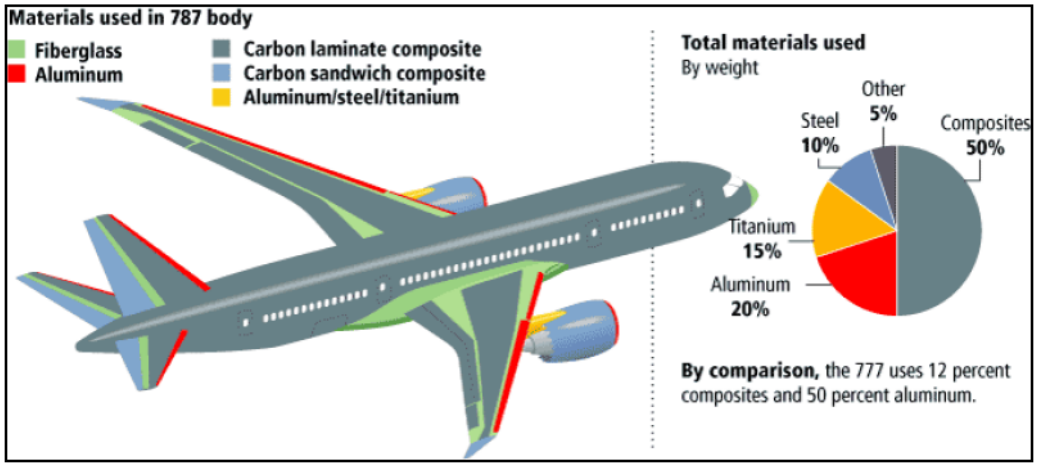

Figure 4.2. Composition of a *Boeing 787* structure [57].

Another hazardous and more dynamic event that may occur in aircrafts is flutter, a phenomenon that can happen when a structure is subject to aerodynamic

forces, causing the wings and/or the stabilizers to oscillate. When the airspeed increases the energy added in each oscillation to the structure by the aerodynamic forces increases. At some speed the damping of the structure may be insufficient to absorb the energy increase from the aerodynamic loads and the amplitude of the harmonic oscillations will grow until the structure breaks. The video shown in [59] displays a Twin Comanche aircraft during a flutter test. As shown in the video, once the vibrations are introduced into the tail of the aircraft, in this case a stabilizer, the flutter increases dramatically, causing tremendous oscillations in the horizontal surface making the stabilizer as flex as if it was made of rubber. This kind of phenomenon can occur in all kind of aircraft structures, including the ones made of composite materials where it may cause internal delamination of the reinforcing fibers.

In order to test an aircraft resilience to flutter, tests regarding the response of the structure to vibrations are carried out [60]. There are plenty of flutter test procedures, but one of these tests in particular is the sweep test, in which a range of oscillations, usually between 5 to 60 Hz, are introduced in-flight by a function generator to flight-control surface such as the ailerons, the rudder or the elevator. Then, the frequency response of the structure along with the damping are analyzed in order to evaluate in which conditions the flutter occurs. Thus, the vibration frequency of the structure is a parameter of high interest for these structure health monitoring tests.

In this scenario, optical fiber sensors have been emerging as feasible solutions due to their higher sensitivity, immunity to electromagnetic interferences, flexibility, durability and small dimensions, which make then capable to be embedded into structures in a low intrusive way [57]. Furthermore, the distributed and quasi-distributed solutions reported in Chapter 3 offer high multiplexing capability, the possibility to reduce the bulky wiring required by traditionally used electronic sensors and to work as an aircraft nervous system, as depicted in Figure 4.3 [61]

Figure 4.3. Concept of an aircraft with embedded optical fiber sensors displaced as a nervous system [61].

It has been reported that these fiber OFS are already employed for both SHM ground tests and on flight measurements [57], *Airbus* has recently announced that the long-term roadmap is that all new aircraft will present embedded FBG optical sensors, which highlights the ever growing evolution of these fiber optic based techniques.

In this work, a composite board sample was designed and fabricated with embedded optical fibers and the phase-OTDR technique was employed to measure vibrations in two layers of this board and also to listen to the sound of knockings on the structures and objects dropping upon it. In this chapter, it was performed an investigation regarding the influence of embedding optical fibers into composite materials, also the fabrication process of the sample board is explained, along with the experimental tests regarding vibration frequency measurement. The sound listening experiments, their motivations and results discussions are presented later in Chapter 6, after the developed phase-OTDR based microphone is introduced and explained.

4.2. INFLUENCE OF OPTICAL FIBERS EMBEDMENT INTO COMPOSITE MATERIALS

As previously stressed, optical fibers can be embedded into composite material structures with minimum intrusion due to their geometric versatility and small size [62]. However, even though very small (around 100 to 200 μm), the optical fiber diameter is still considerable in comparison to the sandwich composite material reinforcing fibers (around 5 to 10 μm) [63]. Thus, in order for embedded optical fiber sensors to be accepted into aircraft composite structures, it must be proved that the insertion of these fibers does not reduce the mechanical properties of the material, like lifetime, strength, and resistance to fatigue.

In literature, previous studies addressed this concern. According to these studies, there are many considerations to successfully integrating fiber sensors into composite materials, and this is itself an active area of research. Issues include the manufacturing process to integrate the sensors without compromising the composite matrix, sensor ingress/egress, and sensor survivability maintenance [65].

Figure 4.4 shows pictures of the cross sections of the composite boards with embedded optical fibers in different orientations.

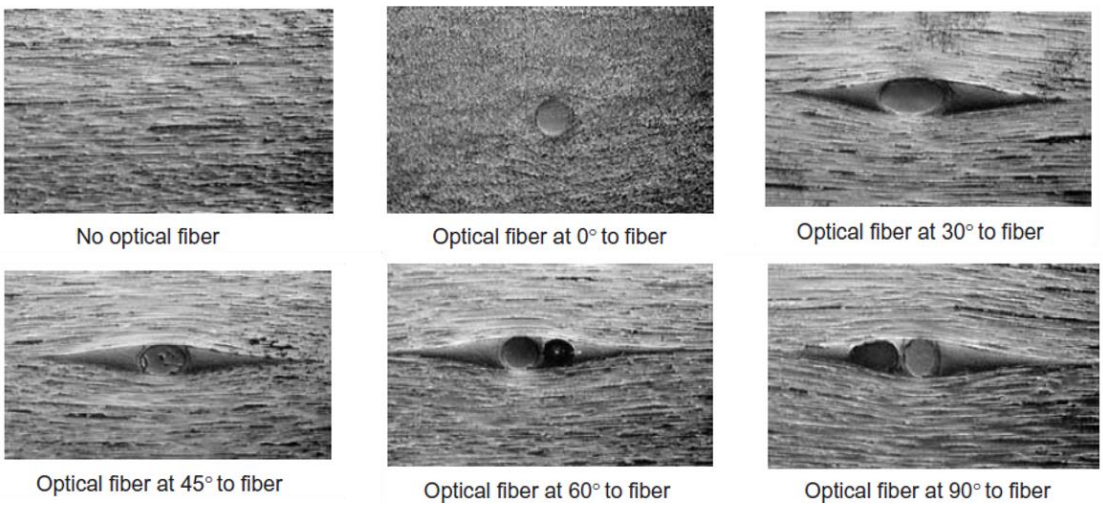

Figure 4.4. Cross section pictures of embedded optical fibers at different orientations with respect to the composite reinforcing fibers [65].

According to the pictures shown in Figure 4.4, it is visible that when the optical fiber is embedded in parallel to the ply reinforcing fibers (0°), no resin pockets are formed around the optical fiber after the fabrication process, presenting then a high absorption by the composite material. However, for embedment angles different from 0°, these pockets, i.e. lenticular regions rich in resin and without reinforcing fibers, appear around the fiber and acts like a interlaminar discontinuity that can be a potential source of damage when submitted to loads [65]. Figure 4.5 illustrates the concept of these resin pockets.

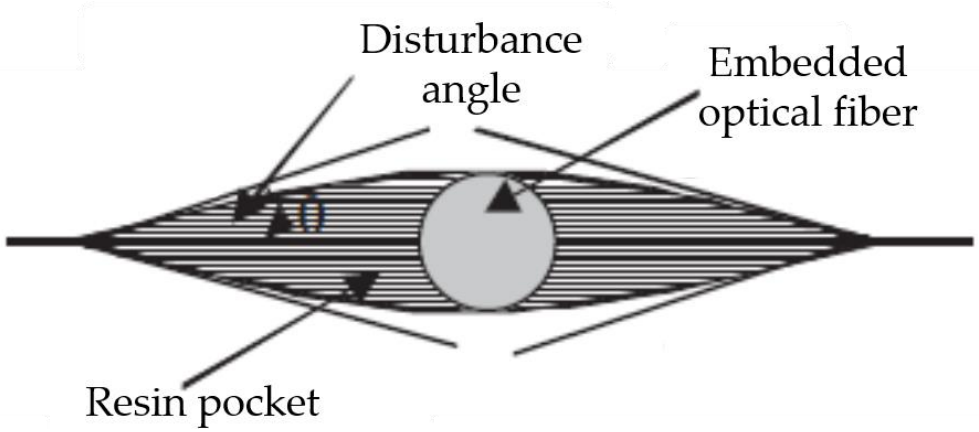

Figure 4.5. Depiction of an arbitrary resin pocket formed by the embedment of an optical fiber not in parallel with the material reinforcing fibers.

These lenticular regions occur due to the fact that when submitted to high temperature and pressure in the curing process, the optical fibers keep their volume and geometry, while the composite plies have the tendency to shrink due to their different thermal expansion coefficients. Thus, the presence of a not aligned optical fiber becomes a local flaw that disturbs the ply sequence and compromises the integrity of the composite structure.

According to the literature, the composite flexure strength and modulus were not significantly influenced by the optical fibers embedded in parallel with respect to the material reinforcing fibers. Also, the impact seems to be more critical in specimen configurations containing embedded optical fibers in the laminate middle plane. This fact was even more notorious for cross-ply laminates, which revealed premature

ruptures for the higher stress ratio (90%) used in previously reported researches; for the lower loading condition (75%), a significant stiffness reduction of about 20% was detected. This behavior seems to be related to higher shear stress levels present in the middle plane [64]. Also, the negative influence proved to be higher in composites with less number of plies. Thus, embedding the fiber optics in the same orientation as the carbon fiber plies is pointed as the best option.

Although this subject has many potential to be explored, this is not the goal of this thesis, which is focused on the vibration monitoring itself. Nevertheless, it is important to acknowledge the need to guarantee a good interface between composite materials and embedded fiber optics. Future investigations in this regard could comprise the development of a dedicated smart composite topology that solve both the structure requirements and the capability to have embedded fibers actuating as a nervous system with the least negative impact possible.

4.3. DESIGN AND MANUFACTURING OF COMPOSITE BOARD SAMPLE WITH EMBEDDED OPTICAL FIBERS

In order to evaluate the capability of the phase-OTDR method in measuring vibration frequencies in composite with embedded optical fibers, a composite board was manufactured for this purpose at Saab AB, Linköping, Sweden, facilities. A sample with 24 plies was build, containing four 2.5 m length embedded 0.24 NA polyimide coating optical fibers with 125 μm of diameter. The use of polyimide coating is due to the fact that this coating solution can resist to temperatures up to 300 °C [66], an important feature since it must endure the high temperature curing process in the composite board manufacturing.

The stacking sequence of the composite board plies is shown in Table I, where the angles refer to the orientation of the material reinforcing carbon fibers. The painted numbers refers to the plies in between an optical fiber was inserted.

Table II. Ply sequence and angles**.**

Ply	1	2	3	4	5	6
Angle	45°	-45°	0°	90°	45°	-45°
Ply	7	8	9	10	11	12
Angle	0°	90°	45°	-45°	0°	90°
Ply	13	14	15	16	17	18
Angle	90°	45°	-45°	0°	90°	45°
Ply	19	20	21	22	23	24
Angle	-45°	0°	90°	45°	-45°	0°

The board size was 50 cm x 50 cm and it was 3 mm thick after the curing process, which was performed as follows:

1. Firstly, the composite plies were cut at the desired shape and quantity;
2. Then, the composite sample board was built by superposing the plies according to the mentioned stacking sequence, putting 2.5 m of optical fibers between some plies as showed in Figure 4.6. The fibers were inserted between the plies: 4-5, 8-9, 12-13 (middle plane) and 17-18. Since the plies were already very sticky, no extra glue were need to bond the optical fibers to the material. Also, the fiber optics were inserted in parallel to the plies orientation as much as possible and the stacking was already built upon a curing table;

Figure 4.6. Stacked plies with embedded optical fibers.

3. After building the samples, the curing table was covered with proper tissue layers and all air between them is removed, as shown in Figure 4.7;

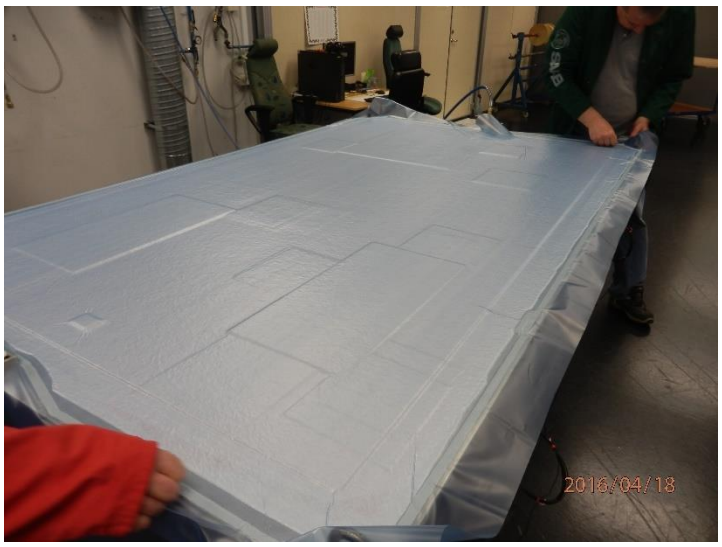

Figure 4.7. Curing table with tissue layers and at the required vacuum conditions.

4. The curing table was then inserted into an autoclave in which temperature and pressure were monitored controlled during the whole curing process. The temperature in the autoclave was varied from 24 °C to 180 °C in the first 176 minutes and from 180

°C to 37 °C after 112 minutes more. During almost the whole process, which takes 286 minutes, the pressure inside the autoclave was kept around 310 kPa;

5. After the curing time, the table was removed from the autoclave and the cover layers were gently removed, always taking care with the optical fibers in the output of the composite. Figure 4.8 shows the final composite sample with embedded fibers, a zoom in the fibers coming out of the material, which will be used to access the embedded fibers, and also a microscope picture of a transversal cut view of one sample where one can see the optical fiber totally absorbed by the plies, as recommended;

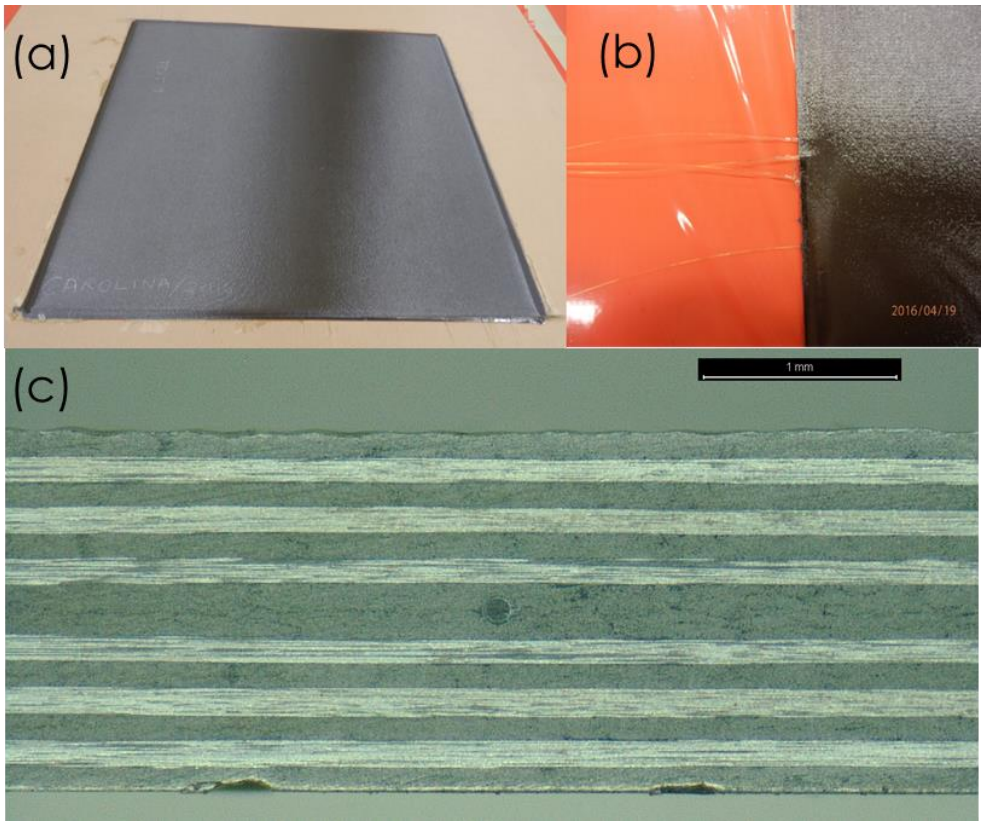

Figure 4.8. (a) Final composite sample with embedded optical fibers, (b) zoom in the fibers inserted in the material and (c) transversal cut view of a sample with the embedded optical fiber in parallel to the carbon reinforcing fibers.

When finished, the composite board was taken to Acreo's facilities in Kista, Stockholm. Both endings of the four embedded optical fibers were then connectorized and tested with a red light, as shown in Figure 4.9, in order to investigate if some fibers

were broken in the curing process. All the four embedded fibers passed the test and thus the embedding process was successful.

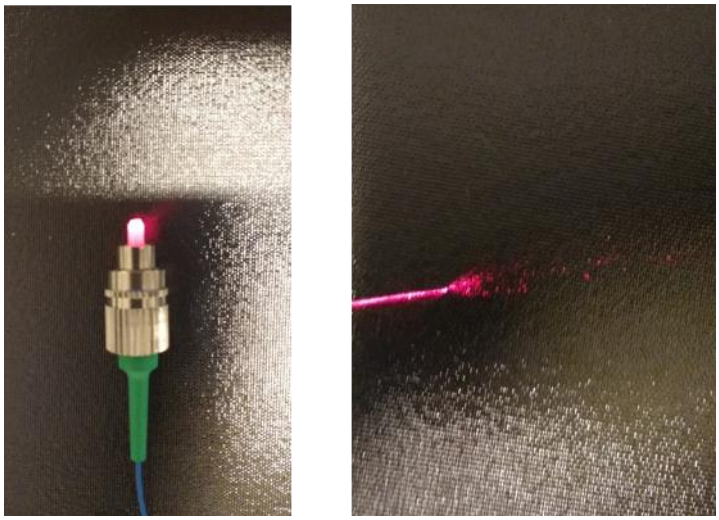

Figure 4.9. Tests with red light to verify the quality of the embedded fibers after the curing process.

4.4. VIBRATION FREQUENCY MEASUREMENTS ON COMPOSITE BOARD SAMPLE

After building the composite sample with the embedded optical fibers, vibration frequency measurements were performed in both one and two layers of the composite. In order to do so, the phase-OTDR setup presented in Figure 4.10 was used.

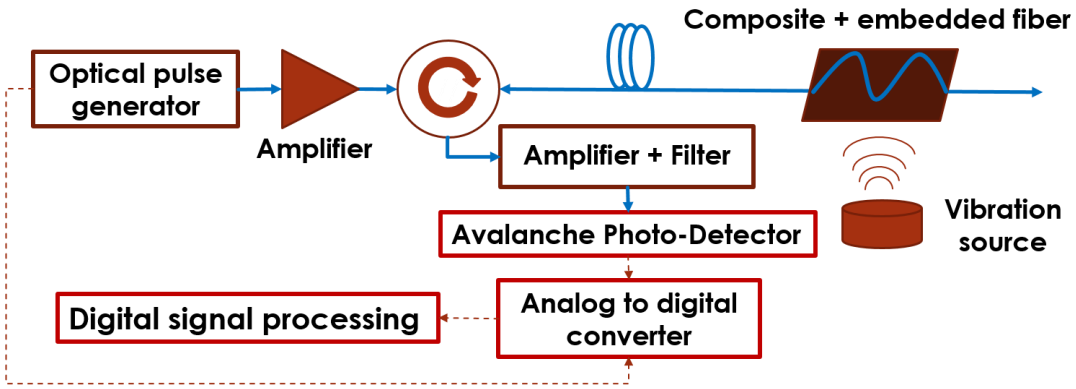

Figure 4.10. Experimental setup comprising the phase-OTDR apparatus and the composite board with embedded optical fiber.

The experimental setup comprises an ANDO AQ4321A narrow linewidth laser (NLL) with bandwidth ~200 kHz, a Thorlabs BOA1004PXS gated semiconductor optical amplifier (SOA) to both amplify and trigger the laser light into optical pulses, a GNNettest BT-17 erbium-doped fiber amplifier (EDFA), an optical circulator and a 45.5 m of 0.24 N.A. single mode optical fiber. The other end of this fiber was connected to one of the 2.5 m optical fibers embedded into one layer of the composite board and used as the fiber under test (FUT). The circulator directs the Rayleigh backscattered signal into the receiver-side of the setup, which incorporates a second EDFA, a 1 nm wide optical bandpass filter (BPF) tuned to the wavelength of the laser, a 400 MHz avalanche photodetector (APD) and a TSW14J56 analog-to-digital converter (ADC) to acquired and store the phase-OTDR traces. The duration of the optical probing pulses is a ~8 ns, thus limiting the spatial resolution to ~80 cm. Figure 4.11 shows pictures of the experimental setup.

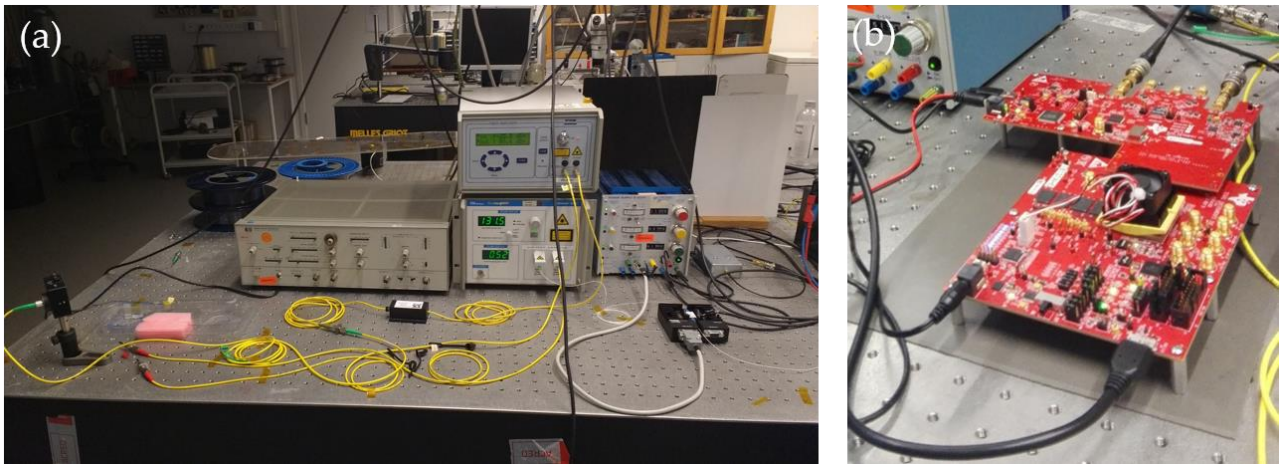

Figure 4.11. (a) Optical transmitter and receiver-side of the employed phase-OTDR setup; (b) ADC to acquire and store the phase-OTDR traces.

Figure 4.12 depicts the composite board with its embedded fibers already connectorized and mounted upon a structure where an electromagnetic mini shaker of 10 cm diameter controlled by a sinewave generator is placed underneath and used as a vibration source.

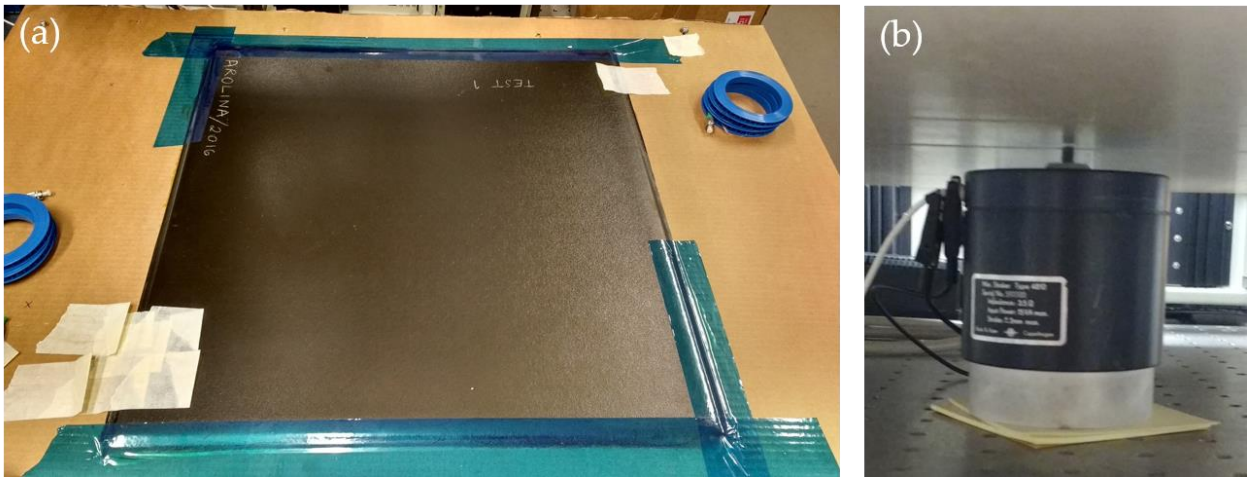

Figure 4.12. (a) Composite board with connectorized embedded optical fibers (blue coils); (b) mini shaker placed underneath the board to generate vibrations.

Firstly, just one layer of the composite was evaluated and the frequency applied to the shaker was swept from 0 to 1000 Hz. For each value of frequency, the phase-OTDR technique was used to measure the vibration frequency of the composite board. In this case, the sensing fiber was located at the middle plane (90°/90°). Figure 4.13 shows the squared differential phase-OTDR traces obtained when applying vibration to the composite. It is visible that the disturbed track of the fiber is between 45.5 and 48 m, which is the fiber section embedded into the composite.

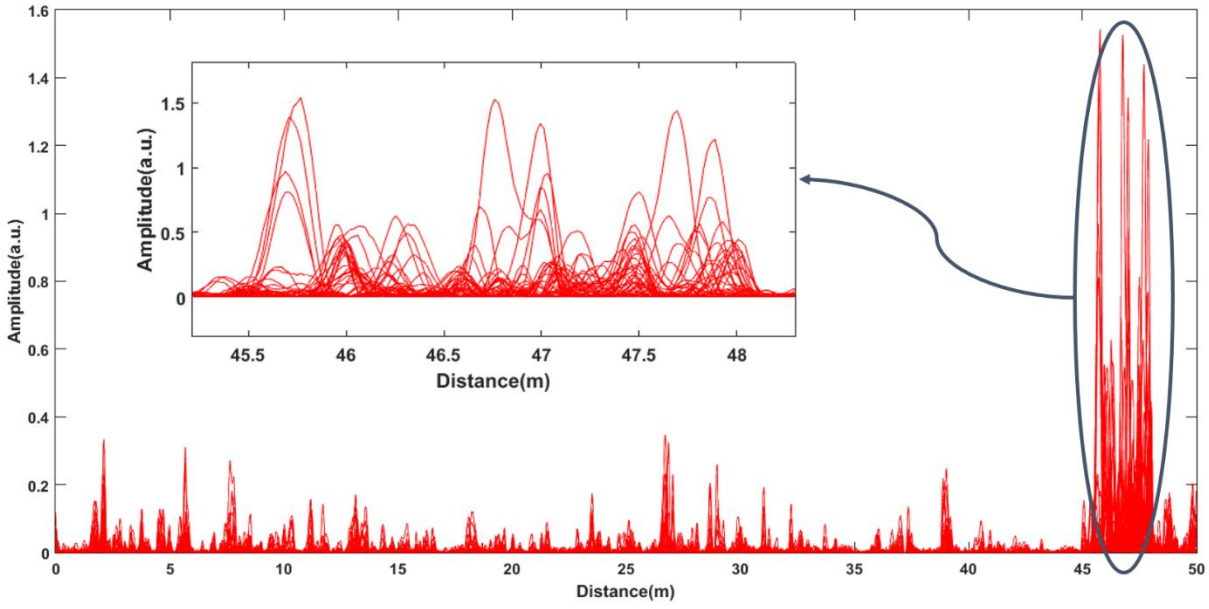

Figure 4.13. Squared differential phase-OTDR traces, highlighting the fiber section embedded into the composite submitted to periodic disturbance (inset).

One can recover the disturbance signal in time-domain by sampling the consecutive obtained phase-OTDR traces in one point among the localized disturbed section within the composite board. For example, Figure 4.14 exhibits the recovered time-domain disturbance signal of 1000 Hz from 393 consecutive phase-OTDR traces.

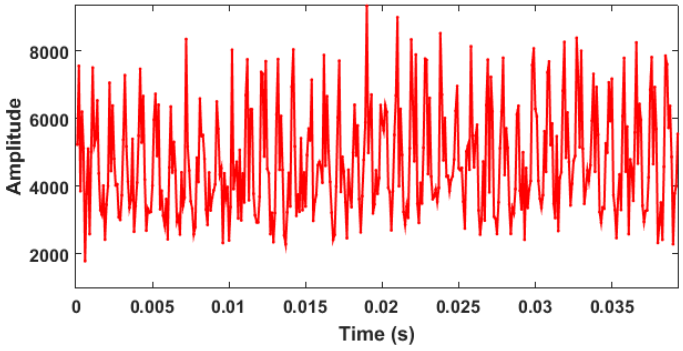

Figure 4.14. Measured time-domain disturbance signal of 1000 Hz from 393 consecutive phase-OTDR traces.

In order to obtain the frequency profile of the disturbance signal, a fast Fourier transform is applied to its time-domain signal. Figure 4.15 exhibits the frequency measurements for each vibration frequency applied to the composite board.

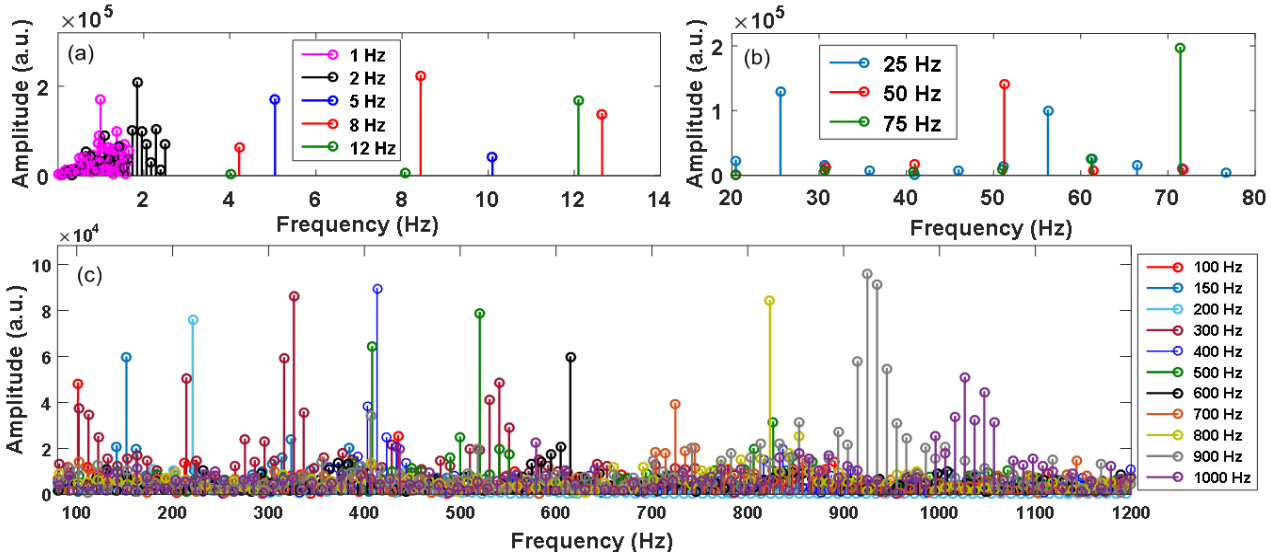

Figure 4.15. Vibration frequency measurements using the phase-OTDR technique: (a) 0 to 12 Hz; (b) 250 to 75 Hz and (c) 100 to 1000 Hz.

It is noticeable that the value of the frequencies measured by the phase-OTDR technique are similar to the frequency of the vibration applied to the composite. The slight differences between applied and measured frequencies may be due to the mini shaker – composite – fiber coupling and can be considered subject of further investigations in future works.

Besides, it is also observed the capability of the sensor to measure low-frequency vibrations around 0 to 100 Hz. Since the natural frequency of airplane wings and the undesirable flutter phenomenon can range around some dozens of herz, it is important for the proposed sensor to be able to detect vibrations with these frequency values. Also, the capability to measure higher frequencies might be also of interest, since fatigue tests can occur at frequency ranges beyond 100 Hz.

Lastly, we tested embedded fiber in the 90°/90° layer was connected to another embedded fiber in the 90°/45° layer, thus analyzing two layers simultaneously. The two layers were connected externally by a 2 m optical fiber spliced between both layers, thus it is seem a 2 m distance between layer 1 and layer 2 in the phase-OTDR traces. The mini shaker controlled by a sine generator was placed beneath the composite board and used again as a vibration source. Figure 4.16 shows the squared differential phase-OTDR traces obtained when applying vibration to the composite in this two layers configuration, where we can clearly distinguish the presence of vibration in both layers.

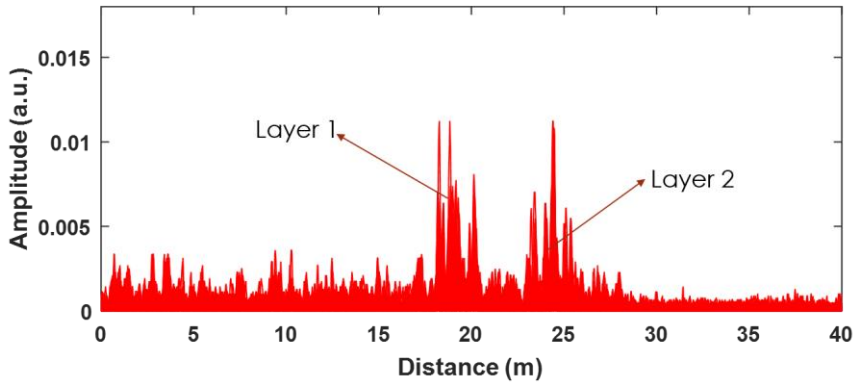

Figure 4.16. Experimental results obtained from disturbing the composite board with an optical fiber embedded in two layers.

The frequencies applied to the board were 1 Hz, 100 Hz and 200 Hz, and the phase-OTDR was used to measure the vibration frequency in both layers. The results are depicted in Figure 4.1.7

The value of the frequencies measured by the phase-OTDR technique are compatible to the frequency of the vibration applied to the composite and also a similar frequency spectrum is observed in both layers for each scenario. The capability to evaluate two layers separately and simultaneously is important when analyzing material fatigue, that may vary from layer to layer according to the curing process and environmental conditions to which the composite is exposed.

Thus, this experimental validation proved the capacity of the presented method to evaluate vibration frequencies in composite boards with embedded optical fibers, which shows the suitability of the technique for aeronautic applications.

4.5. CHAPTER CONCLUSION

This chapter showed the experimental validation of a phase-OTDR technique to localize and measure vibration frequencies in composite materials. In order achieve this goal, 0.24 numerical aperture SMFs were embedded into aircraft composite material and the proposed phase-OTDR method was applied to measure frequencies in one layer, from 0 to 1000 Hz, and in two layers simultaneously, where vibration frequency measurements of 1 Hz, 100 Hz and 200 Hz were demonstrated.

Since the natural frequency of airplane wings and the undesirable flutter phenomenon can range around some dozens of herz, it is important for the proposed sensor to be able to detect vibrations within these frequency values. Also, the capability to measure higher frequencies might be also of interest, since fatigue tests can occur at frequency ranges beyond 100 Hz. Thus, according to the experimental results, the capacity of the presented method to evaluate vibration frequencies in composites with embedded optical fibers was proved, which highlights its usefulness for aeronautic applications.

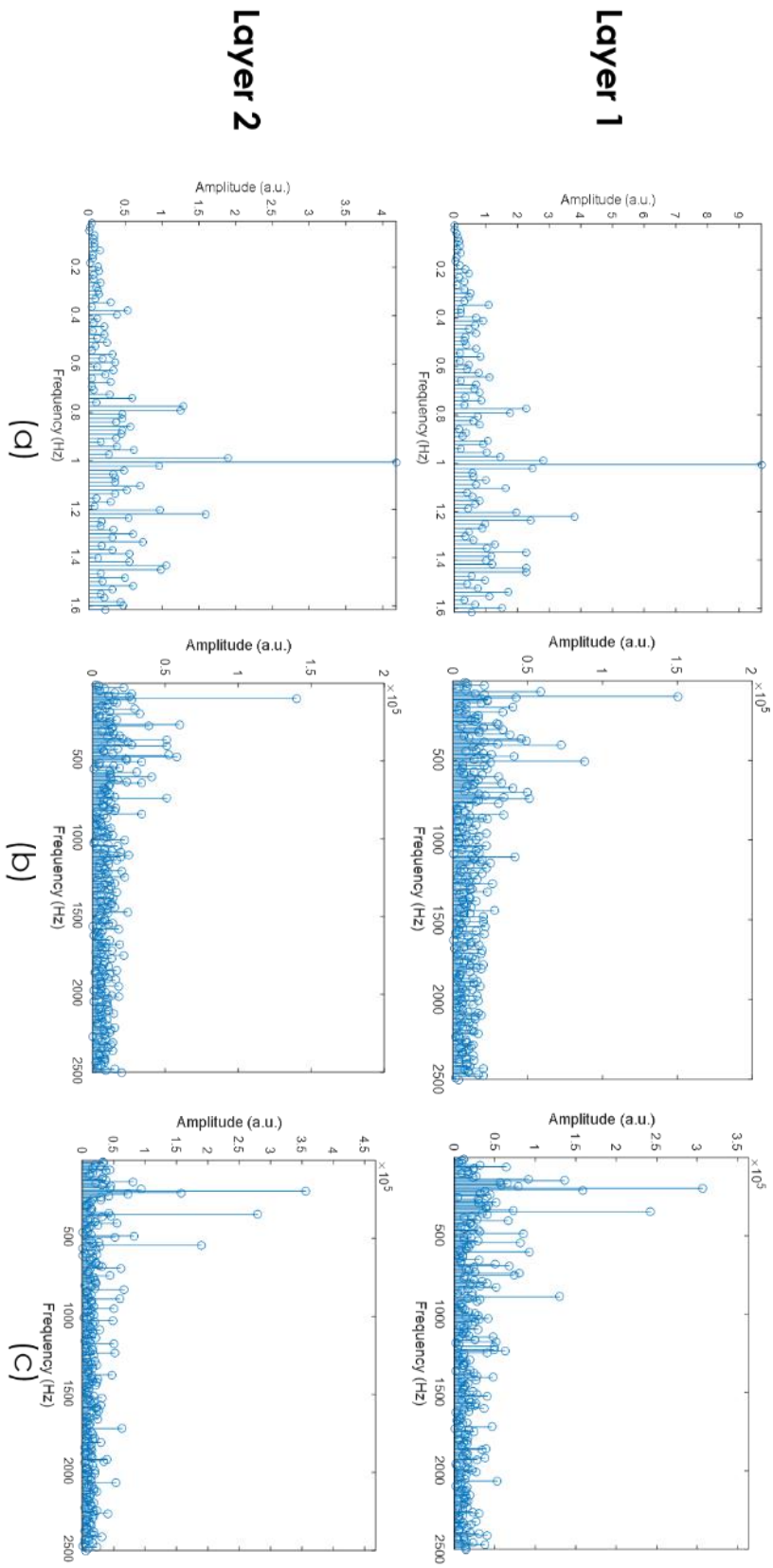

Figure 4.17. Frequency measurements in two layers using the phase-OTDR technique: (a) 1 Hz; (b) 100 Hz and (c) 200 Hz.

CHAPTER 5

5. REAL-TIME DISTRIBUTED OPTICAL FIBER MICROPHONE BASED ON PHASE-OTDR

The use of an optical fiber as a novel real-time distributed microphone is demonstrated employing a phase-OTDR with direct detection. The method comprises a sample-and-hold circuit capable of both tuning the receiver to an arbitrary section of the fiber considered of interest and to recover in real-time the detected acoustic wave. The system allows listening to the sound of a sinusoidal disturbance with variable frequency, music, footsteps, machines, human voice, knocks and underwater sounds with ~60 cm of spatial resolution through hundreds of meters of optical fiber. Part of the experimental results obtained in this chapter were published at the Optics Express Journal and to the IMOC 2017.

5.1. OVERVIEW

Distributed acoustic sensors (DAS) based on optical fibers and Rayleigh scattering have been widely exploited in the last three decades, as reported in Chapter 2, exploiting the fibers small dimensions, immunity to electromagnetic interference, long perimeter coverage and large bandwidth [67]. Like other distributed fiber sensing techniques, DAS also offers high multiplexing capability as well as the possibility of using standard telecommunication fibers and telecommunication demodulation techniques [68].

The use of DAS as a distributed microphone allows extracting information from sound which is useful to monitor perimeter security and equipment in industrial plants, since it allows spatially locating the acoustic disturbance and its frequency content. Recently, a distributed fiber microphone was reported based on the phase-sensitive optical time-domain reflectometry technique (phase-OTDR) [44]. The amount of data generated by a system used to monitor the acoustic response of the entire fiber all the time is massive, and data acquisition to a memory followed by off-line processing is required. This is a serious limitation, and most DAS systems reported in the literature involve a posteriori analysis of recorded data. In that publication [44], for example, consecutive phase-OTDR curves were acquired and processed off-line to recover the sound signal.

In some cases, it would be very advantageous to listen to the acoustic signal in real-time, without additional signal processing. In perimeter security for instance, conventional DAS could be used in a distributed way to define when and where intrusion takes place. From then on, one could listen to the sound generated at the intrusion location in real-time, paying full attention to that point of the fiber, while maintaining the distributed measurement capability in parallel, to keep tracking possible new disturbance points. Another potential application of the technique would be monitoring from the control room in real-time the sound from various machines in a factory, one at a time.

In the present work, we demonstrate the implementation of a simple phase-OTDR, capable of reproducing in real-time the sound detected along an arbitrary section of a fiber length, while maintaining a good spatial resolution of ~60 cm. The system developed is similar to a traditional phase-OTDR setup. In addition, it incorporates a simple low-cost electronic sample-and-hold circuit providing short reading time for good spatial resolution and storing the information for sufficiently long time to reconstruct the detected acoustic wave. The sample-and-hold is triggered after a delay which defines the point of the fiber to which one listens. An audio circuit plays the recovered sound in real-time. In contrast to distributed microphones

reported in the literature, direct detection is employed, simplifying the receiver-side topology and minimizing polarization fading phenomena [25].

In order to evaluate the proposed technique, sound disturbed a section of optical fiber along a fiber link. A frequency-sweeping sinusoidal signal, music, footsteps, machines, human voice, knocks and screw drops were used as acoustic disturbance for testing. After tuning the delay, it was possible to recover and listen to the applied disturbances, proving the suitability of this simple system as a real-time fiber microphone capable of interrogating a fiber link.

5.2. METHODOLOGY

The experimental setup of the modified phase-OTDR is shown in Figure 5.1. The transmitter-side of the setup comprises an ANDO AQ4321, which is a narrow linewidth laser (NLL) with bandwidth ~ 200 kHz tuned to 1543.7 nm and producing 0 dBm power. This signal passes an external isolator and inputs a Thorlabs BOA1004PXS gated semiconductor optical amplifier (SOA) to both amplify to 18 dBm and to carve the cw laser light into optical pulses. The current pulse supplied to the SOA has 600 mA, lasts for 8 ns and has a repetition rate 20 kHz, which is the sampling rate of this experiment. They are further amplified in a GNNettest BT-17 erbium-doped fiber amplifier (EDFA). An optical circulator sends the coherent optical pulses into the fiber under test, whose numerical aperture is 0.24. The length of the fiber and the sound source depends on the experiment performed, as addressed in section 5.4.

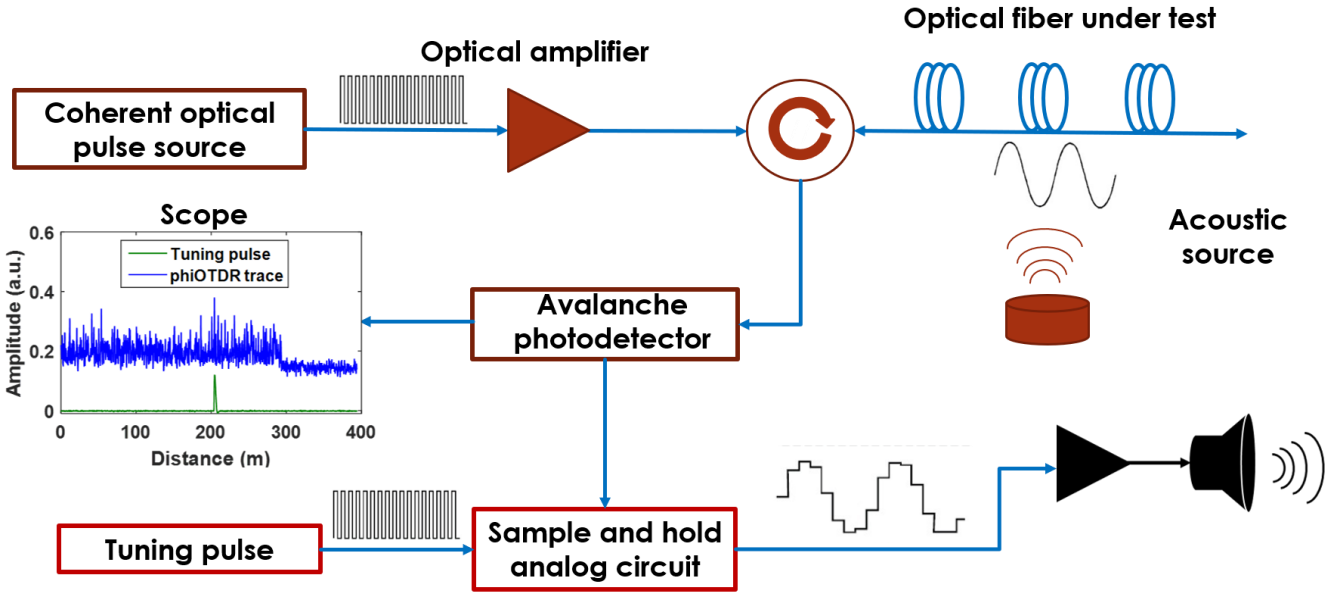

Figure 5.1. Experimental setup displaying the real-time distributed fiber microphone technique.

The circulator directs the Rayleigh backscattered signal into the receiver-side of the setup, which incorporates a second EDFA, a 1-nm wide optical bandpass filter (BPF) tuned to the wavelength of the laser, a 400 MHz avalanche photodetector (APD), the sample-and-hold (S/H) electronic circuit shown in detail in Figure 5.2, an audio amplifier and a loudspeaker to reproduce the recovered sound.

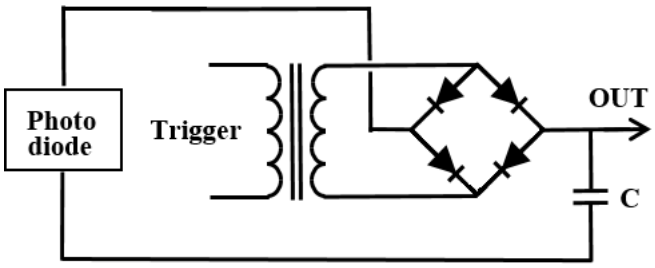

Figure 5.2. Schematic of the sample-and-hold circuit used to recover the acoustic signal.

The APD was employed because of its bandwidth, but the same experiment could be performed with alternative sufficiently fast detectors. A Tektronix AFG3252 two-output pulse generator triggers both the SOA and the sample-and-hold circuit, ensuring synchronization of the reading with the beginning of the sweep. A Tektronix TDS3034 300 MHz 2.5 GS/s digital scope shows in real-time both the phase-OTDR trace and the sample-and-hold trigger pulse. When a disturbance is seen on the backscattered trace, the delay of the trigger pulse is tuned to match the location of the

disturbance. The sample-and-hold circuit zooms in only in the region of interest and rebuilds in real-time the acoustic disturbance signal at this particular location in the fiber. It consists of a small transformer with 7 windings in primary and secondary, a diode bridge with 1N4138 diodes and a storage capacitor (C=100 pF). The latter feeds a high-impedance audio amplifier and holds the voltage value read from the photodiode until the next sampled pulse comes in. This home built sample-and-hold circuit performed better than a commercial circuit tested previously.

It is worth stressing the importance of the hold function of the sample-and-hold device to recover the signal. The samples have very short duration (ns) to allow for good spatial resolution. It was found that reading only a sequence of such samples at 20 kHz rate with conventional audio circuitry was insufficient to reconstruct the sound wave. Holding the sampled voltage value until the next sample is acquired allows the system to recover the acoustic disturbance signal in real-time, which is later amplified sufficiently to drive a loudspeaker.

5.3. SYSTEM CHARACTERIZATIONS

The spatial resolution of the system depends on the sample-and-hold time-window (sampling time) and the pulse duration. In order to quantify the sampling time, square pulses of three different widths (5, 10 and 20 ns) are fed into device input, replacing the photodiode signal (Figure 5.2). If these pulses come much before or much after the sampling, no charge is stored in the capacitor and the output is zero. Convolved measurements are obtained by sweeping the delay between these input pulses and the sample-and-hold trigger pulse, while monitoring the output voltage. The sampling time is then found from the empiric deconvolution of the measured data and the known durations of the input pulses. The experimental results of each convolution are shown in Figure 5.3 (blue traces). The value of the sampling time found empirically that best fits the data in Figure 5.3 is 6 ns, as seen in the simulated convolutions (red dotted curves). In the calculations, it is assumed that the sampling is a square function.

This is in good agreement with the RC charging time of the circuit of Figure 5.2 with a 100 pF capacitance and total impedance slightly above 50 Ω.

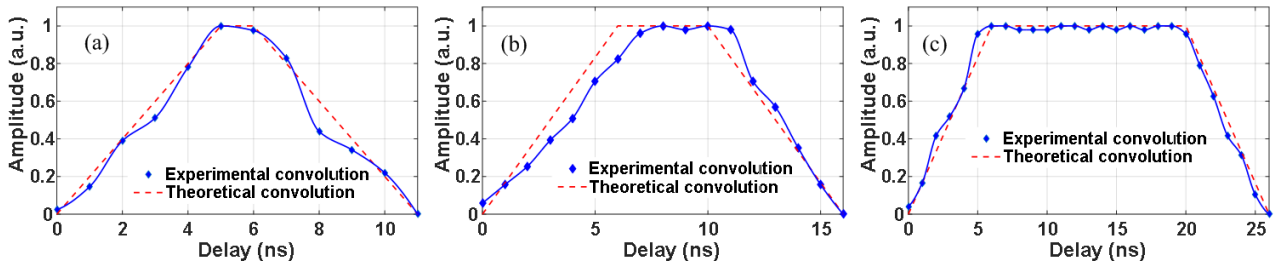

Figure 5.3. Theoretical and experimental results of the convolution between the sampling time and electrical pulses of (a) 5 ns, (b) 10 ns and (c) 20 ns width.

From these experiments, it is concluded that the sampling time is 6 ns, which limits the spatial resolution to around 60 cm, even if the phase-OTDR pulses are very short. Faster response time can be achieved for example by reducing the capacitance value.

The time resolution of the total system including optical pulses was investigated by probing acoustic disturbance employing the experimental setup depicted in Figure 5.1. The FUT was disturbed by driving the actuator loudspeaker with a continuous 80 Hz sinusoidal signal. The sample-and-hold device was triggered after a delay adjusted in steps of 2 ns. This corresponded to scanning the disturbance location in the phase-OTDR curve in 20-cm steps. The sound waveform was recorded during 3 s for every delay. A total tuning interval of 16 ns was covered. Figure 5.4a shows the time-domain sound waveforms for each tuning position. It is seen that the disturbing acoustic wave is detectable only in the central traces (6-10 ns) of the phase-OTDR response. The average of the absolute value of the amplitude for each delay is plotted in Figure 5.4b (blue dots). Its full-width-at-half-maximum (FWHM) measures 6 ns, which indicates a spatial resolution ~60 cm for the phase-OTDR system.

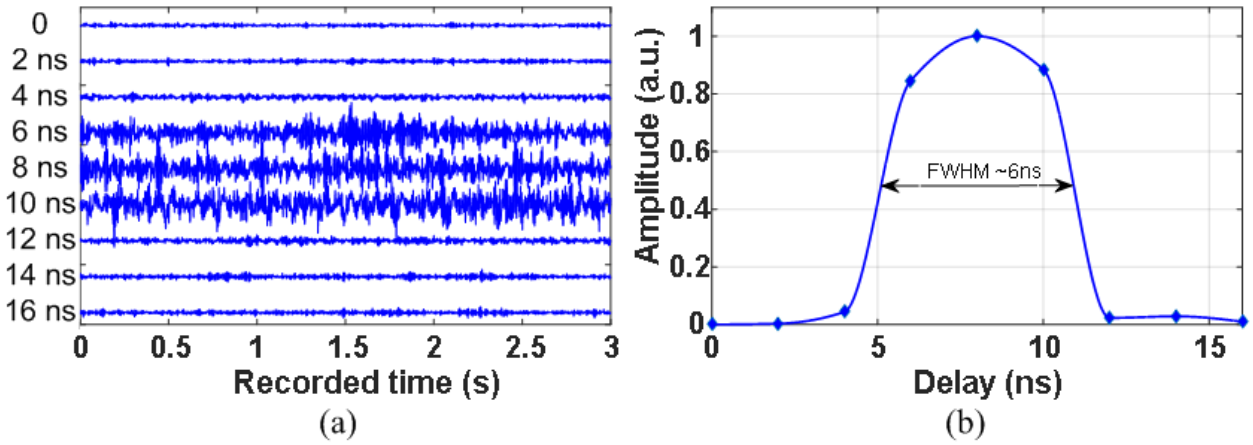

Figure 5.4. (a) Experimental results of the system spatial resolution evaluation using acoustic disturbance; (b) Measurement of the FWHM of the delay which captures a signal of large amplitude.

5.4. SOUND LISTENING EXPERIMENTS

5.4.1. FREQUENCY SWEEP, VOICE AND MUSIC

In order to evaluate the ability of the system to reproduce intelligible sound a sinusoidal signal was used to disturb a 60-cm section of a 300 m fiber. The frequency was swept manually from ~0 to 2000 Hz. The reproduced sound was recorded by tuning the delay of the sample-and-hold circuit to match the disturbed section of the fiber, as explained in Section 2. The recording is available in [69]. From this audio file, it is possible to recognize the frequency sweep in time, which validates the technique for listening to single tone sounds.

The capability of the system to detect and reproduce music was tested in the following. A 20 seconds segment of Beethoven's 5th Symphony played through the actuator loudspeaker was reproduced by the phase-OTDR system in real time and recorded. The detected sound can be found in [69]. Figure 5.5a shows the acquired sound waveform in the time-domain. The capability of the system to detect and reproduce in real-time complex acoustic disturbance such as music is noticeable.

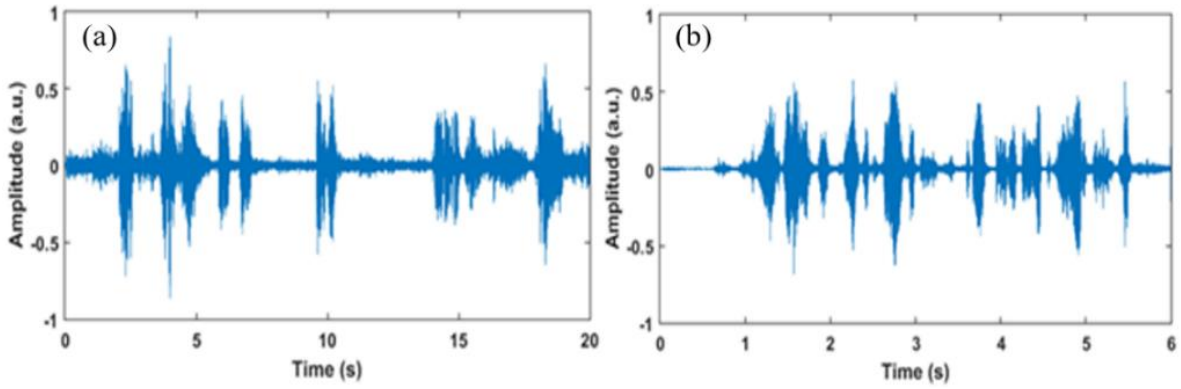

Figure 5.5. Time-domain waveforms of (a) music and (b) voice acquired by the proposed technique.

Lastly, the setup was probed with human voice. The file in [69] contains the input audio sample used to disturb the fiber under test. The recorded voice acquired through the present technique along the fiber link can be accessed in [69], and its time-domain waveform is seen in Figure 5.5b. Although the quality of the acquired sound is considerably worse than the input sample, the spoken words are still distinguishable. Techniques to improve the performance of the sensor and the quality of the acquired sound are the subject of future work. Besides the limitation imposed by the quadratic photodetector that reads the amplitude of the signal but not its phase, the main source of distortion here is in transducing the sound wave to phase disturbance in the optical signal.

5.4.2. FOOTSTEPS ON WOODEN PLANK

As previously stressed in chapter 3, the sound listening proposal could be also used for intrusion detection. In this section, the phase-OTDR method was used to listen to footsteps on a wooden plank, as depicted in Figure 5.6a. One meter of optical fiber was coiled and taped upon the plank and spliced to 300 m of the same fiber used in the previous subsection. Both fibers have the same N.A. = 0.24. The setup used to listen to the footsteps is the same as the one presented in Figure 5.1.

The receiver side of the phase-OTDR scheme was tuned to the plank location at the same time it was stepped on several times, as indicated in Figure 5.6b. The time-domain waveform of the 10 s of the footsteps acquired signal is shown in Figure 5.7 and its sound can be listened to in [70].

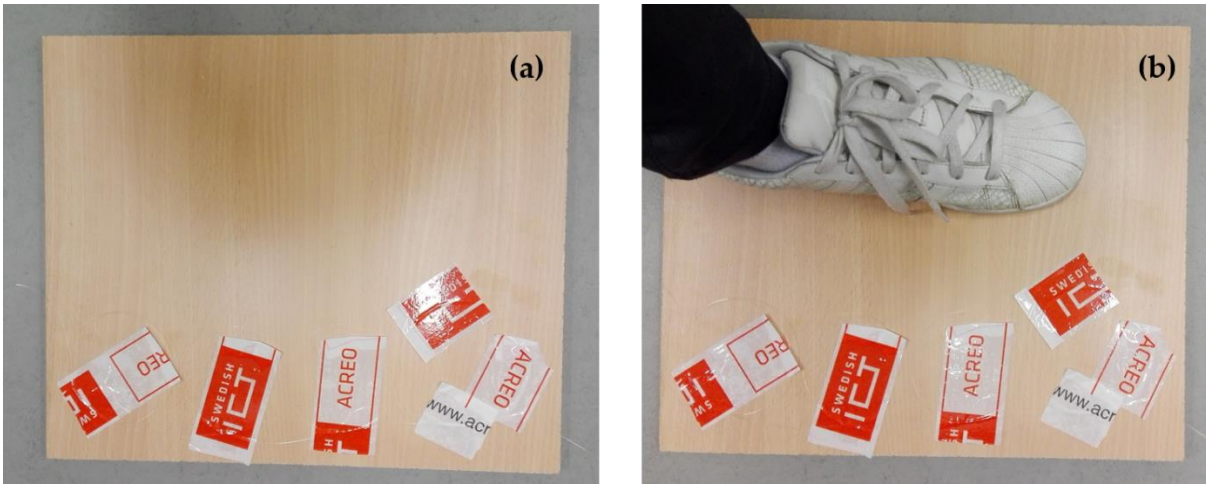

Figure 5.6. (a) Wooden plank with sensing optical fiber; (b) footsteps sound listening experiment.

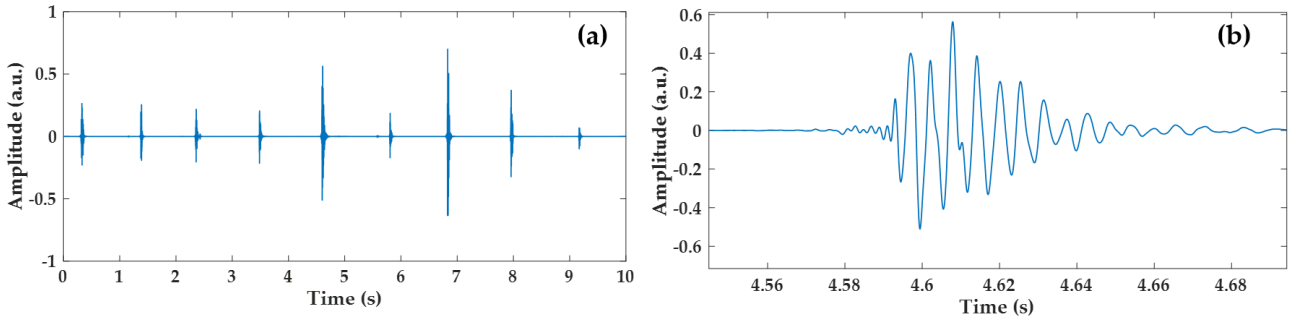

Figure 5.7. (a) Time-domain waveform of the footsteps on the wooden plank; (b) Zoomed section showing the dumped sound waveform of a footstep.

The results shown in Figure 5.7 and in the audio file confirm the capability of the phase-OTDR system to listen to footsteps when the sensing fiber and the disturbing source share the same medium, i.e. the wooden plank. The approximate frequency of the acquired sound is ~1Hz, which within the 1 to 4 Hz frequency range expected for footsteps.

5.4.3. COMPOSITE KNOCKING AND SCREW DROP

In this section, sound listening experiments were performed using the phase-OTDR method and the composite board with embedded optical fibers used in chapter 4. In these experiments, the receiver-side of the setup was tuned to the composite board location and the following acoustic stimuli on the board were recorded: the sound of a person knocking upon the composite and the sound of a screw dropped on the board.

Figure 5.8 depicts the composite board used in the experiments.

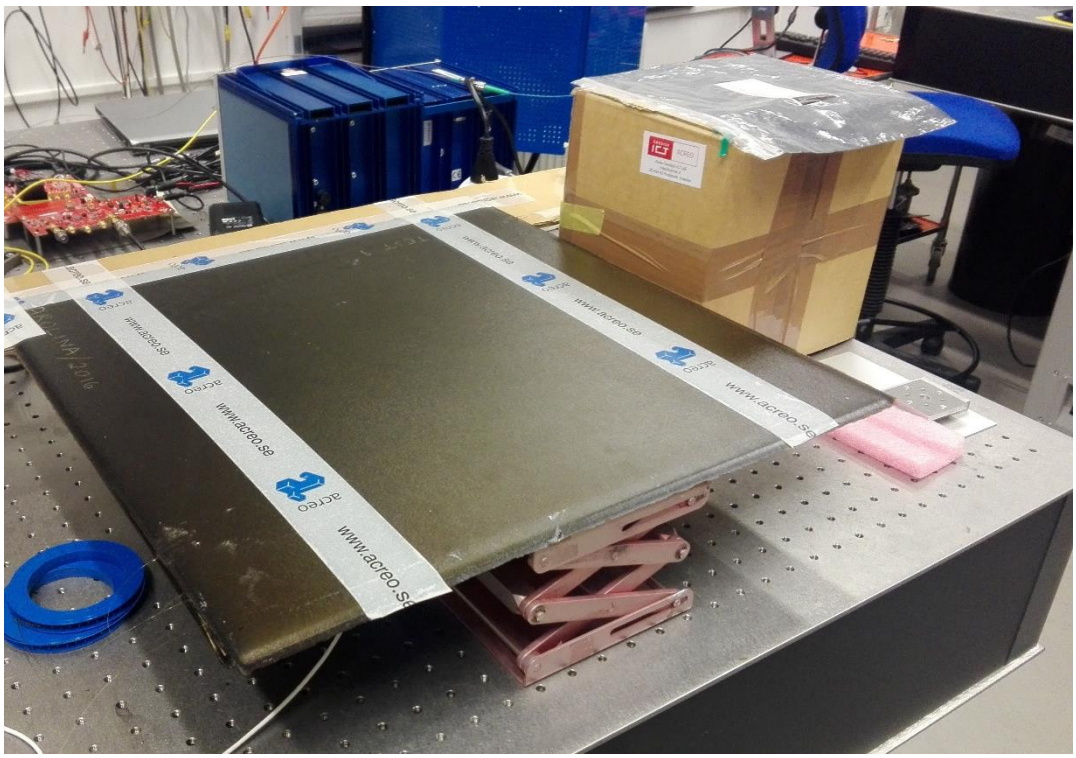

Figure 5.8. Composite board with embedded fibers used in the sound listening experiments.

Firstly, a person knocked upon the board surface and the sound was recorded by the phase-OTDR based microphone and can be listened to in [71]. Figure 5.9 shows the time-domain waveform of the recorded sound.

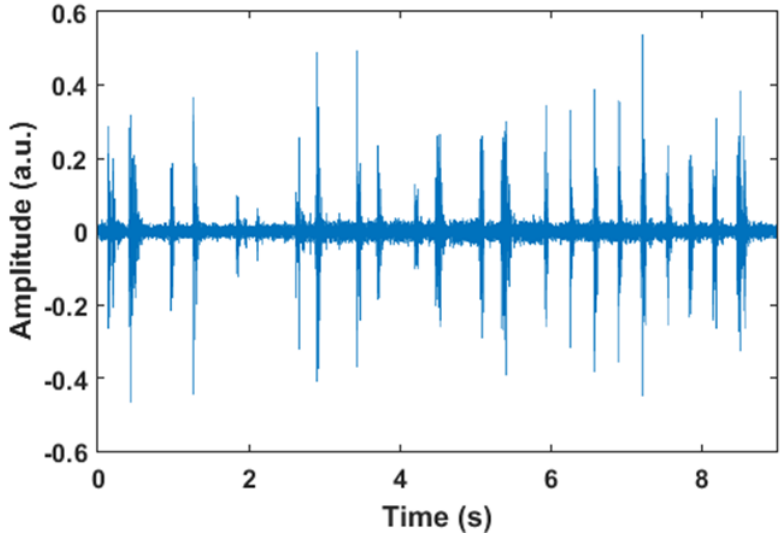

Figure 5.9. Recorded waveform of the composite knocking experiment.

As shown in Figure 5.9, the recorded waveform matches with the knocking events. This application is useful to detect failures in the structure, since they can be identified according to the way the material responds acoustically to the knocking. Thus, it is suitable for structure health monitoring proposals.

The next experiment consisted of dropping a screw upon the composite and recording the sound with the optical fiber microphone. The recorded sound can be heard in [72] and its waveform is shown in Figure 5.10.

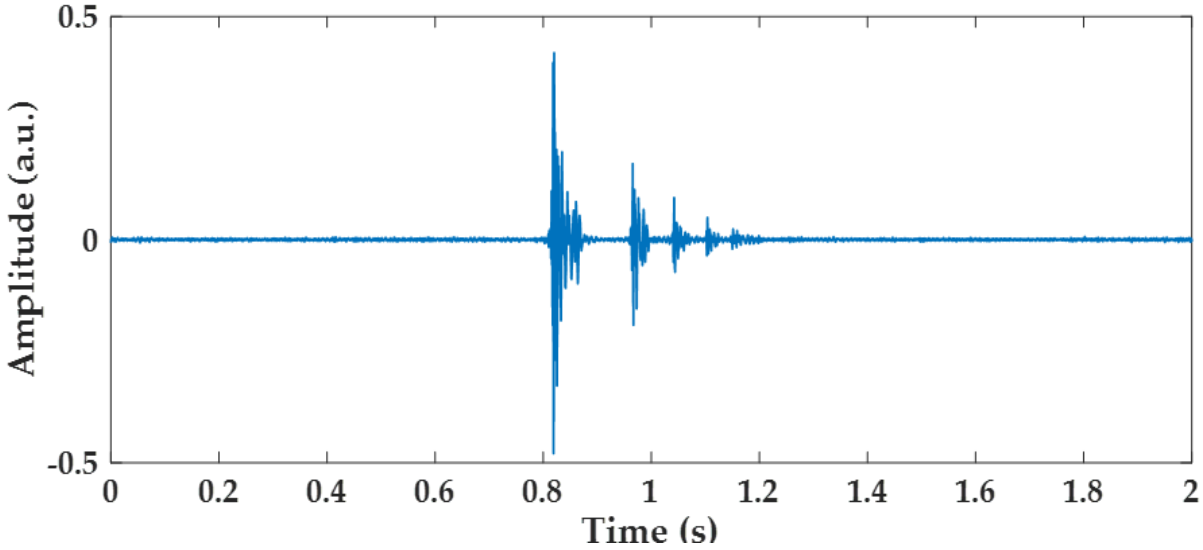

Figure 5.10. Recorded soundwave of a screw dropped upon the composite board.

According to the sound recorded and to its waveform, it is noticeable that the screw bounces upon the board surface a couple of times before stopping, each time exhibiting a lower amplitude. The results are in accordance to the event, which testifies this method capability to detect and reproduce such impacts on a structure.

5.4.4. MULTIPLE MACHINES SIMULTANEOUS LISTENING

The distributed capability of this system allied with the real-time spatial tuning makes this method suitable for listening to several machines in a workshop, one at a time. In this section, the phase-OTDR real-time microphone technique was employed to listen to two different machines, a drill and a cooling water system pump, using a single optical fiber. Both machines were attached to two different sections of the optical fiber, as shown in Figure 5.11, and they were working simultaneously.

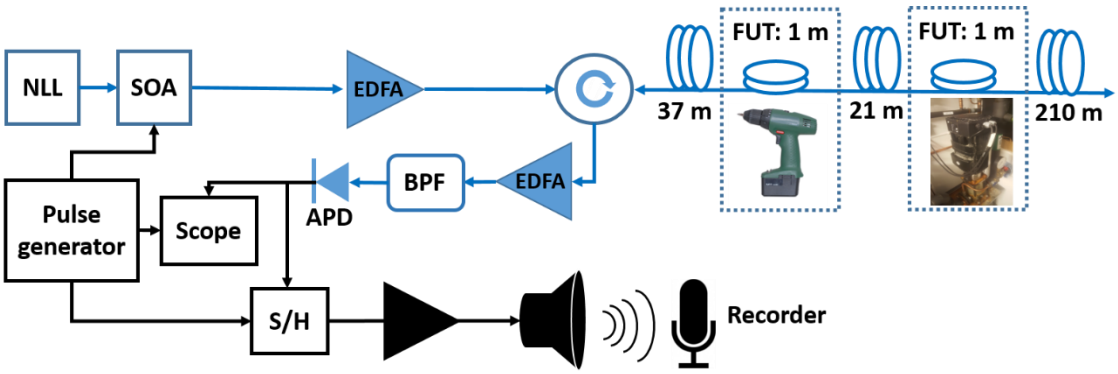

Figure 5.11. Phase-OTDR microphone applied to listen to two machines simultaneously.

Firstly, their locations along the optical fiber were tracked by monitoring on the oscilloscope screen and locating the two amplitude changing points in the phase-OTDR corresponding to the acoustic disturbance caused by both machines. Then, the delay of the sample-and-hold circuit is adjusted by spatially tuning the trigger pulse, matching it to the disturbed fiber section in the phase-OTDR curve, i. e. the machine one wants to listen to first. Initially, the system was tuned to listen to the sound of the

drill, which was intermittently switched on and off. Then, 10 s of the detected sound were recorded, which can be listened to in the link present in [73]. Also, its time-domain waveform is shown in Figure 5.12.

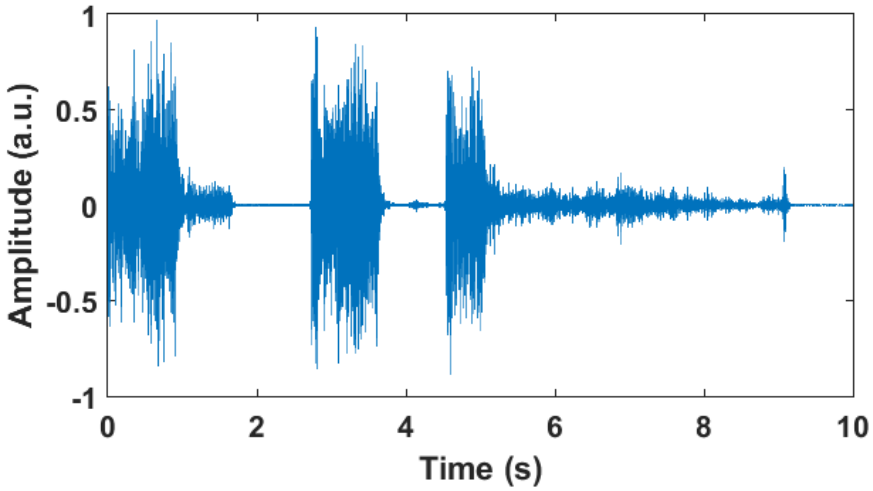

Figure 5.12. Time-domain waveform of the drill sound acquired with the proposed method.

By analyzing and listening to the drill sound recorded with the proposed distributed microphone, it is possible to distinguish between the time slots corresponding to the machine switching on (slots 0~1 s, 2.7~3.7 s and 4.5~5 s) and to the operating regimes (slots 1~1.7 s and 5~9.1 s). The occurrence of a higher amplitude, i.e. louder sound in the switching events than in the operating regime time slots is noticeable.

Further, the system was spatially tuned to listen to the cooling water system pump sound. Forty seconds of its acoustic waveform are recorded and shown in Figure 5.13. Also, the acquired sound can also be listened to in this link present in [73].

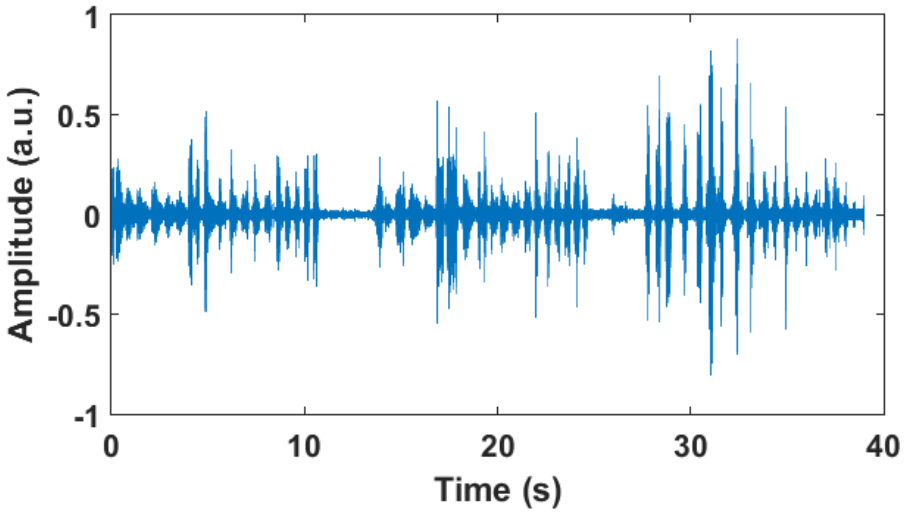

Figure 5.13. Time-domain waveform of the cooling water system pump sound acquired with the proposed method.

The recorded sound revealed the pump operation cycle: its system actuates for ~11 s, every 2.5 s, as it is depicted in Figure 5.13, where acoustic signal is observed from 0 to 11 s, from 13.5 to 24.5 s and from 27 to 38.5 s. Outside these time slots only noise is detected, and the observed behavior agrees with the pump operating cycles.

It is also important to mention that although both machines were in the same room and operating simultaneously, the generated sounds were successfully distinguished through the proposed method, i. e. there was no appreciable crosstalk between both acoustic sources. The experimental results validate then the application of the newly developed phase-OTDR based distributed microphone for listening to and evaluating the operation of multiple machines in a workshop.

5.5. CHAPTER CONCLUSION

In this section a novel distributed optical fiber microphone based on phase-OTDR was demonstrated. The method is capable to tune to different parts of the optical fiber with 60 cm of spatial resolution and listen to nearby sound disturbances in real time. The method comprises a simplified phase-OTDR setup and, in addition, it incorporates a simple low-cost electronic sample-and-hold circuit providing short reading time for

good spatial resolution and storing the information for sufficiently long time to reconstruct the detected acoustic wave.

It was demonstrated that this technique can be used for both SHM and surveillance applications. Sound sources like a frequency-sweeping sinusoidal signal, music, footsteps, machines, human voice, knocks and screw drops were used as acoustic disturbance for testing. After tuning the delay, it was possible to recover and listen to the applied disturbances. Moreover, tests with two simultaneous acoustic sources proved the capability to successfully recover both soundwaves without crosstalk between them. Also, small disturbance events like the drop of a screw upon a composite structure could be heard and recorded to analysis. It was proven as well that the disturbance source does not have to be directly upon the sensing fiber to be listened to, all it takes is to share a common medium with the optical fiber, e.g. the wooden plank used for the footsteps listening experiment.

Although no quantitative tests were performed to investigate the capacity limits of this microphone, it is worth mentioning that a qualitative experience was performed by dropping a 10 x 5 cm piece of foam, 5 cm thick upon the composite with the embedded optical fiber. The sound of the foam touching the composite surface was clearly detected by the developed technique.

Thus, the experiments performed in this section prove the suitability of this simple system as a real-time fiber microphone capable of interrogating a fiber link. Next goals comprise the study of the sensitivity of the microphone regarding minimum detectable acoustic pressure and also an optimized specialty fiber to enhance the sound coupling between source and sensor.

CHAPTER 6

6. CONCLUSIONS

The main goal of this thesis was to make use of the phase-OTDR features to employ this DAS technique as key enabling technology solution for applications concerning SHM and surveillance. The motivations relied on the fact that both areas can be covered using the same phase-OTDR method with minor setup changes, which highlights the adaptability feature of this DAS approach. In this work, phase-OTDR based techniques were investigate and the thesis main contributions were focused on bringing innovative solutions and validations for SHM and surveillance applications.

The contribution of this thesis regarding aircraft SHM was the evaluation of the phase-OTDR technique to measure vibration frequencies in carbon composites using embedded optical fibers. Frequencies ranging from 0 to 1000 Hz were correctly measured in two layers of the investigated composite board and this work was published in the SPIE Smart Structures NDE Conference, 2107. Also, a literature review was also performed in order to evaluate the influence of the embedded optical fibers in the composite reinforcing carbon fibers, showing that no significant resistance reduction is observed when the optical fibers are embedded in parallel with respect to the material carbon fibers.

This work also contributed with intrusion detection systems based on DAS, by proposing the use of parallel hardware architectures to implement real-time detecting and locating perturbations through a phase-OTDR distributed vibration sensor. In this multidisciplinary investigation, hardware architectures of the iterative moving average filter and the Sobel filter were mapped on field programmable gate arrays, exploring the intrinsic parallelism in order to achieve real-time requirements. Experimental results validate the employment of this DAS technique allied with FPGA

solutions for surveillance applications. The experimental results were published in the 14th EEE International Conference on Networking, Sensing and Control, 2017.

Lastly, a novel distributed optical fiber tunable microphone was proposed is demonstrated employing a phase-OTDR with direct detection. This technique covers both the surveillance and SHM applications. The method comprises a sample-and-hold circuit capable of both tuning the receiver to an arbitrary section of the fiber considered of interest and to recover in real-time the detected acoustic wave. The system allows listening to the sound of a sinusoidal disturbance with variable frequency, music and human voice with ~60 cm of spatial resolution through a 300 m long optical fiber. The experimental results were published in the Optics Express journal, 2016, as show in Appendix A.

The developed system distributed capability allied with the real-time spatial tuning makes it also suitable for listening to several machines in a workshop, one at a time. Thus, the phase-OTDR real-time microphone technique was also employed to listen to two different machines, a drill and a cooling water system pump, using a single optical fiber. Both machines were attached to two different sections of the optical fiber and they were both working simultaneously. By triggering the sample-and-hold device, both machines were successfully listened to, along with the recording of their soundwaves. These results were published in the IMOC 2017 International Conference. Also, the knocking sounds on the carbon composite border evaluated in the previous SHM section were also listened to, a result that reinforce the use of this microphone for SHM. It is expected that these results will feed further researches regarding sound coupling and analysis in optical fibers.

It is worth mentioning that this research drove the RISE Acreo laboratories into a new business area of distributed acoustic sensors, a field yet unexplored by the company, which aggregates a technological effort value to this work.

Thus, this thesis accomplished its main goal which was to employ DAS techniques as key enabling technologies solutions for several applications. It is worthy stressing that with a single setup of the parameters addressed in Table I it was possible

to cover the three proposed applications, reinforcing the versatility of this method. Thus, phase-OTDR based techniques were studied and innovative solutions were proposed and validated for SHM and surveillance applications.

BIBLIOGRAPHY

1. A. Barrias, J. R. Casas and S. Villalba, “A review of distributed optical fiber sensors for civil engineering applications,” Sensors, vol. 16, n. 5, 738, May 2016.
2. Q. Cui, S. Pamukcu and M. Pervizpour, “Impact wave monitoring in soil using a dynamic fiber sensor based on stimulated Brillouin scattering,” Sensors, vol 15, n.4, pp. 8163-8172, April 2015.
3. L. S. Grattan and B. T. Meggitt, “Optical fiber sensor technology,” Springer Science & Business Media, 2013.
4. F. Peng, H. Wu, X. Jia, Y. Rao, Z. Wang and Z. Peng, “Ultra-long high-sensitivity Φ-OTDR for high spatial resolution intrusion detection of pipelines,” Optics Express, vol. 22, n. 11, pp. 13804-13810, May 2014.
5. Z. Qin, L. Chen and X. Bao, “Continuous wavelet transform for non-stationary vibration detection with phase-OTDR,” Optics Express, vol. 20, n. 18, pp. 20459-20465, August 2012.
6. Q. He, T. Zhu, X. Xiao, B. Zhang, D. Diao and X. Bao, “All fiber distributed vibration sensing using modulated time-difference pulses,” IEEE Photonics Technology Lettters, vol. 25, n. 20, pp. 1955-1957, October 2013.
7. D. Balageas, C. Fritzen and A. Guemes, “Structural health monitoring,” Wiley-ISTE, 2006.
8. Z. Qin, L. Chen and X. Bao, “Continuous wavelet transform for non-stationary vibration detection with phase-OTDR,” Optics Express, vol. 20, n. 18, pp. 20459-20465, August 2012.
9. J. C. Juarez, E. W. Maier, K. N. Choi and H. F. Taylor, “Distributed fiber-optic intrusion sensor system,” Journal of Lightwave Technology, vol. 23, n. 6, pp. 2081-2087, June 2005.
10. C. F. Bohren and D. R. Huffman, “Absorption and scattering of light by small particles,” Wiley- VCH, 1998.
11. Q. Zengguang, “Distributed optical fiber vibration sensor based on Rayleigh backscattering,” PhD Thesis, Univ. of Ottawa, Canada, 2013.
12. X. Bao and L; Chen, “Recent progress in distributed fiber optic sensors,” Sensors vol. 12, pp-8601-8639, June 2012.
13. H. F. Martins, “Distributed and remote fiber sensing assisted by Raman effect,” PhD Thesis, Univ. do Porto/Univ. de Alcalá, Portugal/Spain, 2014.

14. Link: http://febus-optics.com/1/en/technology/systeme/
15. R. Billington, “Measurement methods for stimulated Raman and Brillouin scattering in optical fibres,” NPL Report COEM 31, June 1999.
16. Link: http://hyperphysics.phy-astr.gsu.edu/hbase/atmos/blusky.html
17. I. Bikandi et al, “Spectral dependence of scattered light in step-index polymer optical fibers by side-illumination technique,” Journal of Lightwave Technology, vol. 32, n.23, pp. 4539-4543, December 2014.
18. M. Nakazawa, “Rayleigh backscattering theory for single-mode optical fibers,” J. Opt. Soc. Am., vol. 73, n. 9, pp. 1175-1180, September 1983.
19. R. Hui and M. O’Sullivan, “Fiber optics measurement techniques,” Elsevier Academic Press, USA 2009.
20. M. Barnoski and S. Jensen, “Fiber waveguides: a novel technique for investigating attenuation characteristics,” Applied Optics, vol.15, n. 9, pp. 2112-2115, September 1976.
21. D. Derickson, “Fiber optic test and measurement,” Prentice Hall PTR, USA 1998.
22. H. Taylor and C. Lee, “Apparatus and method for fiber optic intrusion sensing,” US Patent 5194847, 1993.
23. P. Healey, “Fading in heterodyne OTDR,” Electronic Letters, vol. 20, n.1, pp. 30-32, November 1983.
24. J. Park, W. Lee and H. Taylor, “A fiber optic intrusion sensor with the configuration of an optical time domain reflectometer using coherent interference of Rayleigh backscattering,” SPIE vol. 3555, pp. 49-56, 1998.
25. M. Ren, L. Chen and X. Bao, “Theoretical and experimental analysis of phase-OTDR based on polarization diversity detection,” IEEE Photonics Technology Letters, vol. 28, n. 6, pp. 697-700, December 2015.
26. Y. Lu, T. Zhu, L. Chen and X. Bao, “Distributed vibration sensor based on coherent detection of phase-OTDR,” Journal of Lightwave Technology, vol. 28, n. 22, pp. 3243-3249, November 2010.
27. J. Juarez, E. Maier, K. Choi and H. Taylor, “Distributed fiber-optic intrusion sensor system,” Journal of Lightwave Technology, vol. 23, n. 6, pp. 2081-2087, June 2005.
28. J. Juarez and H. Taylor, “Field test of a distributed fiber-optic intrusion sensor system for long perimeters,” Applied Optics, vol. 46, n. 11, pp. 1968-1971, April 2007.
29. C. Madsen, T. Bae and R. Atkins, “Long fiber-optic perimeter sensor: signature analysis,” Photonic Applications Systems Technologies Conference, PWA5, May 2007.

30. Y. Rao, J. Li, Z. Ran and K. Xie, “Distributed intrusion detection based on combination of phase-OTDR and pOTDR,” Proc. of SPIE, vol. 7004, May 2008.
31. Z. Ran, Y. Rao, L. Luo, S. Xiong, Q. Deng, “Phase-OTDR used for providing security service in EPON,” 14th OECC, July 2009.
32. Z. Pan, K. Liang, Q. Ye, H. Cai, Q. Qu and Z. Fang, “Phase-sensitive OTDR system based on digital coherent detection,” Proc. of ACP, vol. 8311, 2011.
33. Z. Qin, L. Chen and X. Bao, “Continuous wavelet transform for non-stationary vibration detection with phase-OTDR,” Optics Express, vol. 20, n. 18, pp. 20459-20465, August 2012.
34. T. Zhu, X. Xiao, Q. He and D. Diao, “Enhancement of SNR and spatial resolution in phase-OTDR system by using two-dimensional edge detection method,” Journal of Lightwave Technology, vol. 31, n. 17, pp. 2851-2856, September 2013.
35. H. Martins et al, “Coherent noise reduction in high visibility phase-sensitive optical time domain reflectometer for distributed sensing of ultrasonic waves,” Journal of Lightwave Technology, vol. 31, n. 23, pp. 3631-3637, December 2013.
36. Q. et al, “All fiber distributed vibration sensing using modulated time-difference pulses,” IEEE Photonics Technology Letters, vol. 25, n. 20, pp. 1955-1957, October 2013.
37. Z. Zhong et al, “Influences of laser source on phase-sensitivity optical time-domain reflectometer-based distributed intrusion sensor,” Applied Optics, vol. 53, n. 21, pp. 4645-4650, July 2014.
38. Z. Wang et al, “Phase-sensitive optical time-domain reflectometry with Brillouin amplification,” Optics Letters, vol. 39, n.15, pp. 4313-4316, August 2014.
39. H. Martins et al, “Phase-sensitive optical time domain reflectometer assisted by first-order Raman amplification for distributed vibration sensing over > 100 km,” Journal of Lightwave Technology, vol. 32, n. 8, pp. 1510-1518, April 2014.
40. F. Peng et al, “Ultra-long high-sensitivity Φ-OTDR for high spatial resolution intrusion detection of pipelines,” Optics Express, vol. 22, n. 11, pp. 13804-13810, June 2014.
41. C. Wang et al, “Distributed acoustic mapping based on self-interferometry of phase-OTDR,” ACP 2014, ATh3A, 2014.
42. H. Wu et al, “Separation and determination of the disturbing signals in phase-sensitive optical time domain reflectometry (phase-OTDR),” Journal of Lightwave Technology, vol. 33, n. 15, pp. 3156-3162, August 2015.

43. G. Fang, T. Xu, S. Feng and F. Li, “Phase-sensitive optical time domain reflectometer based on phase-generated carrier algorithm,” Journal of Lightwave Technology, vol. 33, n. 13, pp. 2811-2816, July 2015.
44. Y. Wu et al, “Distributed fiber voice sensor based on phase-sensitive optical time-domain reflectometry,” IEEE Photonics Journal, vol. 7, n. 6, 6803810, December 2015.
45. C. Baker et al, “Enhancement of optical pulse extinction-ratio using the nonlinear Kerr effect for phase-OTDR,” Optics Express, vol. 24, n.17, pp. 19424-19434, August 2016.
46. M. Zhang, S. Wang, Y. Zheng and Y. Yang, “Enhancement for phase-OTDR performance by using narrow linewidth light source and signal processing,” Photonic Sensors, vol. 6, n.1, pp. 58-62, 2016.
47. J. Zhang et al, “Modulated pulses based high spatial resolution distributed fiber system for multi-parameter sensing,” Optics Express, vol. 24, n. 24, pp.27482-27493, November 2016.
48. Y. Shang et al, “Phase-OTDR based on space difference of Rayleigh backscattering,” 15th ICOCN, 2016.
49. D. Iida, K. Toge and T. Manabe, “Distributed measurement of acoustic vibration location with frequency multiplexed phase-OTDR,” Optical Fiber Technology, vol. 36, pp. 19-25, February 2017.
50. J. Pastor-Graells, “Chirped-pulse phase-sensitive reflectometer assisted by first-order Raman amplification,” Journal of Lightwave Technology, vol. 35, n. 21, pp. 4677-4683, September 2017.
51. C. Franciscangelis, C. Floridia and F. Fruett, “Optical fibre intrusion detection method based on Lefevre-loop and bidirectional polarization optical time-domain reflectometer-C technique,” The Journal of Engineering, 2 pp., November 2015.
52. A. Owen, G. Duckworth and J. Worsley, “OptaSense: Fibre optic distributed acoustic sensing for border monitoring,” IEEE Conf. Intelligence and Security Informatics, pp. 362-364, August 2012.
53. X. Yu et al, “Phase-sensitive optical time domain reflectometer for distributed fence-perimeter intrusion detection,” SPIE Int. Conf. Optical Fiber Sensors and Applications, October 2015.
54. D. M. Munoz, C. Franciscangelis, W. Margulis and I. Söderquist, “Low latency disturbance detection using distributed optical fiber sensors,” Proc. of IEEE 14th International Conference on Networking, Sensing and Control (ICNSC), May 2017.

55. K. Diamanti and C. Soutis, “Structural health monitoring techniques for aircraft composite structures,” Progress in Aerospave Sciences 46, pp. 342-352, May 2010.
56. M. Kehow, “A historical overview of flight flutter testing,” NASA Technical Memorandum 4720, October 1995.
57. R. Di Sante, “Fibre optic sensors for structural health monitoring of aircraft composite structures: recent advances and applications,” Sensors, vol. 15, pp. 18666-18713, July 2015.
58. Link: http://www.quartus.com/resources/white-papers/composites-101/
59. Link: https://www.wired.com/2010/03/flutter-testing-aircraft/
60. T. Krishnamurthy, “Frequencies and flutter speed estimation for damaged aircraft wing using scaled equivalent plate analysis,” 51st AIAA, 2010-2759, April 2010.
61. Link: https://www.compositesworld.com/articles/structural-health-monitoring-composites-get-smart
62. C. Franciscangelis et al, “Vibration measurement on composite material with embedded optical fiber based on phase-OTDR,” Proc. of SPIE Smart Structures NDE, 101683Q, March 2017.
63. Link: http://altairenlighten.com/in-depth/fiber-reinforced-composites/
64. J. Silva et al, “Mechanical characterization of composites with embedded optical fibers,” Journal of Composite Materials, vol. 39, n. 14, pp. 1261-1281, October 2004.
65. K. Shivakumar, “Mechanics of failure of composite laminates with an embedded fiber optic sensor,” Journal of Composite Materials, vol. 38, n. 8, pp. 669-680, 2004.
66. Link: https://fibercore.com/product/polyimide-coated-sm-fiber
67. L. Palmieri and L. Schenato, “Distributed optical fiber sensing based on Rayleigh scattering,” The Open Opt. Journal 7, 104-127 (2013).
68. Z. Wang, L. Zhang, S. Wang, N. Xue, F. Peng, M. Fan, W. Sun, X. Qian, J. Rao, and Y. Rao, "Coherent Φ-OTDR based on I/Q demodulation and homodyne detection," Opt. Express, vol. 24, n. 2, 853-858, 2016.
69. C. Franciscangelis, W. Margulis, L. Kjellberg, I. Söderquist and F. Fruett, “Real-time distributed fiber microphone based on phase-OTDR,” Opt. Express, vol. 24, n. 26, pp. 29597-29602, December 2016.
70. Link: https://clyp.it/ypv3zvfv
71. Link: https://clyp.it/4t43xzr4
72. Link: https://clyp.it/yyzb2cek

73. C. Franciscangelis, W. Margulis, L. Kjellberg, C. Floridia and F. Fruett, “Real-time multiple sound listening using a phase-OTDR based distributed microphone,” Proc. of IMOC 2017, August 2017.

APPENDIX A: PUBLISHED PAPERS

This appendix section summarizes the papers published by the author during the PhD period.

1. **C. Franciscangelis**, C. Floridia, G. C. Simões, F. Schmmidt and F. Fruett, "On-field distributed first-order PMD measurement based on pOTDR and optical pulse width sweep," Opt. Express, vol. 23, n. 10, pp. 12582-12594, May 2015.
2. **C. Franciscangelis**, C. Floridia and F. Fruett, "Optical fibre intrusion detection method based on Lefevre-loop and bidirectional polarisation optical time-domain reflectometer-C technique," The Journal of Engineering, pp. 1-2, October 2015.
3. **C. Franciscangelis**, W. Margulis, L. Kjellberg, I. Söderquist and F. Fruett, "Real-time distributed fiber microphone based on phase-OTDR," Opt. Express, vol. 24, n. 26, pp. 29597-29602, December 2016.
4. **C. Franciscangelis** et al, "Vibration measurement on composite material with embedded optical fiber based on phase-OTDR," Proc. of SPIE Smart Structures NDE, 101683Q, March 2017.
5. D. M. Munoz, **C. Franciscangelis**, W. Margulis and I. Söderquist, "Low latency disturbance detection using distributed optical fiber sensors," Proc. of IEEE 14th International Conference on Networking, Sensing and Control (ICNSC), May 2017.
6. **C. Franciscangelis**, W. Margulis, L. Kjellberg, C. Floridia and F. Fruett, "Real-time multiple sound listening using a phase-OTDR based distributed microphone," Proc. of IMOC 2017, August 2017.